Phonon-mediated Casimir effect

Dissertation

zur Erlangung des akademischen Grades

Doctor rerum naturalium

(Dr. rer. nat.)

vorgelegt der

Fakultät Physik

der Technischen Universität Dresden

von

Andrei Pavlov

geboren am 13. Dezember 1990 in Moskau

Contents

Chapter 1

Introduction

1.1 Preface

The concept of vacuum energy (also referred as the zero-point energy or energy of the vacuum fluctuation) is one of the most fundamental and counter-intuitive predictions of quantum mechanics and quantum field theory. What is even more fascinating - this energy manifests itself in a number of various measurable phenomena, so it astonishes physicists since early days of the quantum theory. Arguably, one of the most profound and well-known of these phenomena is the so-called Casimir effect [1]. Casimir in his original work showed that an attractive force between two separated uncharged metallic objects arises as a consequence of local change of the vacuum energy. Besides the Casimir effect, there are other predicted and observed vacuum energy manifestations, such as the van der Waals forces [2]. The Lamb shift (found experimentally in [3] and explained theoretically in [4, 5]) is also among them - the effect of displacement of the

$2s$ energy level of hydrogen due to interaction of the electron with the zero mode of the electromagnetic field. Other benchmark examples are anomalous magnetic moment of electron [6] and spontaneous emissions [5, 7].

The concept of vacuum energy can be illustrated by the following consideration. Let us take the Hamiltonian of a harmonic oscillator:

$$H_0 = \frac{1}{2} \sum_{\mathbf{k}} \hbar \omega_{\mathbf{k}} \left(a_{\mathbf{k}}^{\dagger} a_{\mathbf{k}} + a_{\mathbf{k}} a_{\mathbf{k}}^{\dagger} \right) \tag{1.1}$$

$a_{\mathbf{k}}^{\dagger}$ and $a_{\mathbf{k}}$ are bosonic creation and annihilation operators in momentum space, $\omega_{\mathbf{k}}$ is its frequency (dispersion). With the commutation rule $[a_{\mathbf{k}}, a_{\mathbf{k}'}^{\dagger}] = \delta_{\mathbf{k}, \mathbf{k}'}$ and the particle number operator $n_{\mathbf{k}} = a_{\mathbf{k}}^{\dagger} a_{\mathbf{k}}$, the energy vacuum expectation value for the Hamiltonian (1.1) is

$$\langle 0 | H_0 | 0 \rangle = \sum_{\mathbf{k}} \hbar \omega_{\mathbf{k}} \langle 0 | n_{\mathbf{k}} + \frac{1}{2} | 0 \rangle = \frac{1}{2} \sum_{\mathbf{k}} \hbar \omega_{\mathbf{k}}. \tag{1.2}$$

Therefore, even the vacuum state, though there are no particles (quasiparticles), is characterized by non-zero energy. Presence of external objects in the system leads to a change of this energy, which can be an experimentally measurable quantity. In particular, it may lead to an effective interaction between this objects. A majority of the effects mentioned above arises due to coupling of a particle (e.g. an electron) to a fluctuating Goldstone mode. The Casimir effect stands unique even among the vacuum energy related phenomena - unlike others of them, it appears due to a direct local shift of the vacuum energy (1.2) as a consequence of the imposed boundaries or due to the non-Euclidean topology [8].

In this thesis I focus on phenomena arising due to the vacuum fluctuations in condensed matter systems. The subject of our prime interest is the Casimir interaction between impurities mediated by phonons (Chapters 2-4). In Chapter 5 we consider an itinerant electron in a two-dimensional anisotropic ferromagnet in an eternal magnetic field. The particle distorts magnetic order of the system creating virtual magnons. These magnons significantly change mobility of the quasiparticle. We show that in this situation the spectral weight is not described by a pole structure anymore.

1.2 Casimir effect

1.2.1 Original Casimir approach

To understand the difference between the origins of the Casimir interaction in electrodynamics and in condensed matter physics, it is worth to consider the original derivation of the vacuum fluctuation induced interaction made by H. Casimir in his milestone paper [1]. We consider a simplified system consisting of two parallel large conducting plates with sides L placed close to each other and depicted in Fig. 1.1. The plates are separated by distance which can vary from some very small value a up to a large d (but $d \ll L$). The spectrum of fluctuating photons between the plates is quantized and changes depending on the separation between the plates due to the boundary conditions imposed by the plates. Following the Casimir's arguments, we calculate a difference in energy of the vacuum fluctuations within the plates and without. The zero-point energy Eq. (1.2) given by the sum over all possible zero-point frequencies between the plates is divergent, but the difference of the zero-point energies for

3

different separations between the plates is well-defined and finite. This energy difference is interpreted as the interaction between the plates and referred as the Casimir energy.

We choose z-axis perpendicular to the plates. The plates are separated by distance a, so the coordinates inside the area of interest are in the range $0 \leq z \leq a$, momentum of the zero-point field is quantized in this direction and reads

$$k_z = \frac{\pi}{a} n_z$$

with positive integer n_z.

The total zero-point energy Eq. (1.2) for the linear spectrum $\omega_{\mathbf{k}} = c\sqrt{k_x^2 + k_y^2 + k_z^2}$ (c is the speed of light here) is given then as

$$\frac{1}{2}\sum_{\mathbf{k}} \hbar \omega_{\mathbf{k}} = \hbar c \frac{L^2}{(2\pi)^2} \int_{-\infty}^{\infty} dk_x \int_{-\infty}^{\infty} dk_y \left[\frac{1}{2}\sqrt{k_x^2 + k_y^2} + \sum_{n=1}^{\infty} \sqrt{k_x^2 + k_y^2 + \frac{\pi^2}{a^2}n^2} \right].$$

(1.3)

The electromagnetic field has two polatizations, i.e. two standing waves for each mode, except $n = 0$. For a massless scalar field the second term in Eq.(1.3) would have the $\frac{1}{2}$ prefactor.

It is easier to treat the integrals over k_x and k_y in polar coordinates, with the polar angle $\theta \in [0, \frac{\pi}{2}]$ and radius $\varkappa = \sqrt{k_x^2 + k_y^2} \in [0, \infty)$. We are interested in the difference of energy δE for two configurations: when a is small and when a is very large. In the second case the summation can be changed to integration, the same way as previously for k_x and k_y:

$$\delta E = \hbar c \frac{L^2}{\pi^2} \frac{\pi}{2} \int_0^{\infty} d\varkappa \left[\frac{1}{2}\varkappa^2 + \sum_{n=1}^{\infty} \varkappa \sqrt{\varkappa^2 + \frac{\pi^2}{a^2}n^2} - \frac{a}{\pi} \int_0^{\infty} dk_z \varkappa \sqrt{\varkappa^2 + k_z^2} \right].$$
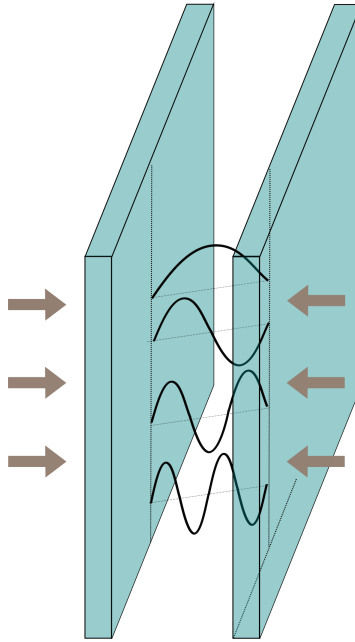
Figure 1.1. Principal set-up for the Casimir effect as formulated in [1]. Quantization of the electromagnetic waves between the plates leads to the attractive force between the plates (depicted as brown arrows).

$$\tag{1.4}$$

To evaluate the expression above, we introduce the cut-off function $f(\frac{k}{k_m}) = e^{-\frac{k}{k_m}}$, $k_m \simeq \frac{\omega_p}{c}$, ω_p the plasma frequency for the metal. The physical meaning of this cut-off is that there are no ideally conducting plates and high frequency waves leak out of region confined by the metal plate. In principle, there are other ways to renormalize Eq. (1.4), for instance, the so-called dimensional regularization method is discussed in [9].

After substitution of a new variable $u = \frac{a^2 \varkappa^2}{\pi^2}$ into Eq.(1.4), the energy

difference becomes

$$\delta E = \hbar c \frac{L^2 \pi^2}{4a^3} \left[\frac{1}{2} F(0) + \sum_{n=1}^{\infty} F(n) - \int_0^{\infty} dn F(n) \right],$$

with $F(n) = \int_0^{\infty} du \sqrt{u + n^2} f \left(\frac{\pi \sqrt{u + n^2}}{a k_m} \right)$.

The Euler–Maclaurin formula, which reads as

$$\sum_{n=1}^{\infty} F(n) - \int_0^{\infty} dn F(n) = -\frac{1}{2} F(0) - \frac{1}{12} F'(0) + \frac{1}{720} F'''(0) + \ldots,$$

can be applied here. Differentiation of this function gives

$$F'(0) = 0,$$
$$F''(0) = 0,$$
$$F'''(0) = -4.$$

Higher order derivatives contain derivatives of the $f(n)|_{n=0}$ function, which are small, and powers of the small parameter $\frac{\pi}{a k_m}$, so the resulting energy difference per unit of square, which is usually referred as the Casimir energy, is $E_{Cas}^{(3D)}(a) = \frac{\delta E}{L^2} = -\hbar c \frac{\pi^2}{720} \frac{1}{a^3}$. As a consequence, the attractive force between the plates is

$$F_{Cas}(a) = \frac{\pi^2}{240} \frac{\hbar c}{a^4}. \tag{1.5}$$

The finite temperature corrections for the Casimir force between conducting plates were calculated by Mehra [10]. The free energy of the

6

system is defined as

$$\mathcal{F} = -\frac{1}{k_B T} \log \left[Tr \left(e^{-\frac{H}{k_B T}} \right) \right], \; H = \sum_{\mathbf{k}} \hbar \omega_{\mathbf{k}} \left(n_{\mathbf{k}} + \frac{1}{2} \right).$$

It gives the Casimir force

$$F_{Cas}(a, T) = \frac{1}{L^2} \frac{\partial \mathcal{F}}{\partial a}, \; \mathcal{F} = \sum_{\mathbf{k}} \left[\frac{\hbar \omega_{\mathbf{k}}}{2} + k_B T \log \left(1 - e^{-\frac{\hbar \omega_{\mathbf{k}}}{k_B T}} \right) \right]. \quad (1.6)$$

For high temperatures $\frac{4\pi a k_B T}{\hbar c} \equiv t \gg 1$, Eq.(1.6) yields

$$F_{Cas}(a) = \frac{k_B T}{4\pi a^3} \zeta(3) + \frac{k_B T}{2\pi a^3} \left[1 + t + \frac{1}{2} t^2 \right] e^{-t},$$

where $\zeta(3) \simeq 1.2$ is the Riemann zeta-function.

At low temperatures $t \ll 1$, the solution of Eq.(1.6) is

$$F_{Cas}(a) = \frac{\pi^2}{240} \frac{\hbar c}{a^4} \left[1 + \frac{t^4}{48\pi^4} - \frac{60t}{\pi^2} e^{-\frac{4\pi^2}{t}} \right].$$

In the limit of zero temperature, this expression is the same as Eq. (1.5). This force between metallic plates is proportional to $\hbar$, which illustrates the fact that it is purely quantum and disappears in the classical limit.

1.2.2 Experimental realizations and further extensions of the Casimir effect

The Casimir effect was measured experimentally for the first time in 1956 [11, 12] in insulating systems (the theory for the Casimir effect in such system was developed by Lifschitz, Dzyaloshinskii and Schwinger [13, 14, 15]). In metallic systems, the Casimir effect was measured for the first

time in 1958 [16]. Later on, several observations of the Casimir effect were reported in [17, 18, 19, 20]. In the high precision experimental measurements, the agreement with theory was achieved with a margin of error 5% and then 1% [21, 22]. Improvement of the measuring devises and development of nanoscale electromechanical devices surged a new wave of interest towards the experimental manifestations of the Casimir effect in systems with nontrivial geometries and in gases or liquids (e.g. [23, 24, 25, 26, 27, 28]).

Beside the experimental studies, there are novel theoretical works which extend the Casimir effect on unusual systems and interactions. A lot of attention is paid recently to the Casimir effect in systems with nontrivial geometry or topology [8, 29, 30, 31, 32, 33], to the Casimir effect mediated by massive bosonic fields [34, 35, 36, 37] and by fermions [38, 39]. Furhermore, repulsive Casimir forces were predicted theoretically and found experimentally [40, 41, 42, 43, 44, 45, 46].

Varieties of the Casimir interaction can have significant manifestations in other broad classes of problems. It is found that under certain conditions the Casimir effect is important in helium films [47, 48, 49], quantum fluids [50, 51, 52, 53, 54, 55], graphene [56, 57], optical systems [58, 59, 60]), high energy physics and cosmology [61, 62, 63, 64, 65, 66].

Due to the development of nanoscale devices, the Casimir effect became important not only from a point of fundamental science, but for applications as well, as it was argued for the first time in [67]. Applications of the Casimir effect were proposed for advanced nanomechanical devices, such as microelectromechanical systems in the production of sensors and actuators. As it was shown in [68], the Casimir effect indeed influences

devices containing a micromachined cantilever beam with a size of a few μm. The cantilever is placed above a substrate and moves in response to applied voltages on the substrate, or in response to incoming radio-frequency signals [69]. The Casimir forces make the cantiliver move as well, which must be taken into account for the correct interpretation of the resulting cantilever movement and optimizing of the devices' performance. This principle was used for an actuator based on the Casimir force developed at Bell labs [70].

1.2.3 Casimir effect in condensed matter physics

In condenced matter physics, a broken continuous symmetry in media generates Goldstone modes, so the media can exhibit long-range interactions [71]. The quantum fluctuations of the Goldstone modes are crucial in a number of the condensed matter systems, for instance, they are present in superfluids [72], e.g. superfluid ^4He [73] and superfluid systems of bosonic or fermionic cold atoms. Another example is liquid crystals [74], their existence is possible due to these fluctuations. In both cases, the arising Goldstone modes are phonons. The long-range interactions appear when perturbing objects or impurities are introduced into a medium with long-range fluctuations. Bosons corresponding to the given Goldstone mode scatter on the perturbing objects creating effective interaction between them.

In this thesis I concentrate on the phonon-induced Casimir effect in condensed matter physics. Recently substantial interest in the Casimir effect in one-dimensional systems has appeared due to new opportunities for experimental realizations as a result of the significant progress in the ex-

perimental techniques in cold atoms [75, 76, 77, 78, 79, 80, 81]. Several set-ups were proposed for studying the Casimir interaction in cold atoms. [82, 83, 84, 85, 86, 87, 88, 89]. Among them is the Luttinger liquid in 1D atomic gases, in which phonons may mediate the Casimir interaction between the impurity atoms.

It was shown by Recati et al. [50] that the phonon-mediated Casimir attraction between two static impurities can be observed experimentally in a Luttinger liquid, in the setup of Moritz et at. [76]. In this experiment, an atomic 1D gas of fermions in two hyperfine states was created by use of a two-dimensional optical lattice. The two internal states play a role of spin$-1/2$ states. It was proposed to introduce in this gas atomic quantum dots (AQD) as impurities (AQD's coupled to quantum liquid were studied in [90, 91, 92]). AQD consists of a single atom confined in a tight trap created either magnetically or optically, this confining potential is assumed to be adjusted so that it does not affect the atoms of the bath. The impurity atom, which is trapped in a certain internal state $|a\rangle$, interacts with the atoms of the bath through $s-$wave collisions. In the case where two such AQD's are embedded in the bath and both impurity atoms are in state $|a\rangle$, the system precisely realizes the situation of two localized impurities interacting via a 1D quantum liquid. The scheme of the proposed experiment is given in Fig. 1.2. A possible way to detect the interaction energy $U_{Cas}(r)$ is to do spectroscopy of a single trapped atom as a function of the distance r to a neighboring trapped atom. In addition to the mean-field line shifts modifying the internal levels of the impurity atom, the Casimir interaction produces a line shift depending on distance as $1/r$. In the experiment of [76] $N \sim 400$ ^{40}K atoms were used.
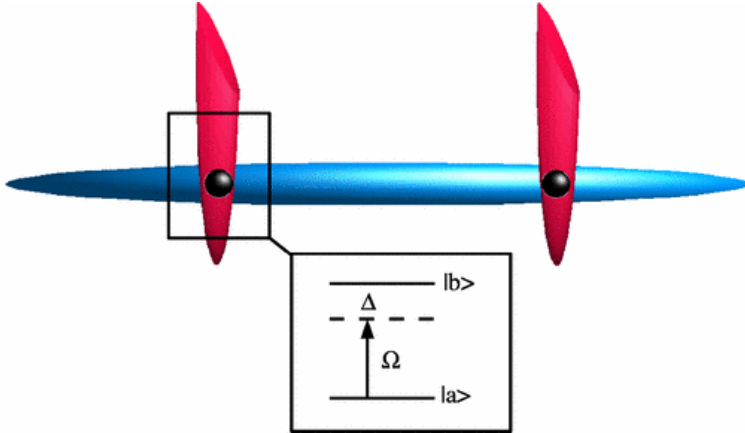
Figure 1.2. Schematic set-up of two AQD's coupled to a 1D atomic reservoir. The impurity atoms in a tightly confining potential interact with the bath when their internal level is $|a\rangle$. Here Δ is the renormalized detuning and Ω is the Rabi frequency coming from a laser-induced coupling. The figure is reprinted with permission from[50]. Copyright 2005 by the American Physical Society.

They form an atomic wire of length $L \sim 10\mu m$, the inter-particle distance is estimated as $0.1\mu m$, the speed of sound $c \sim 4cm/s$, temperature corrections are neglected, since $T \sim 50nK$ is smaller than other energy scales of the systems. Recati et al. estimated the Casimir energy (and the related shift between two levels) for two AQD's separated by the inter-impurity distance $r \sim 1\mu m$ for this system as $E_{Cas}(r) \sim 1kHz$, which is in an experimentally accessible range.

The authors of [51] estimated applicability of the considered model for experimentally realized Luttinger liquid, using a set-up provided in [79], a 1D system of ^{87}Rb atoms with ^{40}K impurities (Fig. 1.3). With density of the system $n \simeq 7(\mu m)^{-1}$ and a speed of sound $c \simeq 1cm/s$, $T \simeq 300nK$, the magnitude of the potential at the closest applicable separation $r = 1/n \simeq 0.14\mu m$ is $U_{Cas}(r) \simeq 1kHz$, while for $r = 5L_T \simeq 0.39\mu m$
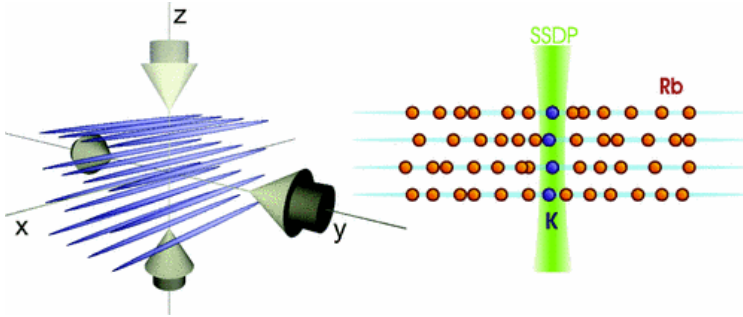
Figure 1.3. Ultracold Rb atoms with K impurities are loaded into an array of 1D systems, "tubes" (left). The species selective dipole potential (SSDP) light blade [93] spatially localizes the impurities into the center of the Rb tubes. The figure is reprinted with permission from [79]. Copyright 2012 by the American Physical Society.

$(L_T = \frac{2\pi c}{T})$ one finds $U_{Cas}(5L_T) \simeq 1Hz$, indicating 3 orders of magnitude variation over a $\simeq 0.25\mu m$ range of separations. The magnitude of the effect $\sim 1kHz$ is thus within an experimentally accessible range, with the scale of applicable separations increasing as one goes deeper into the quantum degenerate regime, $T \ll mc^2$.

1.3   Outline of the chapters

Bellow I briefly highlight the main results presented in the thesis.

1.3.1   Chapter 2

In this chapter we consider how the Casimir interaction is generated between the impurities due to changes in the spectrum of phonons of the lattice induced by these impurities. We use the exact diagonalization method for this study. We analyze two different types of impurities that perturb the kinetic and potential terms of the Hamiltonian correspond-

ingly. The first one corresponds to heavy or light impurities in atomic chains with periodic boundary conditions, the second one - an external potential applied to two given sites of the lattice. We show that these two different mechanisms for the phonon-induced Casimir interaction lead to different spacial laws.

1.3.2 Chapter 3

We find the Casimir interaction in the one-dimensional atomic chain with impurities from Chapter 2 using the perturbation theory approach. We expand obtained solution on a continuum case and, after a short introduction to Luttinger liquids, discuss the mapping of a Luttinger liquid with impurities to our continuum model. The main result of this chapter is the exact solution of the considered model. We consider two types of impurities introduced in the previous chapter and show that their asymptotical spacial dependence differs and exhibits two universal power laws. At shorter distances the spacial behavior of the Casimir interaction is non-universal. The characteristic scaling for the universal spacial laws is defined by the relation between masses of the impurities and particles of the medium. The temperature corrections for the effects are found for the cases of low and high temperatures.

1.3.3 Chapter 4

In this chapter, we generalize the results obtained in the previous chapter in the framework of the T-matrix approach. It allows us to connect the experimentally measurable single-particle scattering amplitude with the Casimir interaction. Our consideration applies to the cases of dynamical

and static impurities discussed in previous chapters. This approach is especially important for the external potential case, since the problem is non-perturbative. The corresponding Casimir interactions are found in dimensions $D = 1..3$. In addition, we consider the Casimir interaction at finite temperatures and show that at finite temperatures the Casimir interaction becomes exponential at large distances with two characteristic distances defining scaling crossovers in the system.

1.3.4 Chapter 5

We move from the Casimir interaction and discuss another effect involving the Goldstone mode properties. We study analytically and numerically how an itinerant hole propagates in a two-dimensional ferromagnetic system with spin-flip processes. This spin-flip processes create virtual magnons that strongly couple to the hole changing its properties. Applying an external magnetic field to the ferromagnet, one can achieve the regime where the quasiparticle description of the system is no longer valid. We demonstrate that the van der Waals crystals with antiferromagnetic interlayer and ferromagnetic intralayer alignments can realize the proposed mechanism of the spin-flip hopping.

Chapter 2

Origin of the phonon-mediated Casimir interaction

2.1 Lattice model for phonon-mediated Casimir interaction

In this chapter, we show that the Casimir effect between impurities mediated by phonons is different to the one mediated by photons. The crucial difference comes from the fact that in the system considered originally by Casimir the plates imposing boundary conditions are static. In contract, the impurities on a lattice (or in a medium) move coherently with atoms

of the lattice. The dynamic nature of the impurities reflects itself in the power law of the Casimir interaction.

We start from the most simple physical system where excitations are described by phonons - a harmonical oscillator, which describes atoms in an ideal lattice, and study how perturbation of the phonon's spectrum created by two separated impurities generates the Casimir interaction between them. The calculation of the Casimir interaction will be done numerically by means of the exact diagonalization method. We examine the properties of the system for different relative positions of the impurities.

We analyze an ideal harmonic cubic lattice, described by the Hamiltonian

$$H_0 = \sum_i \frac{p_i^2}{2m} + \frac{m\omega_0^2}{2} \sum_{<i,j>} (u_i - u_j)^2, \tag{2.1}$$

with two embedded impurity atoms, which have their mass different from the mass of the atoms of the lattice. In Eq.(2.1) p_i and u_i are the momentum and coordinate operators, m is the mass of the atoms of the cubic lattice and $m\omega_0^2$ is the harmonic potential of the lattice. Introduction of the impurity atoms creates an additional term V in the full Hamiltonian of the system $H = H_0 + V$. The structure of this term depends on the considered problems and is discussed in next sections. We consider only the longitudinal mode here and below. The extension to the transverse modes is trivial and leads to D factor, which we neglect for simplicity.

We express Eq.(2.1) in terms of bosonic operators $b_{\mathbf{k}}$, $b_{\mathbf{k}}^\dagger$. Quantized operators p_i and u_i read as $p_i = -i\sqrt{\frac{m\omega_0}{2}} \int \frac{d\mathbf{k}}{(2\pi)^D} e^{i\mathbf{r_i k}} \left(b_{\mathbf{k}}^\dagger - b_{\mathbf{k}} \right)$ and $u_i =$

$\sqrt{\frac{1}{2m\omega_0}} \int \frac{d\mathbf{k}}{2\pi)^D} e^{i\mathbf{r_i k}} \left(b_{\mathbf{k}}^\dagger + b_{\mathbf{k}} \right)$, where D is dimensionality, we obtain H_0 as

$$H_0 = \sum_{\mathbf{k}} \omega_{\mathbf{k}} \left(b_{\mathbf{k}}^\dagger b_{\mathbf{k}} + \frac{1}{2} \right) \tag{2.2}$$

with the phonon spectrum: $\omega_{\mathbf{k}} = \omega_0 \sqrt{Z(1 - \gamma_{\mathbf{k}})}$. Here $\gamma_{\mathbf{k}} = \frac{1}{Z} \sum_{\delta} e^{i\mathbf{k}\delta}$ with summation over the nearest neighbours and Z is the number of the nearest neighbors. In one-dimensional case it reduces to: $\omega_k = 2\omega_0 |\sin(k\delta/2)|$, where δ is the lattice constant. In the low energy limit $\omega_k = c|k|$ with the phonon's speed (speed of sound) $c = \omega_0 \delta$. Further for simplicity we put $\delta = 1$.

2.2 Exact diagonalization

2.2.1 Two impurity atoms with different masses

At first, we consider two impurity atoms with masses M located at sites a and b. The resulting Hamiltonian of the system is $H = H_0 + V$ with the perturbation term of the kinetic energy:

$$V = -\frac{g}{2m}(p_a^2 + p_b^2) \tag{2.3}$$

where the effective coupling constant $g = (1 - m/M)$.

The Hamiltonian with two embedded impurity of the masses M can not be reduced to the Hamiltonian of free phonons. However, one can find the Casimir interaction, i.e the dependence of the total energy of zero point motion $E = \frac{1}{2} \sum_{ka} \tilde{\omega}_k$ of the all atoms of the lattice on the distance between the impurity atoms.

We employ the exact diagonalization method by considering atomic chains with periodic boundary conditions of various sizes with two impurities put at some fixed positions a and b. The energy of the system is a function of distance between the impurities $U(r_a - r_b)$. The detailed explanation of the employed method is given in Section 2.4.

The result of the exact diagonalization for a 200 atoms chain for various masses of impurity atoms is shown in Fig. 2.1. The Casimir interaction $U(r)$ between finite mass impurities does not follow $U(r) \sim 1/r^3$ in the whole range of distances. Rather the interaction is non-universal. One can note that the normalized Casimir interaction for heavy impurities $(M > m)$ scales in the range $1/r^3 < U < 1/r$, and for light impurities $(M < m)$ it is $U < 1/r^3$. For impurity masses close to m, the Casimir interaction tends to $1/r^3$ law and in the limit $M \to \infty$ (infinitely heavy impurities) one observes the $1/r$ law. Impurity with large but finite masses demonstrate behavior close to $1/r$ at short distances with the crossover to the $1/r^3$ law at large distances. The scale of these crossover depends on the M/m relation.

2.2.2 External potential

Now we consider a lattice with periodic boundary conditions where two atoms are placed in an external harmonic potential which is defined by the following Hamiltonian:

$$V = gm\omega_0^2(u_a^2 + u_b^2), \tag{2.4}$$
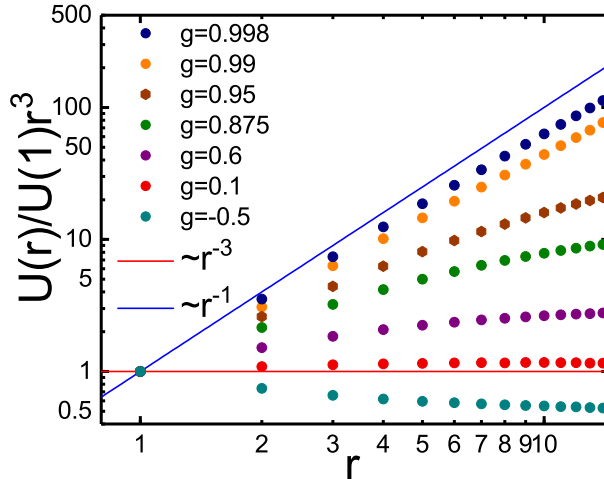
Figure 2.1. Normalized by $U(1)r^3$ Casimir interaction $U(r)$ calculated for a chain of 200 atoms with two impurity atoms with various masses (to check the finite size effects we examined various sizes of the chain, up to a 800 atoms chain, and found no difference at such distances): Red dots - $g = 0.1$ ($M/m = 1.1$), purple - $g = 0.6$ ($M/m = 2.5$), green - $g = 0.875$ ($M/m = 8$), brown - $g = 0.95$ ($M/m = 20$), orange - $g = 0.99$ ($M/m = 100$), blue - $g = 0.998$ ($M/m = 500$), turquoise - $g = -0.5$ ($M/m = 0.5$). The red line shows $1/r^3$ law, the blue line - $1/r$.

with the interaction constant $g \geq 0$.

This term is quantized in terms of the phonon operators and the whole system is diagonalized in the same fashion as in the previous case (see Section 2.4).

The spacial dependence of the resulting energy is non-universal as well. It behaves as $U(r) < \frac{1}{r}$, as it is shown in Fig.2.2. The Casimir interaction in this case demonstrated the non-universal spacial behavior at short distances a falls off slower than for the impurities considered in Section.2.2.1,

reaching the $1/r$ at large distance. In the limit of infinitely strong confining potential $g \to \infty$, the interaction becomes universal and falls off exactly as $\sim \frac{1}{r}$, as the boundary conditions imposed by the impurities in this case are identical to the ones created by metallic plates in vacuum for photons in the original paper of Casimir.
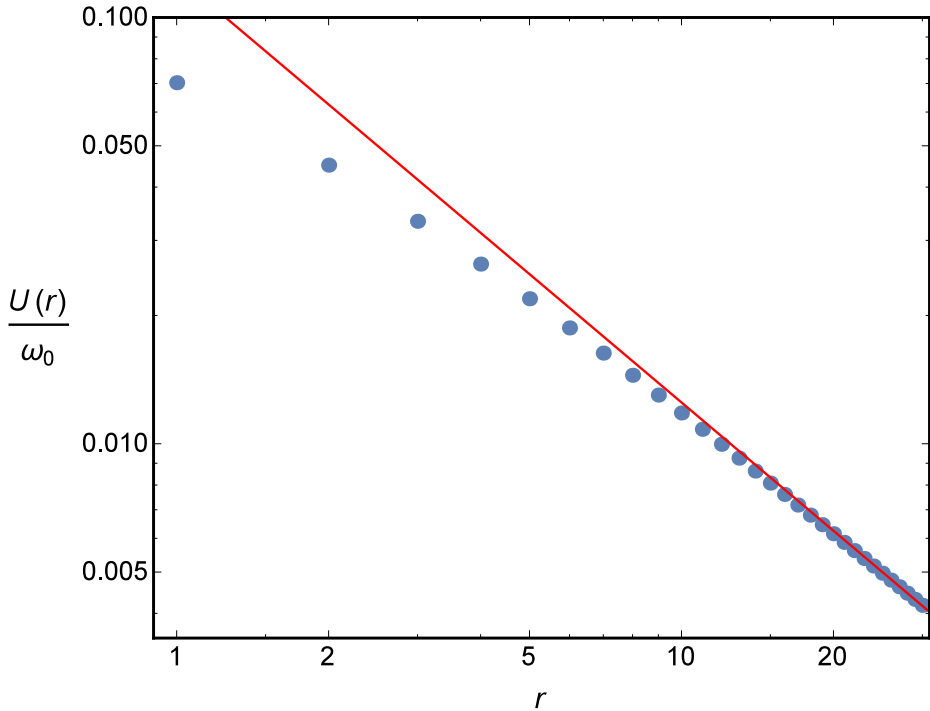
Figure 2.2. Casimir interaction $U(r)$ calculated for a chain of 200 atoms with an external potential applied to two sites separated by the distance r. The potential strength from Eq.(2.4) is chosen as $g = 0.5$

2.2.3 Multidimensional lattice

The exact diagonalization procedure discussed in this chapter can be directly applied to harmonic lattices in dimensions $D > 1$. Due to the re-

source consumption, the computed cluster sizes are considerably smaller. We considered here the case of heavy impurities in a $20x20$ square (2D) or a cubic $8x8x8$ (3D) lattice. The behavior of the Casimir interaction between them demonstrates the same features in these dimensions as in $1D$ - its behaviour is non-universal, but at sufficiently large distances its asymptotic behavior is $\sim \frac{1}{r^{2D+1}}$, as illustrated in Fig.2.3. With increase of dimensionality, this spacial law is reached much faster than in $1D$. The characteristic distance where the crossover between different scalings happens, as well as the spacial behavior in the $M \to \infty$ limit will be discussed further in this thesis during the analytical study of the Casimir interaction in dimensions $D > 1$.

(a) **(b)**
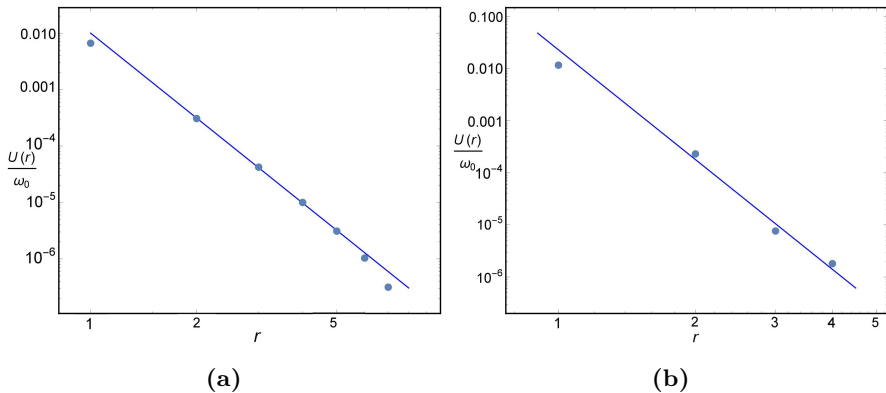
Figure 2.3. Exact diagonalization of the Casimir interaction between heavy impurities $(M/m = 2)$ in higher dimensions in a cubic lattice, $\tilde{\omega} = \frac{\omega}{\omega_0}$ **(a)** $D = 2$, $20x20$ lattice, blue line $\sim 1/r^5$ **(b)** $D = 3$, $8x8x8$ lattice, blue line $\sim 1/r^7$

2.3 Physical origin of the Casimir interaction between impurities on a lattice

Now we show where the principal difference between the two considered cases comes from. Dispersion of phonons of the lattice is given in Fig.2.4. Fig.2.4a illustrates an ideal lattice composed of 12 identical atoms with periodical boundary conditions. Now let us add a small perturbation to the lattice. Depending on which term from Eq.(2.1) we perturb, we get drastically different results. If we perturb the kinetic term, as is the case in the Section 2.2.1, a small perturbation leads to considerable change of the phonon dispersion at high energy, but without serious influence on the lowest ones (Fig.2.4b). While perturbing the potential term, as it is done in Section 2.2.2, we see that the lowest mode instantly becomes gapped (Fig.2.4c), so the linear gapless spectrum is no longer here. These two cases converge only in the limiting case then the bands become completely flat (which corresponds to infinite mass of the impurities or infinite confining potential).

In this chapter, we have analyzed numerically the evolution of the phonon induced Casimir interaction between two impurity atoms embedded in an ideal lattice. This interaction at small distances differs from the power law $1/r^{(2D+1)}$ realized at large separations between the impurities. For static impurities the interaction tends to the $1/r$ law. The reasons for such behavior and crossover between them is demonstrated in next chapters.
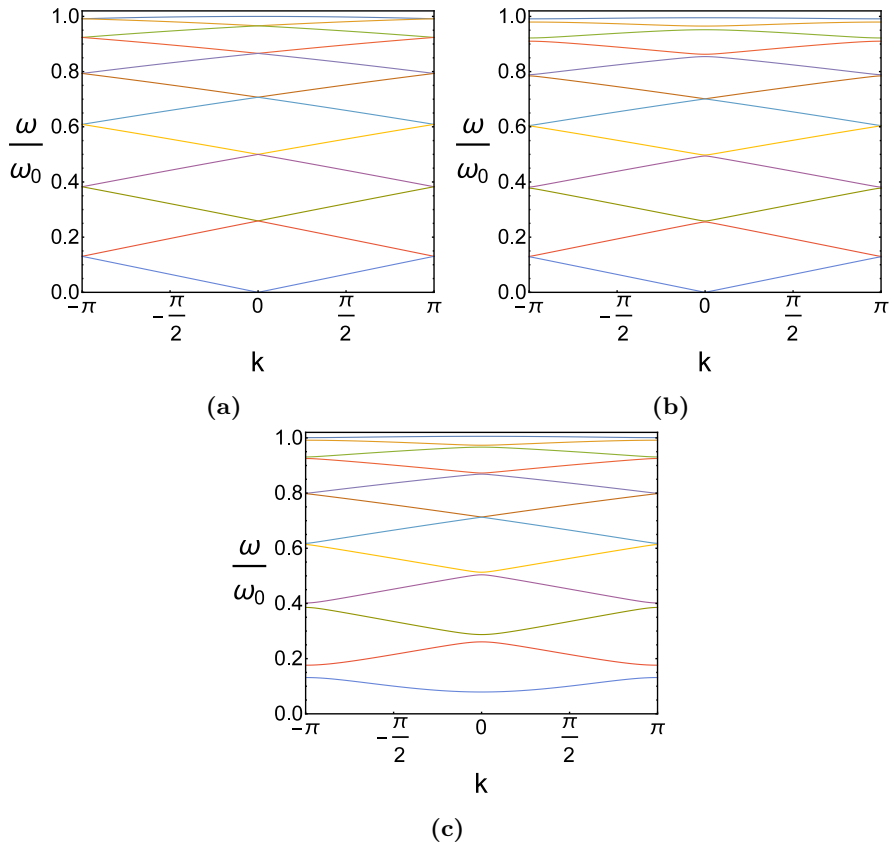
Figure 2.4. Phonon dispersion for a chain of 12 atoms with periodic boundary conditions. **(a)** An ideal lattice withut impurities. **(b)** A lattice with two heavy impurities $M = 1.1m$. **(c)** a lattice with external potential applied to two sites, $g = 1.1$

2.4 Appendix: Exact diagonalization method

Here we describe the technical details of the exact diagonalization method with respect to our model.

We start from the harmonical oscillator Hamiltonian which includes impurities. Let us consider an ideal lattice with two impurities at sites a and

b of masses $M \neq m$.

$$H = \sum_i \frac{\mathbf{p}_i^2}{2m_i} + \sum_{<i,j>} \frac{m\omega_0^2}{2}(\mathbf{u}_i - \mathbf{u}_j)^2,$$

where

$$m_i = \begin{cases} m, & \text{if } i \neq a, b \\ M, & \text{if } i = a, b. \end{cases}$$

The sum is taken over all positions, so m_i is either m or M. We stay in r-space, so this Hamiltonian is represented through the second quantization operators of the real space

$$p_i = -i\sqrt{\frac{m\omega_0}{2}}(b_i^\dagger - b_i),$$

$$u_i = \sqrt{\frac{1}{2m\omega_0}}(b_i^\dagger + b_i).$$

This leads us to the expression

$$
\begin{aligned}
H &= \frac{1}{2}\omega_0 \sum_{i=1}^{N} \left[-\frac{m}{m_i}\frac{(b_i^\dagger - b_i)^2}{2} + (b_i^\dagger + b_i)^2 \right. \\
&\quad - \left. (b_{i-1}^\dagger + b_{i-1})(b_i^\dagger + b_i) - (b_i^\dagger + b_i)(b_{i+1}^\dagger + b_{i+1}) \right].
\end{aligned}
\tag{2.5}
$$

N is the number of atoms in the considered chain, ω_0 is the characteristic energy of phonons. This energy depends on a particular system under consideration. In a system of solid hydrogen with deuterium impurities, which is naturally well suited for testing the Casimir forces discussed in this thesis due to high Debye frequency of phonons and relatively large mass ratio of hydrogen and deuterium, this energy is $\omega_0 \sim 10 meV$ [94].

And for hydrates, e.g. H_3S compound, this value can be as high as $\omega_0 \sim 100 meV$ [95].

We apply the Fourier transform to this Hamiltonian and diagonalize it numerically. It means that we have to diagonalize the following matrix for all possible values of k

$$
\begin{pmatrix}
\frac{m}{2M}+D & -\frac{m}{2M}+D & 1 & 1 & 0 & 0 & \cdots & \cdots & e^{ik} & e^{ik} \\
\frac{m}{2M}-D & -\frac{m}{2M}-D & -1 & -1 & 0 & 0 & \cdots & \cdots & -e^{ik} & -e^{ik} \\
1 & 1 & \frac{1}{2}+D & -\frac{1}{2}+D & 1 & 1 & 0 & \cdots & 0 & 0 \\
-1 & -1 & \frac{1}{2}-D & -\frac{1}{2}-D & -1 & -1 & 0 & \cdots & 0 & 0 \\
0 & 0 & 1 & 1 & \frac{m}{2M}+D & -\frac{m}{2M}+D & 1 & 1 & 0 & \cdots \\
0 & 0 & -1 & -1 & \frac{m}{2M}-D & -\frac{m}{2M}-D & -1 & -1 & 0 & \cdots \\
\cdots & \cdots & \cdots & \cdots & \cdots & \cdots & \cdots & \cdots & \cdots & \cdots \\
e^{-ik} & e^{-ik} & 0 & 0 & \cdots & \cdots & 1 & 1 & \frac{1}{2}+D & -\frac{1}{2}+D \\
-e^{-ik} & -e^{-ik} & 0 & 0 & \cdots & \cdots & -1 & -1 & \frac{1}{2}-D & -\frac{1}{2}-D
\end{pmatrix}.
$$

Here D is dimensionality of the problem (the consideration is correct for a cubic lattice). In this example, impurities are located at $a = 1, b = 3$. Even lines of the matrix are taken with the " - " sign to satisfy the bosonic commutation rules.

The diagonalization leads to the Hamiltonian of a diagonal form (α_k is some operator which diagonalizes the Hamiltonian, ω_k' is the energy corresponding to eigenstates of this operator):

$$
\hat{H} = \sum_k \omega_k' \left(\alpha_k^\dagger \alpha_k + \frac{1}{2} \right).
$$

Integration over k gives us energy $\tilde{U}(r_a - r_b) = U_{Cas}(r_a - r_b) + U_\infty$, which is a sum of the Casimir interaction energy and some constant part coming from renormalization of the phonons spectra. By consideration of various

r_a and r_b, the U_∞-term is eliminated, so we get the Casimir interaction energy $U_{Cas}(r_a - r_b)$.

In the case of applied potential, the approach is identical with the only difference that the matrix for diagonalization is now

$$
\begin{pmatrix}
\frac{1}{2}+gD & -\frac{1}{2}+gD & 1 & 1 & 0 & 0 & \cdots & \cdots & e^{ik} & e^{ik} \\
\frac{1}{2}-gD & -\frac{1}{2}-gD & -1 & -1 & 0 & 0 & \cdots & \cdots & -e^{ik} & -e^{ik} \\
1 & 1 & \frac{1}{2}+D & -\frac{1}{2}+D & 1 & 1 & 0 & \cdots & 0 & 0 \\
-1 & -1 & \frac{1}{2}-D & -\frac{1}{2}-D & -1 & -1 & 0 & \cdots & 0 & 0 \\
0 & 0 & 1 & 1 & \frac{1}{2}+gD & -\frac{1}{2}+gD & 1 & 1 & 0 & \cdots \\
0 & 0 & -1 & -1 & \frac{1}{2}-gD & -\frac{1}{2}-gD & -1 & -1 & 0 & \cdots \\
\cdots & \cdots & \cdots & \cdots & \cdots & \cdots & \cdots & \cdots & \cdots & \cdots \\
e^{-ik} & e^{-ik} & 0 & 0 & \cdots & \cdots & 1 & 1 & \frac{1}{2}+D & -\frac{1}{2}+D \\
-e^{-ik} & -e^{-ik} & 0 & 0 & \cdots & \cdots & -1 & -1 & \frac{1}{2}-D & -\frac{1}{2}-D
\end{pmatrix}.
$$

Chapter 3

Exact solution for the phonon-mediated Casimir effect in 1D

3.1 Introduction

In this chapter we consider the phonon-mediated Casimir interaction in one dimension. Using the diagrammatic technique, we evaluate this interaction analytically. The series of the diagrams contributing to this interaction can be summed up, so we obtain the exact solution of the model. Phonons of the system couple to separated impurities. This coupling leads to an effective exchange of the virtual phonons between impurities that it

turn creates an attractive force between them. We consider the solution both for a lattice and continuum models. The latter situation has a direct relation to the Casimir effect arising between impurities in Luttinger liquids. It is worth to discuss the phonon-impurity coupling in the Luttinger liquid in greater details to see how the Casimir interaction arises there, which is done in next sections. After that, we move directly to consideration of our model and its relation to experimentally achievable systems.

3.2 Phonon-mediated Casimir effect in one-dimensional quantum liquids

3.2.1 Littinger liquid

The Tomonaga-Luttinger model, formulated initially by Tomonaga [96] and Luttinger [97] for one-dimensional spinless fermions, has been explicitly solved by Mattis and Lieb [98]. This model was generalized for the so-called Luttinger liquids by Haldane [99]. The excitations in the model can be represented as non-interacting bosons (namely, phonons). As argued by Haldane, the Luttinger liquid description is valid for conducting spinless fermion systems in one dimension as the effective low energy model, it also can be generalized to spin$-\frac{1}{2}$ fermions. Since then, the realization of the Luttinger liquids and their bosonic analogues (the Luttinger liquid model can be applied as an effective low-energy theory of one-dimensional bosons) in cold atoms have been extensively discussed [85, 86, 87, 88, 89].

Haldane developed the Luttinger liquid approach to one-dimensional interacting systems in [99, 100] for both fermionic and bosonic systems. The general form of the Hamiltonian employed for the description of this system is

$$H = \frac{1}{2m} \int dx |\nabla \psi(x)|^2 + \frac{1}{2} \int dx dy \rho(x) V(x-y) \rho(y). \qquad (3.1)$$

The operator $\psi(x)$ can obey either Fermi or Bose statistics. For now, we choose a system of fermions. This system can be bosonized in multiple ways (see [101] for a review). Details of this procedure are given in Section 3.6.1.

Using the so-called phenomenological bosonization [100, 102], one can rewrite the Luttunger liquid Hamiltonian in the following form [102]

$$H_{LL} = \frac{c}{2\pi} \int dx \left[K \left(\nabla \theta(x) \right)^2 + \frac{1}{K} \left(\nabla \phi(x) \right)^2 \right]. \qquad (3.2)$$

Fields $\theta(x)$ and $\phi(x)$ describe the phase and the density of the wave-function $\psi(x)$ corresponding to operators from Eq.(3.1), $\psi(x) \simeq |\rho_0 + \frac{\nabla \phi(x)}{\pi}|^{\frac{1}{2}} e^{i\theta(x)}$ (see Section 3.6.1 for details). K is the Luttinger liquid parameter, $K < 1$ for repulsive fermions or attractive bosons, $K > 1$ for attractive fermions or repulsive bosons, $K = 1$ for non-interacting fermions and $K \to \infty$ for non-interacting bosons. In the approach of the phenomenological bosonization, this Hamiltonian is obtained by substituting the fields $\psi_F(x)$ or $\psi_B(x)$ into Eq.(3.1) and retaining only the leading orders of $\theta(x)$ and $\phi(x)$ (fluctuations over the ground state are assumed to be small).

Let us perform this procedure for bosonic fields. Choosing the interac-

tion between bosonic particles as $V(x - y) = \frac{c}{m}\delta(x - y)$, we come to the Lieb-Liniger model [103]. The Hamiltonian for this model reads [104]

$$H = \frac{1}{2m} \int dx \left[\left(\rho_0 + \frac{\nabla\phi(x)}{\pi} \right) (\nabla\theta(x))^2 + \frac{(\nabla^2\phi(x))^2}{4\rho_0} \right] + \frac{c}{2m} \int dx \, (\nabla\phi(x))^2 .$$

Retaining the operators of scaling dimension two, we come at low energies to the Luttinger liquid Hamiltonian Eq.(3.2).

3.2.2 Mapping between a Luttinger liquid and a harmonical oscillator

The Luttinger liquid Hamiltonian Eq. (3.2) can be rewritten in the form identical to the Hamiltonian of the harmonical oscillator [102]. Expressing the operators $\theta(x)$ and $\phi(x)$ explicitly via phonon operators b, $b^\dagger$ as

$$\partial_x\theta(x) \;=\; -i\sum_q \sqrt{\frac{\pi K|q|}{2L}}\,\mathrm{sgn}(q)\left(b_q + b_{-q}^\dagger\right)e^{-iqx}, \qquad (3.3)$$

$$\partial_x\phi(x) \;=\; i\sum_q \sqrt{\frac{\pi|q|}{2KL}}\left(b_q - b_{-q}^\dagger\right)e^{-iqx}, \qquad (3.4)$$

one can rewrite Eq. (3.2) as $H_{LL} = c\sum_q |q| b_q^\dagger b_q$.

Now we move to the Casimir interaction realized between two impurities embedded in the Luttinger liquid. The impurities under consideration are electrically neutral and spinless, separated by distances much larger then their size. The elementary Goldstone excitations in the Luttinger liquids are phonons [102], so the Casimir interaction between impurities in these systems is realized foremost via exchange of virtual phonons. We consider impurities of two different types. The static impurities in the Luttinger

liquid do not posses kinetic energy and perturb the potential term in Eq. (3.2). They correspond to atoms in an applied external potential in the lattice. In contrary, the dynamic impurities can move coherently with the medium, they perturb the kinetic term in Eq. (3.2) and correspond to heavy/light impurities in a lattice. In both cases a bare impurity-phonon coupling is strongly renormalized in the Luttinger liquid at small energies [105, 106, 107], so we take the interaction constant g as a phenomenological phonon scattering amplitude for a single impurity. As we explicitly show in the further, a system with these types of impurities can be described as a harmonical oscillator with perturbed kinetic and potential energy correspondingly.

Static impurities in a Luttinger liquid

If the impurities are located at fixed positions and create perfectly reflecting barriers for phonons, the Casimir interaction between them is completely analogous to the one originally obtained by Casimir [1]. These impurities in one dimension impose the same boundary conditions for phonons as the conducting walls for photons in the original Casimir problem. The only difference in the result is the "$\frac{1}{2}$" coefficient for phonons, since they are scalar particles, while photons are summed over two spin polarizations [108, 109]

$$U_{Cas}(r) = -\frac{\hbar c\pi}{24r}. \tag{3.5}$$

The mechanism of the Casimir interaction in Luttinger liquids between static impurities when the phonon reflection is not perfect was studied in

[54, 50, 53]. The authors of [50], considered a one-dimensional quantum liquid with two static impurities. Each impurity couples to the particles of the liquid with the given coupling strength g. This value is taken phenomenologically as the phonon-impurity scattering amplitude. They found that for a non-interacting Fermi gas ($K = 1$), the Casimir interaction is strongly affected by the Friedel oscillations [110]. This type of oscillations is typical for fermionic systems with impurities (an impurity creates oscillations of density with period π/k_F, the other impurity senses them). Away from the point of non-interacting fermions ($K \ll 1$), these oscillations quickly vanish and the interaction between two impurities becomes smooth. Each impurity in the Luttinger liquid creates a local perturbaton of density, for two impurities it gives us the additional term for the Luttinger liquid Hamiltonian:

$$H_{int} = g \sum_{i=1,2} \psi^\dagger(x)\psi(x)\Big|_{x=x_i}.$$

The sum is taken over two positions of the impurities. We supposed here that the coupling constant g is identical for both impurities. Using the density-phase representation (see Section 3.6.1) and assuming $K \ll 1$, so the stationary phase approximation can be used, one gets the interaction term as

$$H_{int} = \sum_{i=1,2} 4g\rho_0\phi^2(x_i), \tag{3.6}$$

ρ_0 is the average density of the system, the field ϕ is taken from Eq. (3.2) and corresponds to fluctuations of the density. Eq. (3.6) reads in terms

of the phonon operators as

$$H_{int} = 4g\rho_0 \sum_{i=1,2} \sum_{q,q'} \frac{\text{sign}(q)\text{sign}(q')}{\sqrt{|q||q'|}} \left(b_q^\dagger e^{-iqx_i} + b_q e^{iqx_i}\right) \left(b_{q'}^\dagger e^{-iq'x_i} + b_{q'} e^{iq'x_i}\right).$$

As we show further in this chapter, this expression exactly matches the expression for a perturbation of the potential term of the harmonical oscillator. One should note here, that the sign functions in this expression can be omitted as both of them always appear in even powers for all non-vanishing contributions to the interaction given by this Hamiltonian.

Though this term does not contain any direct coupling between impurities, it generates an effective attraction between them due to exchange of virtual phonons, as it will be discussed in details later. This interaction falls off as $\frac{1}{r}$ at large distances.

Dynamic impurities in a Luttinger liquid

Castro Neto and Fisher showed in [107] that the bare coupling between dynamic impurities and phonons in Luttinger liquids is effectively renormalized towards zero. The long-range Casimir force is still present because it comes not from the ultimate low-energy impurity-phonon coupling strength, but rather relies on the participation of an energy band of quantum fluctuations, with width $\hbar c/r$ [51]. This argument is valid for both fermionic and bosonic systems.

It is shown in [51] that the Casimir interaction in this case arises due to a local change of the kinetic energy and even in the limit of very slow impurities ($V/c \to 0$, V is the speed of the impurities, c is the speed of sound), the interaction can not be reduced to the case of static impurities

and scales differently. The interaction term H_{int}, arising in addition to the non-interacting part Eq.(3.2) of the full Hamiltonian, is expressed through gradients of the fields $\theta(x), \phi(x)$. Introducing the chiral basis

$$\chi_+(x) = \frac{\theta}{\sqrt{\pi K}} + \sqrt{\frac{K}{\pi}}\phi(x),$$

$$\chi_-(x) = \frac{\theta}{\sqrt{\pi K}} - \sqrt{\frac{K}{\pi}}\phi(x),$$

and restricting their consideration analysis to the lowest orders of the perturbation theory, Schecter and Kamenev obtained the interaction term responsible for the Casimir force as

$$g\partial_x\chi_+(x)\partial_x\chi_-(x). \tag{3.7}$$

Terms proportional to $(\partial_x\chi_+(x))^2 + (\partial_x\chi_-(x))^2$ are neglected since they do not contribute to the impurity equations of motion because they do not change a relative number of left- and right-moving particles in the Luttinger liquid. The physically relevant processes are those in which this number changes. Therefore, these terms do not affect physically relevant processes [51]. The interaction term Eq.(3.7) contains not fluctuations of density, but rather their derivative, so this term corresponds to a local perturbation on the kinetic energy in Eq. (3.2). In the explicit form, the phonon-impurity interaction Eq. (3.7) is written as

$$gc\sum_{i=1,2}\sum_{q,q'}\sqrt{|q||q'|}\left(b_q^\dagger e^{-iqx_i} - b_q e^{iqx_i}\right)\left(b_{q'}^\dagger e^{-iq'x_i} - b_{q'} e^{iq'x_i}\right).$$

This term describes the perturbed kinetic energy of the harmonical oscil-

lator.

Considering this term in the second order of the perturbation theory, one obtains the Casimir interaction between two dynamic impurities as

$$U(r) = -mc^2 \frac{\Gamma_1 \Gamma_2}{32\pi} \frac{\xi^3}{r^3},$$

where m is the mass of background particles, c is the speed of sound, $\xi = 1/mc$ and the dimensionless parameters $\Gamma_{1,2}$ is impurity-phonon scattering amplitudes.

3.3 Phonon-induced Casimir interaction between impurity atoms in a lattice. Perturbation theory

In the previous chapter, we have discussed the origin of the Casimir interaction between impurities in a lattice. If is found there that neither the $\frac{1}{r^3}$ spatial law for dynamic impurities nor the $\frac{1}{r}$ for static ones are universal, but represent rather asymptotic behavior of the Casimir energy between impurities in the corresponding cases. Now we use the perturbation theory approach to evaluate the Casimir interaction between two impurities. This approach will allow us to see how the change in the phonon spectrum discussed in Chapter 2 is translated to impurity-phonon scattering processes and where the short distance corrections to the interaction come from. The aim of this approach is to see what defines the crossover between two regimes of the Casimir interaction and whether the $\frac{1}{r}$ scaling law is restored for dynamic impurities on the limit of infinitely large im-

purity mass $M \to \infty$, where impurities become static. After explanation of the mechanisms behind the results obtained in the previous chapter for impurities in a lattice, we apply our results to impurities in continuum medium, i.e. to the Luttinger liquids discussed above.

Casimir interaction in the second order of perturbation theory

We consider an ideal harmonic cubic lattice with impurities described in Chapter 2 by Eqs.(2.1) and (2.3).

To find the reason of the drastic deviation of the r-dependence of the Casimir interaction from the $1/r^3$-law seen in Fig. 2.1, we employ the perturbation theory. For our calculations, we express Eq. (2.3) via the phonon operators (see Section 3.6.2 for details):

$$V(r) = \sum_{q,q'}(V_{q,q'}^{(1)}(r)b_q^\dagger b_{q'} + V_{q,q'}^{(2)}(r)\frac{b_q b_{q'}}{2} + h.c.). \qquad (3.8)$$

Here the vertices are:

$$V_{q,q'}^{(1)}(r) = -V_{q,q'}^{(0)} \cos\frac{(q-q')r}{2},$$
$$V_{q,q'}^{(2)} = V_{q,q'}^{(0)} \cos\frac{(q+q')r}{2},$$

with $r = r_a - r_b$ (r_a and r_b are positions of the impurities). $V_{q,q'}^{(0)} = g\sqrt{\omega_q}\sqrt{\omega_{q'}}$, where ω_q, $\omega_{q'}$ are free phonon spectra in the lattice $\omega_q = \omega_0\sqrt{2-2\cos q}$, $\omega_0 = c/\delta$ is the relation between the speed of sound c and the interatomic distance δ. We put $\delta = 1$ and choose $r_a + r_b = 0$ for simplicity.

The first order term of the perturbation theory is r-independent and

therefore does not contribute to the Casimir interaction. The lowest contributing order is the second order of the perturbation theory

$$U_{\text{eff}}^{(2)}(r) = -2T \sum_{n,k,q} \frac{|V_{k,k+q}^{(2)}|^2 \omega_k \omega_{k+q}}{(\omega_n^2 + \omega_k^2)(\omega_n^2 + \omega_{k+q}^2)}. \tag{3.9}$$

Here $\omega_n = 2\pi Tn$ is the Matsubara frequency.

At large distances $r \gg 1$ the leading contribution comes from the small momenta. At zero temperature the integration in Eq.(3.9) can be performed analytically for the linearized spectrum $\omega_k = ck$ with use of the substitution $T \sum_n \to \int d\omega_n / 2\pi$. The result is the $1/r^3$-law:

$$U_{\text{eff}}^{(2)}(r) = -\frac{g^2 \omega_0}{32\pi} \frac{1}{r^3}. \tag{3.10}$$

This dependence agrees with that previously found in [51], but disagrees with the results of the exact diagonalization.

Higher orders of perturbation theory

To understand the origin of the deviation from $1/r^3$ law, we explore higher order phonon processes, which correspond to multiple scattering of phonons on the impurities.

- Second order – We now write the second order perturbation term integrated over frequency ω_n in the following form:

$$
\begin{aligned}
U_{eff}^{(2)}(r) &= -\int \frac{dkdq}{(2\pi)^2} \frac{|V_{k,k+q}^{(0)}|^2}{\omega_k + \omega_{k+q}} \cos^2\left(\frac{qr}{2}\right) \\
&= -\int \frac{dkdq}{(2\pi)^2} \frac{g^2 \omega_k \omega_{k+q}}{\omega_k + \omega_{k+q}} \cos^2\left(\frac{qr}{2}\right).
\end{aligned}
$$
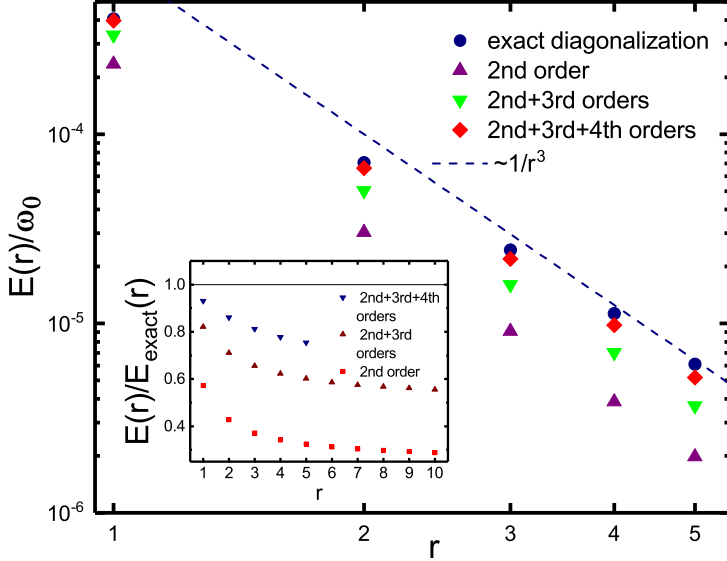
Figure 3.1. Casimir interaction in the perturbation theory: gray dots - second order; brown dots - diagrams up to the third order; red dots - up to the forth order; blue dots - energies obtained by the exact diagonalization. Inset: Contribution of different orders of the perturbation theory to the total result.

- Third order reads:

$$U_{\text{eff}}^{(3)}(r) = -\frac{1}{4}\hbar\omega_0 \int \frac{dq_1 dq_2 dq_3}{(2\pi)^3} \frac{|V_{q_1,q_2}^{(0)} V_{q_2,q_3}^{(0)} V_{q_1,q_3}^{(0)}|}{(\omega_1 + \omega_2)(\omega_2 + \omega_3)}$$
$$*(\cos r(q_1 + q_2) + \cos r(q_2 + q_3) + \cos r(q_1 - q_3)).$$

- Forth order reads

$$
\begin{aligned}
U_{\text{eff}}^{(4,a)}(r) \;=\; & -\frac{1}{8}\hbar\omega_0 \int \frac{dq_1 dq_2 dq_3 dq_4}{(2\pi)^4} \frac{|V_{q_1,q_2}^{(0)} V_{q_3,q_4}^{(0)} V_{q_1,q_3}^{(0)} V_{q_2,q_4}^{(0)}|}{(\omega_{q_1}+\omega_{q_2}+\omega_{q_3}+\omega_{q_4})} \\
\times\; & \frac{1}{(\omega_{q_1}+\omega_{q_2})(\omega_{q_3}+\omega_{q_4})}[\cos r(q_1+q_2) \\
+\; & \cos r(q_3+q_4)+\cos r(q_1+q_3)+\cos r(q_2+q_4) \\
+\; & \cos r(q_1+q_4)+\cos r(q_2+q_3)+\cos r(q_1+q_2+q_3+q_4)],
\end{aligned}
$$

$$
\begin{aligned}
U_{\text{eff}}^{(4,b)}(r) \;=\; & -\frac{1}{8}\hbar\omega_0 \int \frac{dq_1 dq_2 dq_3 dq_4}{(2\pi)^4} \frac{|V_{q_1,q_2}^{(0)} V_{q_1,q_3}^{(0)} V_{q_2,q_4}^{(0)} V_{q_3,q_4}^{(0)}|}{(\omega_{q_1}+\omega_{q_2})(\omega_{q_2}+\omega_{q_3})(\omega_{q_3}+\omega_{q_4})} \\
\times\; & [\cos r(q_1+q_2)+\cos r(q_3+q_4)+\cos r(q_2+q_3) \\
+\; & \cos r(q_1+q_4)+\cos r(q_1-q_3)+\cos r(q_2-q_4) \\
+\; & \cos r(q_1+q_2-q_3-q_4)],
\end{aligned}
$$

$$
\begin{aligned}
U_{\text{eff}}^{(4,c)}(r) \;=\; & -\frac{1}{8}\hbar\omega_0 \int \frac{dq_1 dq_2 dq_3 dq_4}{(2\pi)^4} \frac{|V_{q_1,q_2}^{(0)} V_{q_2,q_3}^{(0)} V_{q_3,q_4}^{(0)} V_{q_1,q_4}^{(0)}|}{(\omega_{q_1}+\omega_{q_2})(\omega_{q_1}+\omega_{q_3})(\omega_{q_1}+\omega_{q_4})} \\
\times\; & [\cos r(q_1+q_2)+\cos r(q_1+q_3)+\cos r(q_1+q_4) \\
+\; & \cos r(q_2-q_3)+\cos r(q_2-q_4)+\cos r(q_3-q_4) \\
+\; & \cos r(q_1+q_2+q_3-q_4)].
\end{aligned}
$$

The result of the perturbation theory up to four-phonon processes for
$g = 0.5$ is presented in Fig.3.1. Here we keep only r-dependent terms. One
immediately notes that the third and fourth orders of the perturbation
theory significantly change the Casimir interaction. Plotting the sum of
all terms up to the fourth order, one can see a good match with the results
of the exact diagonalization.
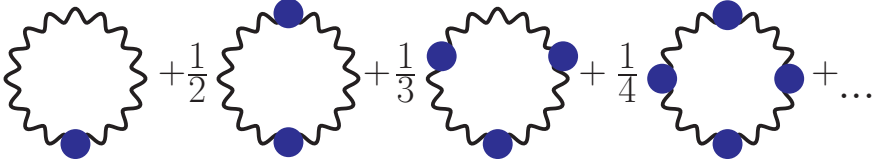
Figure 3.2. The diagrammatic representation of the thermodynamic potential.

One can find exactly the thermodynamic potential in this model. It is given by diagrams shown in Fig.3.2. Following Abrikosov et al. [111], we define the phonon field φ as

$$\varphi(r, t) = \frac{1}{\sqrt{V}} \sum_q \sqrt{\omega_k} \left[b_q e^{iqr - i\omega_q t} + b_q^+ e^{-iqr + i\omega_q t} \right]$$

The phonon Green's function in Matsubara formalism reads:

$$D(q, \omega_n) = \omega_q \left(\frac{1}{i\omega_n + \omega_q} + \frac{1}{-i\omega_n + \omega_q} \right).$$

It's worth to introduce Green's functions in the coordinate space:

$$G_0(\omega_n) - G(r, \omega_n) = \int_{-\pi}^{\pi} \frac{dk}{2\pi} \cos^2\left(\frac{kr}{2} \right) \frac{2\omega_k^2}{\omega_n^2 + \omega_k^2}$$

$$G_0(\omega_n) + G(r, \omega_n) = \int_{-\pi}^{\pi} \frac{dk}{2\pi} \sin^2\left(\frac{kr}{2} \right) \frac{2\omega_k^2}{\omega_n^2 + \omega_k^2}$$

Then the loop of the nth order can be expressed in the compact form:

$$U_{\text{eff}}^{(n)} = -\frac{1}{2} \frac{g^n}{n} \int_{-\infty}^{\infty} \frac{d\omega_n}{2\pi} \left((G_0(\omega_n) + G(r, \omega_n))^n + (G_0(\omega_n) - G(r, \omega_n))^n \right),$$

$$(3.11)$$

where:

$$
\begin{aligned}
G(\omega_n, r) &= \int_{-\pi}^{\pi} \frac{dk}{2\pi} \cos(kr) \frac{\omega_k^2}{\omega_n^2 + \omega_k^2} = \int_{-\pi}^{\pi} \frac{dk}{2\pi} \cos(kr) \frac{4\omega_0^2 \sin^2(\frac{k}{2})}{\omega_n^2 + 4\omega_0^2 \sin^2(\frac{k}{2})} \\
&= \delta_{r,0} - f\left(\frac{\omega_n}{2\omega_0}, r\right) \underset{\frac{\omega_n}{\omega_0} \ll 1}{\simeq} \delta_{r,0} - \frac{|\omega_n|}{2\omega_0} e^{-\frac{|\omega_n|}{\omega_0} r}, \quad (3.12)
\end{aligned}
$$

$$
G_0(\omega_n) = G(0, \omega_n) = \int_{-\pi}^{\pi} \frac{dk}{2\pi} \frac{\omega_k^2}{\omega_n^2 + \omega_k^2} = 1 - f\left(\frac{\omega_n}{2\omega_0}, 0\right) \underset{\frac{\omega_n}{\omega_0} \ll 1}{\simeq} 1 - \frac{|\omega_n|}{2\omega_0},
$$
$$(3.13)$$

$$
f(x, r) = \frac{x}{\sqrt{1+x^2}} (x + \sqrt{1+x^2})^{-2r}. \quad (3.14)
$$

One can note that the Green's function for $r \gg 1$ falls off exponentially $\sim e^{-2r\omega_n/\omega_0}$. It means that the main contribution to the Casimir interaction comes from the low energy acoustic phonons.

The thermodynamic potential at $T = 0$ is

$$
\begin{aligned}
\Phi_{total}(r) &= -\int_0^{\infty} \frac{d\omega_n}{2\pi} \sum_{l=2}^{\infty} \left[\frac{g^l}{l} ((G_0(\omega_n) + G(r, \omega_n))^l \right. \\
&+ \left. \left(G_0(\omega_n) - G(r, \omega_n))^l \right) \right] = \int_0^{\infty} \frac{d\omega_n}{2\pi} \left[\ln\left(1 - \frac{g^2 G^2(r, \omega_n)}{(1 - gG_0(\omega_n))^2} \right) \right. \\
&+ \left. 2\ln\left(1 - gG_0(\omega_n) \right) + 2gG_0(\omega_n) \right].
\end{aligned}
$$

The obtained thermodynamic potential $\Phi(r)$ contains an r-independent term, which is related to perturbation of the zero point motion by uncorrelated impurity atoms ($r \to \infty$). The effective Casimir energy goes to 0 when $r \to \infty$ and should not contain a constant part. Defining

$U_{\text{eff}}(r) = \Phi(r) - \Phi(\infty)$ we arrive to the following expression:

$$
\begin{aligned}
U_{eff}(r) &= \Phi_{total}(r) - \Phi_{total}(\infty) = \int_0^\infty \frac{d\omega_n}{2\pi} \left[\ln \left(1 - \frac{g^2 G^2(r, \omega_n)}{(1 - g G_0(\omega_n))^2} \right) \right] \\
&= \int_0^\infty \frac{d\omega_n}{2\pi} \ln \left[1 - \frac{\left(\frac{g\omega_n}{2c} e^{-\frac{\omega_n}{c} r} \right)^2}{(1 - g + \frac{g\omega_n}{2c})^2} \right].
\end{aligned}
$$

(3.15)

$$
U_{\text{eff}}(r) = \frac{1}{2} T \sum_n \ln \left[1 - \left(\frac{g G(\omega_n, r)}{1 - g G_0(\omega_n)} \right)^2 \right],
$$

(3.16)

where $G(\omega_n, r)$ are the phonon Green's functions in the coordinate space. Let us discuss this derivation in more details.

3.4 Results in continuum limit

3.4.1 Casimir interaction

The low energy Hamiltonian can be obtained from Eqs.(2.2, 3.8) by linearization of the spectrum for small momenta $\omega_k = c|k|$. The corresponding Hamiltonian is

$$
\begin{aligned}
H &= \sum_k c|k| b_k^\dagger b_k \\
&+ gc \sum_{k,k'} \sqrt{|k||k'|} \cos \left[\frac{(k + k')r}{2} \right] \left(b_k^\dagger b_{k'} + \frac{b_k b_{k'} + b_k^\dagger b_{k'}^\dagger}{2} \right).
\end{aligned}
$$

(3.17)

This expression is similar to that used in [51]. To calculate the thermodynamic potential in the continuum limit we use the results of the previous

section, changing the limits of the integration from the Brillouin zone to infinity. Note, that the integral in Eq.(3.13) becomes formally divergent and has to be renormalized. For this we use the mapping to the lattice model of the previous section (this procedure is discussed in next chapter). The Green's functions in the continuum limit can be obtained as

$$
\begin{aligned}
G(r, \omega_n) &\simeq \int_{-\infty}^{\infty} \frac{dk}{2\pi} \cos kr \frac{k^2}{(\frac{\omega_n}{c})^2 + k^2} = -\frac{|\omega_n|}{2c} e^{-\frac{|\omega_n|}{c} r} \\
G_0(\omega_n) &= 1 - \int_{-\pi}^{\pi} \frac{dk}{2\pi} \frac{4\omega_0^2 \sin^2 \frac{k}{2}}{(\frac{\omega_n}{c})^2 + 4\omega_0^2 \sin^2 \frac{k}{2}} \\
&\simeq 1 - \int_{-\infty}^{\infty} \frac{dk}{2\pi} \frac{(\frac{\omega_n}{c})^2}{(\frac{\omega_n}{c})^2 + k^2} = 1 - \frac{|\omega_n|}{2c}
\end{aligned}
$$

In the second order of the perturbation theory we restore the results of [51]:

$$
U_{\text{eff}}^{(2)}(r) = -\frac{g^2}{2} \int_{-\infty}^{\infty} \frac{d\omega}{(2\pi)} \frac{\omega^2 e^{-2\frac{|\omega| r}{c}}}{4\omega_0^2} = -\frac{g^2 \omega_0}{32\pi r^3}.
$$

In this approach, at $T = 0$ the Casimir interaction reads:

$$
U_{\text{eff}}(r) = \int_0^{\infty} \frac{d\omega_n}{2\pi} \ln \left[1 - \left(\frac{\frac{g\omega_n}{2c} e^{-\frac{\omega r}{c}}}{1 - g + \frac{g\omega_n}{2c}} \right)^2 \right]. \tag{3.18}
$$

To trace the dependence of the Casimir interaction on the coupling constant $g < 1$ and distance r at $T = 0$ we introduce the logarithmic derivative $\nu = -\frac{d \ln(E(r))}{d \ln(r)}$. For power law functions $1/r^\nu$ it gives the power ν. The results are summarized in the Fig. 3.3. The interval $0 < g \le 1$ describes the impurity masses $m < M \le \infty$. The line $g = 0$ is the singular line where $U_{\text{eff}} = 0$. And the interval $-\infty < g < 0$ corresponds to $M < m$.
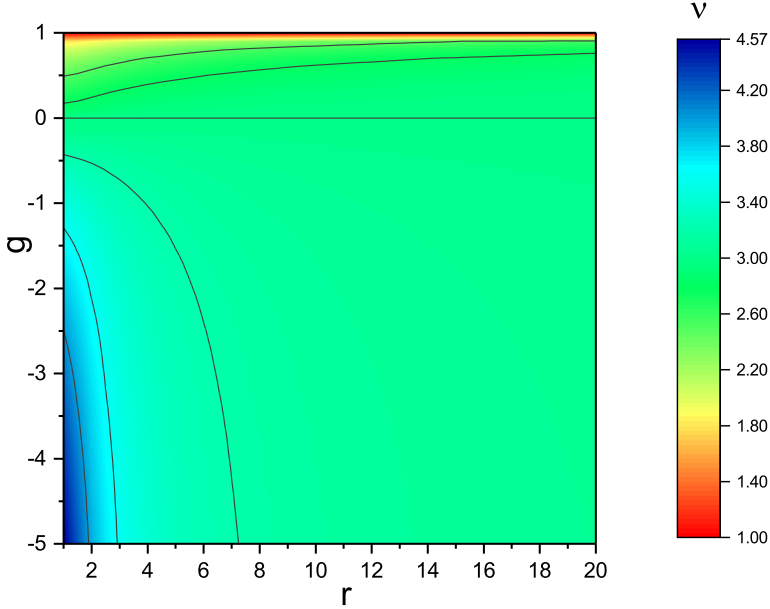
Figure 3.3. Logarithmic derivative $\nu = -\frac{d \ln U_{\text{eff}}(r)}{d \ln r}$ as the function of r and g of the Casimir interaction between two impurity atoms having different masses.

One can see from the figure that although for small distances the Casimir interaction cannot be described as a function $1/r^{\nu}$, at large distances the dependence tends to $1/r^3$. The characteristic distance of the crossover to the $1/r^3$-law is $r_g = \frac{g}{1-g}$ (see 3.4.2). Finally, in the limit $g \to 1$ the Casimir interaction depends as $1/r$ from the distance between the impurity atoms and coincides with Eq. (3.5).

3.4.2 Casimir force

The Casimir force reads:

$$F(r) = -\frac{\partial U_{eff}}{\partial r} = -\int_0^\infty \frac{d\omega}{2\pi} \frac{\frac{\tilde{g}^2 \omega^3}{2c^3} e^{-2\frac{\omega r}{c}}}{(1 + \tilde{g}\frac{\omega}{2c})^2 - (\tilde{g}\frac{\omega}{2c} e^{-\frac{\omega r}{c}})^2}, \qquad (3.19)$$

where we use a new constant $\tilde{g} = \frac{g}{1-g}$ for convenience. For heavy impurities ($\tilde{g} > 0$), one can approximate Eq. (3.19) omitting the exponentially small term from the denominator. It reads then as

$$F(r) \simeq -\int_0^\infty \frac{d\omega}{2\pi} \frac{\frac{\tilde{g}^2 \omega^3}{2c^3} e^{-2\frac{\omega r}{c}}}{(1 + \tilde{g}\frac{w}{2c})^2} = \frac{c}{\tilde{g}^2 \pi} \left(\frac{1}{4x^2} - \frac{2}{x} - 4 + (12 + 16x)I(4x) \right), \qquad (3.20)$$

where $x = r/\tilde{g}$. Here $I(x) = \int_0^\infty dt \frac{e^{-t}}{x+t}$. The integral $I(x)$ can be expressed through the incomplete gamma function: $I(x) = e^x \Gamma[0, x]$, $\Gamma[\alpha, x] = \int_x^\infty t^{\alpha-1} e^{-t} dt$.

Integration over r with condition $U_{\text{eff}}(r \to \infty) = 0$ gives

$$U_{\text{eff}}(x) \simeq \frac{c}{\tilde{g}\pi} \left(-\frac{1}{4x} + 2(1 + 2x)I(4x) - 1 \right). \qquad (3.21)$$

Expression (3.21) works excellently for small masses, but for infinite masses it gives $\frac{1}{4\pi}$ numerical coefficient instead of $\frac{\pi}{24}$ provided by (3.15) and expected for the Casimir law (Fig. 3.4). Asymptotically, Eq. (3.21) for mass ratio $m/M \to 1$ ($g \to 0$) is:

$$U_{\text{eff}}(x) \underset{x \to \infty}{\simeq} \frac{c}{\tilde{g}} \left(-\frac{1}{32\pi x^3} + \frac{1}{16\pi x^4} - \frac{9}{128\pi x^5} + ... \right).$$

The space dependence for this expression is shown at Fig. 3.5 with three
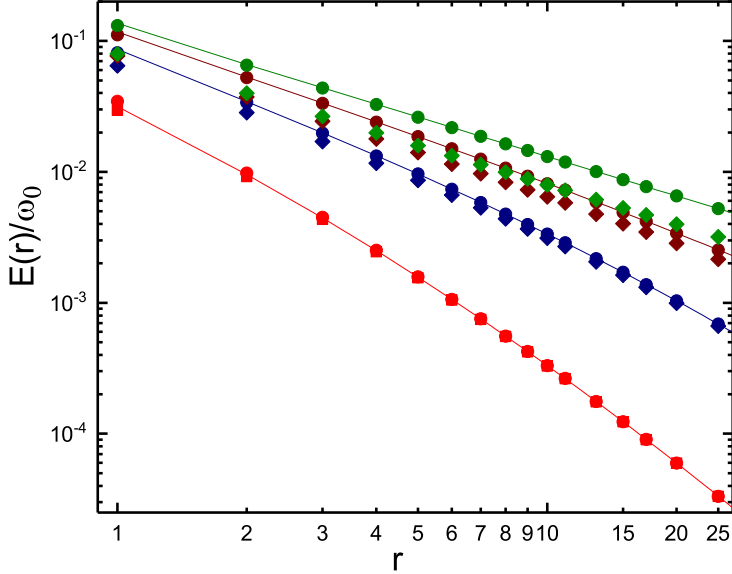
Figure 3.4. Comparison of exact result, result for the linearized vertices and approximate analytical formula. Red color - $g = 0.9$, blue - $g = 0.99$, brown - $g = 0.999$, green - $g = 1$. Circles - exact result, lines - linearized vertices, diamonds - approximate formula.

different values of g.

3.4.3 External potential

Now we consider two atoms in an external harmonic potential which is defined by the following Hamiltonian

$$V = gm\omega_0^2(u_a^2 + u_b^2), \tag{3.22}$$
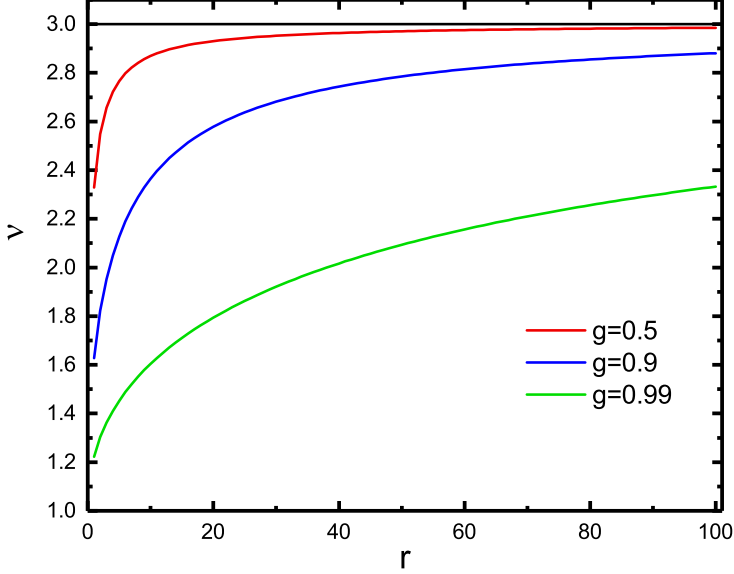
Figure 3.5. Dependence of the logarithmic derivative $\nu(r)$ on distance for various fixed g.

with the interaction constant $g \geq 0$.

It is more convenient to define a free phonon field in this case as

$$\tilde{\varphi}(r,t) = \frac{1}{\sqrt{V}} \sum_q \omega_0 \sqrt{\frac{1}{\omega_k}} \left[b_q e^{iqr - i\omega_q t} + b_q^+ e^{-iqr + i\omega_q t} \right].$$

Eq.(3.22) takes then the same form as Eq.(3.8), but the vertices now are

$$
\begin{aligned}
V_{\mathbf{q},\mathbf{q}'}^{(1)} &= V_{\mathbf{q},\mathbf{q}'}^{(0)} \cos[(\mathbf{q} - \mathbf{q}')\frac{\mathbf{r}}{2}], \\
V_{\mathbf{q},\mathbf{q}'}^{(2)} &= -V_{\mathbf{q},\mathbf{q}'}^{(0)} \cos[(\mathbf{q} + \mathbf{q}')\frac{\mathbf{r}}{2}],
\end{aligned}
$$

with $V_{\mathbf{q},\mathbf{q}'}^{(0)}$:

$$V_{\mathbf{q},\mathbf{q}'}^{(0)} = -\frac{g\omega_0^2}{\sqrt{\omega_q}\sqrt{\omega_{q'}}}, \tag{3.23}$$

The Green's functions $G(\omega_n, r), G_0(\omega_n)$ take form

$$
\begin{aligned}
G(\omega_n, r) &= \int_{-\pi}^{\pi} \frac{dk}{2\pi} \cos(kr) \frac{\omega_0^2}{\omega_n^2 + \omega_k^2} = \int_{-\pi}^{\pi} \frac{dk}{2\pi} \cos(kr) \frac{\omega_0^2}{\omega_n^2 + 4\omega_0^2 \sin^2(\frac{k}{2})} \\
&= \frac{\frac{\omega_0^2}{2|\omega_n|c}}{\sqrt{1 + (\frac{\omega_n}{2\omega_0})^2}} \left(\frac{\omega_n}{2\omega_0} + \sqrt{1 + \left(\frac{\omega_n}{2\omega_0}\right)^2} \right)^{-2r} \\
G_0(\omega_n) &= G(0, \omega_n) = \int_{-\pi}^{\pi} \frac{dk}{2\pi} \frac{\omega_0^2}{\omega_n^2 + \omega_k^2} = \frac{\frac{\omega_0^2}{2|\omega_n|c}}{\sqrt{1 + (\frac{\omega_n}{2\omega_0})^2}}.
\end{aligned}
$$

So they can be written as

$$G(\omega_n, r) = \frac{\omega_0}{c} \frac{\omega_0^2}{\omega_n^2} f(|\omega_n|/2\omega_0, r) \tag{3.24}$$

$$G_0(\omega_n) = \frac{\omega_0}{c} \frac{\omega_0^2}{\omega_n^2} f(|\omega_n|/2\omega_0, 0), \tag{3.25}$$

where the $f(x, r)$ function is the same as before in (3.14). To analyze the Casimir energy, we use the linearized spectrum. The correspondent continuum model is different from Eq. (3.17) and is given by

$$
\begin{aligned}
H &= \sum_k c|k| b_k^{\dagger} b_k \tag{3.26} \\
&+ g\sum_{k,k'} \frac{\omega_0^2}{c\sqrt{|kk'|}} \cos\left[\frac{(k+k')r}{2} \right] \left(b_k^{\dagger} b_{k'} + \frac{b_k b_{k'} + b_k^{\dagger} b_{k'}^{\dagger}}{2} \right).
\end{aligned}
$$
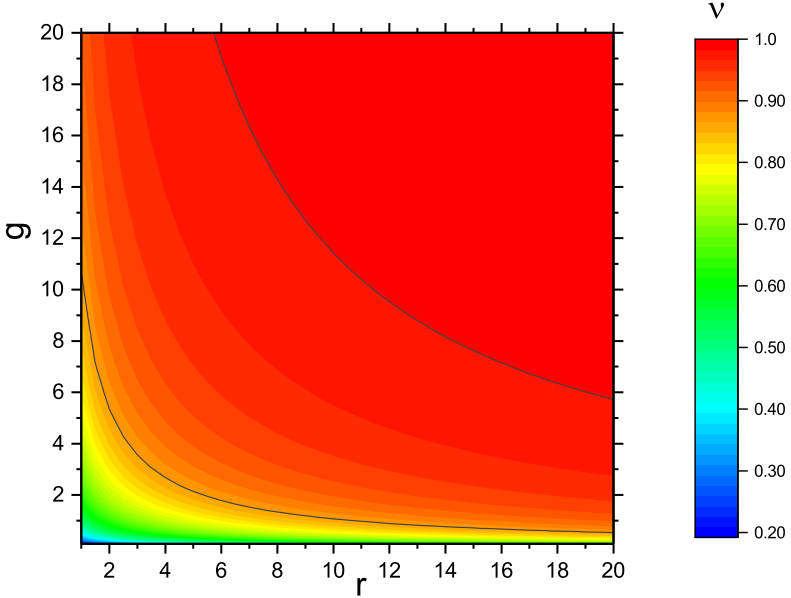
Figure 3.6. Logarithmic derivative $\nu = -\frac{d\ln U_{\text{eff}}(r)}{d\ln r}$ as the function of r and g for the Casimir interaction between two masses in an external potential.

The Green's functions read in this case as

$$
\begin{aligned}
G(\omega_n, r) &= \frac{\omega_0^2}{2c|\omega_n|} e^{-\frac{|\omega_n|}{c}r}, \\
G_0(\omega_n) &= \frac{\omega_0^2}{2c|\omega_n|}.
\end{aligned}
$$

It's worth to consider the second order term of the perturbation theory for the Casimir interaction:

$$
U^{(2)}(r) = -\frac{g^2}{2} \int_{-\infty}^{\infty} \frac{d\omega_n}{2\pi} \frac{\omega_0^4}{4c^2\omega_n^2} e^{-2\frac{|\omega_n|}{c}r}.
$$

This expression diverges at small frequencies, as illustrated in Fig.2.4c. Direct calculations analogous to the previous case give us that all orders of the perturbation theory are divergent at the low energy limit. But the summation of whole series of the diagrams Fig.3.2 leads to cancellation of the singularities and finite expression for the thermodynamic potential Eq.(3.16) is obtained. With the phonon Green's functions given by Eqs. (3.24,3.25), the whole sum of the perturbation theory series remains finite and gives us

$$U_{eff}(r) = - \int_0^\infty \frac{d\omega_n}{2\pi} \ln \left[1 - \left(\frac{g \frac{\omega_0^2}{2c\omega_n} e^{-\frac{\omega_n}{c} r}}{1 + \frac{g\omega_0^2}{2c\omega_n}} \right)^2 \right]. \qquad (3.27)$$

The distance dependence for various given values of g is shown at Fig. 3.7.

At $g = \infty$, from Eq.(3.27) follows $U_{eff}(r) = \frac{\omega_0^2 \pi}{24cr}$. To investigate the finite g case, we use the same approach as before, finding an approximate expression for the Casimir force and integrating it:

$$
\begin{aligned}
F(x) &= \int_0^\infty \frac{d\omega_n}{2\pi} \frac{g^2 \frac{\omega_0^4}{2c^3\omega_n^2} e^{-2\frac{\omega_n}{c} r}}{(1 + \frac{g\omega_0^2}{2c\omega_n})^2 - \frac{g^2\omega_0^4}{4c^2\omega_n^2} e^{-2\frac{\omega_n^2}{c} r}} \\
&\simeq \frac{g^2 \omega_0^4}{4\pi c^3} \left(-1 + (x+1)I(x) \right),
\end{aligned}
\qquad (3.28)
$$

where $x = \frac{gr\omega_0^2}{c^2}$.

$$E_{Cas}(r) \simeq \frac{g\omega_0^2}{4\pi c} \left(1 - xI(x) \right). \qquad (3.29)$$

Logarithmic derivative ν extracted from Eq.(3.29) is shown in Fig.3.6 in
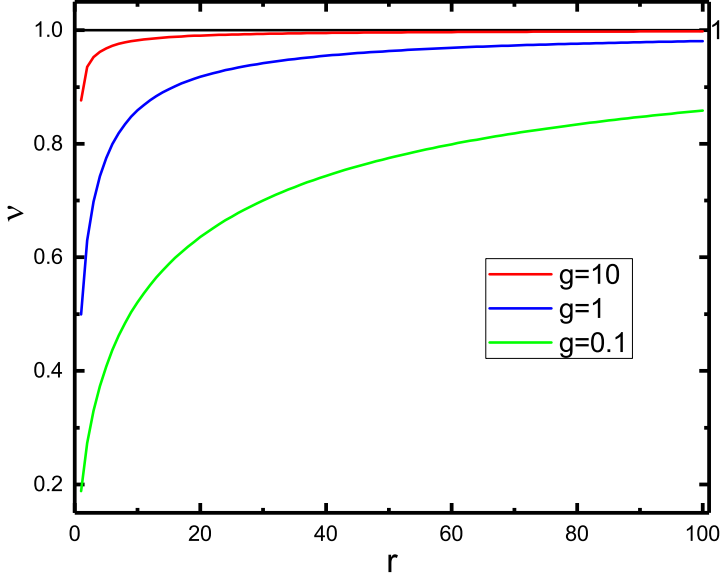
Figure 3.7. Dependence of the logarithmic derivative $\nu(r)$ on distance for various fixed g. Potential energy case.

relation to r and g. The r-dependence for various given values of g is also depicted at Fig. 3.7.

For $gr \gg 1$, the expression for the Casimir force reads

$$F(r) = \frac{\omega_0^2}{cr^2} \left(\frac{\pi}{24} - \frac{c^2\pi}{6gr\omega_0^2} + \frac{\pi^2 + 3\zeta(3)}{2\pi} \left(\frac{c^2}{gr\omega_0^2} \right)^2 + ... \right).$$

Similar to Eq.(3.27) expression was obtained in [50]. To understand the scaling behavior at $T = 0$ we plot the logarithmic derivative ν of the Casimir interaction U_{eff} given by Eq. (3.27) as a function of r and g in Fig. 3.6. For small values gr the law is not universal, but U_{eff} tends to $1/r$

as soon as $gr \ll 1$. The integral Eq. (3.27) in the limit $gr \gg 1$ matches the previously found expression for $M \to \infty$ in Eq.(3.5).

3.5 Estimation of the Casimir interaction for experimental setups

The obtained long-ranged interaction can be observed experimentally in ultra cold atomic gases in the experimental setup of Catani et al. [79] described in Chapter 1. As it follows from this chapter, we argue that the Casimir interaction for dynamic impurities measured in this setup should be stronger than predicted by Schecter and Kamenev [51]. Their estimation is based on the second order of the perturbation theory. As shown in Fig. 3.1, the total Casimir interaction in this case will be approximately three times stronger at large separations between impurities (for this setup, $g \sim \frac{1}{2}$, based in the relative masses of the considered atoms). The characteristic length for the saturation of the $1/r^3$ law in this case is $\sim 0.1 \mu m$, which is comparable to the closes interatomic separation for the setup.

In principle, the competing photon-induced Casimir-Polder interaction is also present for the system mentioned above. But since the Casimir-Polder interaction falls off much faster, namely as $1/r^6$, the phonon induced Casimir interaction should dominate. At the minimal possible distance between the impurity atoms in the setup, the phonon-induced Casimir interaction between two static impurities for this set-up is $1kHz$. At the minimal possible distance between the impurity atoms in the setup of ^{40}K atoms and ^{87}Rb atoms, the Casimir-Polder interaction gives 10^{-6}Hz [112],

which is at least three orders of magnitude smaller than the contribution from the phonon-mediated Casimir interaction.

3.6 Appendices for the main text

3.6.1 Appendix A: Phenomenological bosonization

The density operator of a one-dimensional system with particles located at points x_i is written as

$$\rho(x) = \sum_i \delta(x - x_i). \tag{3.30}$$

Now, following [102] closely, we introduce a labeling field $\phi_l(x)$ such that $\phi_l(x_i) = 2\pi i$. This field shifts at 2π each time it passes a particle (Fig.3.8).
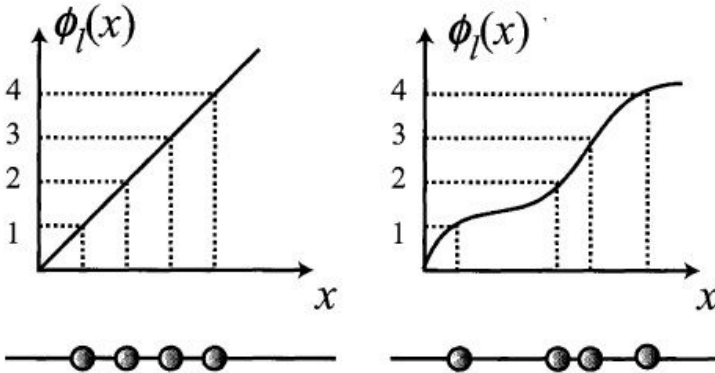
Figure 3.8. Labelling field $\phi_l(x)$ in units of 2π. Choosing a proper function, one can describe any configuration of the particles in space via this field. The figure is reprinted with permission from [102]. Copyright 2003 by the American Physical Society.

The advantage of using this field is that it is unique, since the ordering of the particles is fixed starting from $x = -\infty$ and moving to $x = \infty$ for

any given configuration.

Using the properties of the δ-function from Eq.(3.30), we can write

$$\rho(x) = \sum_n |\nabla\phi_l(x)|\delta(\phi_l(x) - 2\pi n). \tag{3.31}$$

The function $\phi_l(x)$ always can be chosen as non-decreasing, so we drop the absolute value in this formula. Using the Poisson summation formula, we can rewrite Eq.(3.31) as

$$\rho(x) = \frac{\nabla\phi_l(x)}{2\pi} \sum_{p\in\mathbb{Z}} e^{ip\phi_l(x)}.$$

Introducing the average density of the system ρ_0, we express the labelling field through the labelling field for the ideal lattice (left part of Fig.3.8) and a field $\phi(x)$ relative to the perfect crystalline solution

$$\phi_l(x) = 2\pi\rho_0 x - 2\phi(x). \tag{3.32}$$

In terms of this new field $\phi(x)$, the density now takes form

$$\rho(x) = \left(\rho_0 - \frac{\nabla\phi(x)}{\pi}\right) \sum_{p\in\mathbb{Z}} e^{2ip(\pi\rho_0 x - \phi(x))}. \tag{3.33}$$

Averaging density over distances large compared to interparticle distance, we have only the non-oscillating term $(p=0)$ contributing to the density. The smeared density $\rho(x)$ reads then

$$\rho(x) \simeq \rho_0 - \frac{\nabla\phi(x)}{\pi}. \tag{3.34}$$

Now we use the density-phase representation to write the single particle creation operator $\psi^\dagger(x) = |\rho^{\frac{1}{2}}(x)|exp\left[-i\theta(x)\right]$. $\theta(x)$ is some operator describing the phase. Depending whether we deal with a bosonic or a fermionic system, the particle creation and annihilation operators $\psi^\dagger$, $\psi(x)$ obey the commutation/anticommutation relations imposing some commutation relation between the density operators and $\theta(x)$.

The bosonic commutation relation for $\psi_B(x)$ (the label B is introduced to emphasis that we deal with the bosonic operator) rewritten in terms of the density and the phase operators is

$$\left[\rho(x), e^{-i\theta(x')}\right] = \delta(x - x')e^{-i\theta(x')}.$$

Using the expression Eq.(3.31) for the smeared density, one gets the following relation:

$$\left[\frac{1}{\pi}\nabla\phi(x), \theta(x')\right] = -i\delta(x - x'), \tag{3.35}$$

we used here the relation $[A, f(B)] = [A, B] f'(B)$. The higher harmonics from the exact expression for the density contributing to Eq.(3.33) are highly oscillatory, so they are expected to play no role in the continuum limit [102].

As follows from Eq.(3.35), $\theta(x)$ and $\frac{1}{\pi}\nabla\phi(x)$ are canonically conjugate, so the canonically conjugate momentum to $\phi(x)$, denoted as $\Pi_\phi(x)$, is

$$\Pi_\phi(x) = \frac{1}{\pi}\nabla\theta(x).$$

Now we can restore the bosonic single-particle creation operator $\psi_B^\dagger(x)$ substituting Eq.(3.33) into the density-phase representation of the single-

particle operator and noting that the square root of the δ-function is the δ-function with some normalization coefficient, we write

$$\psi_B^\dagger(x) = \left(\rho_0 - \frac{1}{\pi}\nabla\phi(x)\right)^{1/2} \sum_{p\in\mathbb{Z}} e^{i2p(\pi\rho_0 x - \phi(x))} e^{-i\theta(x)}. \qquad (3.36)$$

Now let us consider the single-particle fermionic creation operator $\psi_F^\dagger(x)$. Unlike $\psi_B^\dagger(x)$, it must satisfy the anticommutation relation. To achieve that we need to modify this operator so that it gives the minus sigh each time the fermionic operators are commuted. In general, this can be done by performing the Jordan-Wigner transformation over the $\psi_B^\dagger(x)$ operator. In our case, we can simply note that the labelling field $\phi_l(x)$ in Eq.(3.32) is constructed to be a multiple of 2π at each particle, so the operator $e^{i\frac{1}{2}\phi_l(x)}$ changes the sign at the location of consecutive particle. It allow us to construct the fermionic single-particle creation operator as $\psi_F^\dagger(x) = \psi_B^\dagger(x) e^{i\frac{1}{2}\phi_l(x)}$. It the explicit form of the $\theta(x)$, $\phi(x)$ representation, we have

$$\psi_F^\dagger(x) = \left(\rho_0 - \frac{1}{\pi}\nabla\phi(x)\right)^{1/2} \sum_{p\in\mathbb{Z}} e^{i(2p+1)(\pi\rho_0 x - \phi(x))} e^{-i\theta(x)}. \qquad (3.37)$$

The fields θ and ϕ can have topological excitations in addition to the small oscillations [100]. This excitations can appear since if one imposes periodic boundary conditions $\psi(x+L) = \psi(x)$, where L is the length of the system, on a system, it gives $\theta(x+L) = \theta(x) + \pi J$, $\phi(x+L) = \phi(x) + \pi N$, where numbers N and J are some integers. In a bosonic system, J is an even integer, while in a fermionic system the sum $N + J$ must be even. The fields $\Pi(x)$ and $\phi(x)$ are canonically conjugate, so they can be ex-

pressed in terms of bosonic operators b_p, $b_p^\dagger$ for any Hamiltonian. The field $\phi(x)$ is real, so it contains both b and $b^\dagger$. Substituting operators $\psi_B(x)$ or $\psi_F(x)$ into Eq.(3.1), one gets the Luttinger liquid Hamiltonian written in terms of the $\theta(x)$, $\phi(x)$ fields [100]. By the inversion symmetry requirements, the energy of the system is invariant under $x \to -x$ transformation and therefore $\theta(x) = \tilde{\theta}(-x)\,\phi(x) = -\tilde{\phi}(-x)$, the the effective low energy Hamiltonian contains only $(\nabla\phi(x))^2$ (from the potential energy) and $(\nabla\theta(x))^2$ (from the kinetic energy) terms without the cross-term $(\nabla\theta(x)(\nabla\phi(x))$.

3.6.2 Appendix B: Phonon-impurity scattering on the lattice Effective interaction between two impurities

In this section we derive the effective interaction given by Eq. (3.8). Let us start by considering an ideal cubic lattice in D dimensions with δ_n inter-atomic distance in each dimension. The Hamiltonian, quantized by bosonic operators $\alpha_\mathbf{k}, \alpha_\mathbf{k}^\dagger$, reads

$$
\begin{aligned}
H &= \sum_i \frac{\mathbf{p}^2}{2m} + \frac{m\omega_0^2}{2} \sum_{|i-j|=1} (\mathbf{u}_i - \mathbf{u}_j)^2 = \sum_i \frac{\mathbf{p}^2}{2m} \\
&+ m\omega_0^2 \sum_i (2D\mathbf{u}_i^2 - 2D\mathbf{u}_i\mathbf{u}_{i+1} - 2D\mathbf{r}_{i-1}\mathbf{r}_i) \\
&= \frac{\omega_0}{2} \left[\sum_\mathbf{k} \left(\frac{1}{2} + 2D - 2\sum_{n=1}^{D} \cos(k_n\delta_n) \right) (b_\mathbf{k}^\dagger \alpha_\mathbf{k} + \alpha_\mathbf{k}\alpha_\mathbf{k}^\dagger) \right. \\
&+ \left. \left(-\frac{1}{2} + 2D - 2\sum_{n=1}^{D} \cos(k_n\delta_n) \right) (\alpha_\mathbf{k}^\dagger \alpha_{-\mathbf{k}}^\dagger + \alpha_\mathbf{k}\alpha_{-\mathbf{k}}) \right] \\
&= \sum_\mathbf{k} \left[A_\mathbf{k}(\alpha_\mathbf{k}^\dagger \alpha_\mathbf{k} + \alpha_\mathbf{k}\alpha_\mathbf{k}^\dagger) + B_\mathbf{k}(\alpha_\mathbf{k}^\dagger \alpha_{-\mathbf{k}}^\dagger + \alpha_\mathbf{k}\alpha_{-\mathbf{k}}) \right], \quad (3.38)
\end{aligned}
$$

δ_n are the lattice constants. We introduced coefficients $A_{\mathbf{k}}, B_{\mathbf{k}}$ as

$$A_{\mathbf{k}} = \omega_0 \left(D + \frac{1}{4} - \sum_{n=1}^{D} \cos(k_n \delta_n) \right),$$

$$B_{\mathbf{k}} = \omega_0 \left(D - \frac{1}{4} - \sum_{n=1}^{D} \cos(k_n \delta_n) \right).$$

The Hamiltonian Eq.(3.38) can be diagonalized by the Bogolubov transformation [113]

$$\begin{cases} \alpha_{\mathbf{k}} = U_{\mathbf{k}} b_{\mathbf{k}} + V_{-\mathbf{k}}^* b_{-\mathbf{k}}^\dagger \\ \alpha_{\mathbf{k}}^\dagger = U_{\mathbf{k}}^* b_{\mathbf{k}}^\dagger + V_{-\mathbf{k}} b_{-\mathbf{k}}, \end{cases}$$

with $b_{\mathbf{k}}, b_{\mathbf{k}}^\dagger$ - phonon operators.

The Bogolubov coefficients satisfy the equation

$$(A_{\mathbf{k}} - \omega_{\mathbf{k}}) U_{\mathbf{k}} + B_{\mathbf{k}} V_{\mathbf{k}} = 0,$$

with the condition

$$U_{\mathbf{k}}^2 - V_{\mathbf{k}}^2 = 1.$$

$$U_{\mathbf{k}} = \sqrt{\frac{1}{2} + \frac{A_{\mathbf{k}}}{2\omega_{\mathbf{k}}}}; \ V_{\mathbf{k}} = -\frac{B_{\mathbf{k}}}{A_{\mathbf{k}} + \omega_{\mathbf{k}}} U_{\mathbf{k}}, \qquad (3.39)$$

$$\omega_{\mathbf{k}} = \omega_0 \sqrt{2\nu_{\mathbf{k}}}; \ \nu_{\mathbf{k}} = D - \sum_{i=1}^{D} \cos(q_i \delta_i)$$

Now we can return to our system with impurities and the emerging interaction given by Eq.(2.3). Here and below we first consider the one

dimensional case.

$$\hat{V}(i,j) = g\frac{p_i^2}{2m} + g\frac{p_j^2}{2m} = \frac{g}{4}\omega_0\left((\alpha_i^\dagger - \alpha_i)^2 + (\alpha_j^\dagger - \alpha_j)^2\right)$$

We apply the Fourier transform and than the Bogolubov transformation using coefficients (3.39), so the interaction, expressed via phonon operators turns into

$$
\begin{aligned}
V_{kin} &= \frac{g}{4}\omega_0\sum_{\mathbf{q},\mathbf{q'}}\left[\left(b_\mathbf{q}^\dagger b_\mathbf{q'}^\dagger + b_\mathbf{q}b_\mathbf{q'} - b_\mathbf{q}b_\mathbf{q'}^\dagger - b_\mathbf{q}^\dagger b_\mathbf{q'}\right)(U_\mathbf{q}U_\mathbf{q'} + V_\mathbf{q}V_\mathbf{q'}\right.\\
&- \left. U_\mathbf{q}V_\mathbf{q'} - V_\mathbf{q}U_\mathbf{q'})\left(e^{i(\mathbf{q}+\mathbf{q'})\mathbf{r}_i} + e^{i(\mathbf{q}+\mathbf{q'})\mathbf{r}_j}\right)\right].
\end{aligned}
$$

He we used the fact that $U_\mathbf{q}^* = U_\mathbf{q}, V_\mathbf{q}^* = V_\mathbf{q}$.

This expression immediately leads to Eq.(3.8).

In the case of static impurities, the interaction term reads

$$g\frac{m\omega_0^2}{2}x_i^2 + g\frac{m\omega_0^2}{2}x_j^2.$$

Expressing it via the phonon operators b, $b^\dagger$, we obtain

$$
\begin{aligned}
V_{pot} &= \frac{g}{4}\omega_0\sum_{\mathbf{q},\mathbf{q'}}\left[\left(b_\mathbf{q}^\dagger b_\mathbf{q'}^\dagger + b_\mathbf{q}b_\mathbf{q'} + b_\mathbf{q}b_\mathbf{q'}^\dagger + b_\mathbf{q}^\dagger b_\mathbf{q'}\right)(U_\mathbf{q}U_\mathbf{q'} + V_\mathbf{q}V_\mathbf{q'}\right.\\
&+ \left. U_\mathbf{q}V_\mathbf{q'} + V_\mathbf{q}U_\mathbf{q'})\left(e^{i(\mathbf{q}+\mathbf{q'})\mathbf{r}_i} + e^{i(\mathbf{q}+\mathbf{q'})\mathbf{r}_j}\right)\right].
\end{aligned}
$$

Chapter 4

General T-matrix approach to the phonon-mediated Casimir interaction in $D = 1, 2, 3$ dimensions

4.1 Introduction

It it shown in Chapters 2, 3, that the Casimir interaction in 1D falls off asymptotically with the distance r between the impurities as r^{-1} in the static limit, while as r^{-3} in the dynamic one. The Casimir interaction evolves with increase of the mass of the impurities It is also shown that

the scaling of the Casimir interaction continuously changes from r^{-3} to r^{-1} for dynamic impurities if the mass of the impurities becomes infinitely large.

In the present Chapter, we generalize the theory of the phonon mediated Casimir interaction [114], on two and three dimensional cases and finite temperatures. We investigate the evolution of the Casimir interaction in the full range of the scattering amplitude starting from the weak phonon-impurity scattering till the unitary limit. The impurity scattering T-matrix approach is used, in order to regularize the intrinsic infra-red and ultraviolet divergences [115, 116, 117, 118, 119, 120]. Similar approach was used in earlier works in different contexts [37, 121, 122, 56, 46].

We start this Chapter explaining the T-matrix formalism. The rest of the paper is organized as follows. We describe the model for dynamical impurities. Then we derive the Casimir interaction in terms of the single impurity T-matrix for the considered system. Using the general properties of the T-matrix, we consider the Casimir interaction in dimensions $D = 1..3$. Then, we evaluate the effect of temperature. Finally, we consider a model for static impurities in an external potential. We conclude with a discussion of the obtained results.

4.2 T-matrix formalism

The T-matrix arises in the scattering theory [123]. The operator corresponding to the T-matrix can be obtained from the Lippmann-Schwinger equation [124]. It establishes the relation between the wave function ψ of

a particle in presence of the scattering potential V and the free particle wave function ψ_0. These wave functions satisfy the equations

$$\left(E - \hat{H}_0\right)|\psi_0\rangle = 0, \quad \left(E - \hat{H}_0 - \hat{V}\right)|\psi\rangle = 0,$$

where E is the energy of the free particle. The relation between these functions reads [125] as

$$|\psi\rangle = |\psi_0\rangle + \hat{V}G_0(E)|\psi\rangle,$$

$G_0(E) = (E - H_0)^{-1}$. This equation can be solved by iterations. Expanding it into the Born series [123], we obtain

$$|\psi\rangle = \left(1 + \hat{V}G_0 + \hat{V}G_0\hat{V}G_0 + ...\right)|\psi_0\rangle. \tag{4.1}$$

We introduce the operator T through this series, so that Eq.(4.1) is rewritten as

$$|\psi\rangle = \left(1 + \hat{T}G_0(E)\right)|\psi_0\rangle.$$

The Lippman-Schwinger equation in the operator representation is

$$\hat{T} = \hat{V} + \hat{V}G_0(E)\hat{T}. \tag{4.2}$$

In general form, Eq.(4.2) is an integral equation. For instance, it yields in the momentum representation

$$\langle\mathbf{k}|\hat{T}(E)|\mathbf{k}'\rangle \equiv T(\mathbf{k}, \mathbf{k}', E) = V(\mathbf{k}, \mathbf{k}') + \int \frac{d^D\mathbf{q}}{(2\pi)^D}V(\mathbf{k}, \mathbf{q})G_0(\mathbf{q}, E)T(\mathbf{q}, \mathbf{k}', E).$$

This expression can be simplified if certain restrictions are applied to the scattering potential. If the potential is local, i.e. $\langle \mathbf{x} | \hat{V} | \mathbf{y} \rangle = V(\mathbf{x}) \delta(\mathbf{x} - \mathbf{y})$ in the coordinate representation, it depends on the the difference of momenta - $V(\mathbf{k}, \mathbf{k}') = V(\mathbf{k} - \mathbf{k}')$. Furthermore, if the scattering potential is point-like, i.e. $V(\mathbf{x}) = V\delta(\mathbf{x})$, Eq.(4.2) becomes algebraic. In this case, the T-matrix is simply [126]

$$T(E) = \left(1 + V \int \frac{d^D \mathbf{q}}{(2\pi)^D} G_0(\mathbf{q}, E) \right)^{-1} V. \qquad (4.3)$$

The solution of Eq.(4.3) can be found explicitly, so this kind of potential allows the exact solution of the scattering problem. The T-matrix is directly related to the scattering amplitude [123], and the latter can be extracted in numerous experiments for various physical set-ups [127, 128, 129, 130, 131, 132, 133], including experiments on phonon scattering on impurities [134, 135, 136]. This fact allows to treat some low-energy effective theories containing ultraviolet divergences renormalizing them using the T-matrix.

4.3 Dynamical impurities

Let us now consider free scalar bosons with linear energy dispersion (phonons) which are described by a standard Hamiltonian (e.g. [137])

$$\hat{H}_0 = \sum_{\mathbf{k}} \left(\pi(\mathbf{k})\bar{\pi}(\mathbf{k}) + \omega_{\mathbf{k}}^2 \varphi(\mathbf{k})\bar{\varphi}(\mathbf{k}) \right), \qquad (4.4)$$

where the bosonic fields are:

$$\pi(\mathbf{x}) = \frac{i}{\sqrt{V}} \sum_{\mathbf{k}} \sqrt{\frac{\omega_{\mathbf{k}}}{2}} \left[b_{\mathbf{k}} e^{i\mathbf{k}\mathbf{x}} - b_{-\mathbf{k}}^{\dagger} e^{-i\mathbf{k}\mathbf{x}} \right],$$

$$\varphi(\mathbf{x}) = \frac{1}{\sqrt{V}} \sum_{\mathbf{k}} \sqrt{\frac{1}{2\omega_{\mathbf{k}}}} \left[b_{\mathbf{k}} e^{i\mathbf{k}\mathbf{x}} + b_{-\mathbf{k}}^{\dagger} e^{-i\mathbf{k}\mathbf{x}} \right],$$

with linear dispersion $\omega_{\mathbf{k}} = c|\mathbf{k}|$. Here $b_{\mathbf{k}}, b_{\mathbf{k}}^{\dagger}$ are phonon annihilation and creation operators, V - the volume of the system, c is the sound velocity. We put $\hbar = 1$ here.

The simplest form of the interaction of the phonons with an impurity located at the point $\mathbf{x}$ can be written in the bilinear form of the field operators, i.e. $\pi\bar{\pi}$ and $\phi\bar{\phi}$. These two terms have significantly different physical meaning. The interaction $\pi\bar{\pi}$ may dominate in the systems in which the impurities are moving coherently with the moving media e.g. dynamic impurities in the Luttinger liquid [51], or in atomic chains/lattices (see Section 4.7.1). The interaction $\varphi\bar{\varphi}$ is leading in the case of static impurities, e.g. static impurity atoms in the Luttinger liquid considered in [50].

In this section, we consider the $\pi\bar{\pi}$ impurity-phonon interaction for two impurities, which was previously derived for the Luttinger liquids in [51]. We consider the case when the impurities are much slower then phonons. In this limit, the interaction of phonons with two impurities located at the given time at the coordinates $-\mathbf{r}/2$ and $\mathbf{r}/2$ can be written as

$$\hat{H}_{int} = -g \left(\pi(\mathbf{x})\bar{\pi}(\mathbf{x})\big|_{\mathbf{x}=-\frac{\mathbf{r}}{2}} + \pi(\mathbf{x})\bar{\pi}(\mathbf{x})\big|_{\mathbf{x}=\frac{\mathbf{r}}{2}} \right).$$

$$(4.5)$$

Here g is the interaction constant. The requirement of the positiveness of the kinetic energy leads to $g \leq 1$. It was shown in [114] that $g = 1$ corresponds to the limit of infinite mass of impurities in the lattice model (see Section 4.7.1).

We define the Green's functions on the Matsubara axis at temperature T for non-interacting bosons as [111]:

$$G^{(0)}(\mathbf{x}, \mathbf{x}', \omega_n) = -\int_0^{\frac{1}{T}} d\tau e^{-i\omega_n \tau} \langle\, T_\tau \big(\pi(\mathbf{x}, \tau)\bar{\pi}(\mathbf{x}', 0)\big)\rangle. \qquad (4.6)$$

For the calculations of the Casimir interaction, it is enough to find the Green's functions taken at the coordinates of the impurities $\pm\mathbf{r}/2$. For the sake of simplicity, we use the following notation:

$$
\begin{aligned}
G_r^{(0)}(\omega_n) &\equiv G^{(0)}\big(+\tfrac{\mathbf{r}}{2}, -\tfrac{\mathbf{r}}{2}, \omega_n\big) = G^{(0)}\big(-\tfrac{\mathbf{r}}{2}, +\tfrac{\mathbf{r}}{2}, \omega_n\big), \\
G^{(0)}(\omega_n) &\equiv G^{(0)}\big(+\tfrac{\mathbf{r}}{2}, +\tfrac{\mathbf{r}}{2}, \omega_n\big) = G^{(0)}\big(-\tfrac{\mathbf{r}}{2}, -\tfrac{\mathbf{r}}{2}, \omega_n\big).
\end{aligned}
$$

$$(4.7)$$

The explicit expressions for these Green's functions read as [114]:

$$G_{\mathbf{r}}^{(0)}(\omega_n) = \int \frac{d^D\mathbf{k}}{(2\pi)^D} \left[1 - \frac{\omega_n^2}{\omega_n^2 + \omega_{\mathbf{k}}^2}\right] e^{-i\mathbf{k}\mathbf{r}} \qquad (4.8)$$

and

$$G^{(0)}(\omega_n) = \int \frac{d^D\mathbf{k}}{(2\pi)^D} \left[1 - \frac{\omega_n^2}{\omega_n^2 + \omega_{\mathbf{k}}^2}\right], \qquad (4.9)$$

correspondingly. Note, that $G^{(0)}(\omega_n)$ is formally divergent in the ultraviolet limit. It can be regularized considering a lattice model.
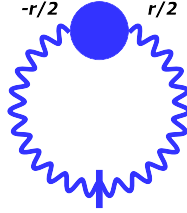
Figure 4.1. Diagrammatic representation of the derivative of the thermodynamic potential with respect to distance of the impurities.

4.4 The Casimir interaction

The starting point is the derivation of the thermodynamic potential of the system of phonons interacting with two impurities located at points $\pm\mathbf{r}/2$ correspondingly. We employ the well-known relation between the derivative of the thermodynamic potential with respect to a parameter and the derivative of the total Hamiltonian $\hat{H} = \hat{H}_0 + \hat{H}_{int}$ with respect to the same parameter [138, 111]. Then one has:

$$\frac{\partial \Omega(\mathbf{r})}{\partial \mathbf{r}} = \left\langle \frac{\partial \hat{H}_{int}(\mathbf{r})}{\partial \mathbf{r}} \right\rangle. \tag{4.10}$$

The right side of Eq.(4.10) can be found using the T-matrix approach. The corresponding diagram is presented in Fig. 4.1. The solid line with a tick stands for the derivative of the Green's function $\frac{\partial G_r^{(0)}(\omega_n)}{\partial r}$. The circle is the two-impurity scattering T-matrix $T_2(-\frac{\mathbf{r}}{2}, \frac{\mathbf{r}}{2}, \omega_n)$. Then Eq.(4.10) takes the form:

$$\frac{\partial \Omega(r)}{\partial r} = T \sum_n \frac{\partial G_r^{(0)}(\omega_n)}{\partial r} T_2 \left(-\frac{\mathbf{r}}{2}, \frac{\mathbf{r}}{2}, \omega_n \right).$$
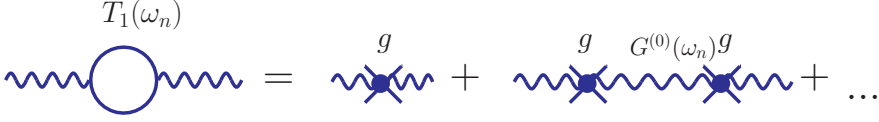
Figure 4.2. Definition of the single-particle T-matrix $T_1(\omega_n)$.

$T_2\left(-\frac{\mathbf{r}}{2}, \frac{\mathbf{r}}{2}, \omega_n\right)$ can be deduced from the single impurity scattering matrix $T_1(\omega_n)$. The series for $T_1(\omega_n)$ is shown in Fig.4.2. The explicit form is:

$$T_1(\omega_n) = \frac{g}{1 - g G^{(0)}(\omega_n)}. \tag{4.11}$$

The two-impurity T-matrix, represented in Fig.4.3, is given by the set of the following equations:

$$T_2\left(\frac{\mathbf{r}}{2}, \frac{\mathbf{r}}{2}, \omega_n\right) = T_1(\omega_n) + T_1(\omega_n) G_r^{(0)}(\omega_n) T_2\left(-\frac{\mathbf{r}}{2}, \frac{\mathbf{r}}{2}, \omega_n\right),$$
$$T_2\left(-\frac{\mathbf{r}}{2}, \frac{\mathbf{r}}{2}, \omega_n\right) = T_1(\omega_n) G_r^{(0)}(\omega_n) T_2\left(\frac{\mathbf{r}}{2}, \frac{\mathbf{r}}{2}, \omega_n\right). \tag{4.12}$$

Solving Eqs.(4.12), one gets

$$\frac{\partial \Omega(\mathbf{r})}{\partial \mathbf{r}} = -T \sum_{n=-\infty}^{\infty} \frac{(T_1(\omega_n) G_{\mathbf{r}}^{(0)}(\omega_n))^2}{1 - \left(T_1(\omega_n) G_{\mathbf{r}}^{(0)}(\omega_n)\right)^2} \frac{\partial_r G_{\mathbf{r}}^{(0)}(\omega_n)}{G_{\mathbf{r}}^{(0)}(\omega_n)}. \tag{4.13}$$

The Casimir interaction can be found by integration of Eq. (4.13) with a condition $\Delta\Omega(r) \to 0$ for $r \to \infty$:

$$U_{Cas}(r) \equiv \Delta\Omega(r) = T \sum_{\omega_n > 0} \log\left(1 - \left(T_1(\omega_n) G_{\mathbf{r}}^{(0)}(\omega_n)\right)^2\right). \tag{4.14}$$

Now, as we have established the general expression for the Casimir energy via the single particle scattering matrix and Green's functions, it
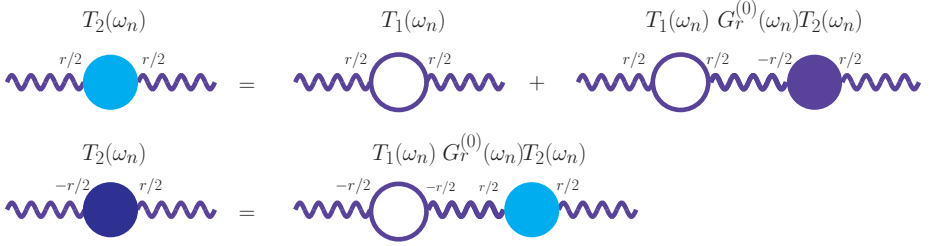
Figure 4.3. Diagrammatic representation of the two-impurity T-matrix. The empty circles here correspond to the $T_1(\omega_n)$, light blue and dark blue circles mean $T_2\left(\frac{\mathbf{r}}{2}, \frac{\mathbf{r}}{2}, \omega_n\right)$ and $T_2\left(-\frac{\mathbf{r}}{2}, \frac{\mathbf{r}}{2}, \omega_n\right)$ correspondingly, the wavy lines are the Green's functions $G_r^{(0)}(\omega_n)$.

is worth to evaluate these Green's functions in various dimensions. The Green's function $G_r^{(0)}(\omega_n)$ $(r \neq 0)$ can be explicitly calculated for the linear boson spectrum $\omega_{\mathbf{k}} = ck$ from Eq.(4.8). It yields in the dimensions $D = 1..3$ (see Section 4.7.2 for details):

$$G_r^{(0)}(\omega_n) = \begin{cases} -\frac{|\omega_n|}{2c}e^{-\frac{|\omega_n|}{c}r}, & D = 1, \\ -\frac{|\omega_n|^2}{2\pi c^2}K_0\left(\frac{|\omega_n|}{c}r\right), & D = 2, \\ -\frac{|\omega_n|^2}{4\pi rc^2}e^{-\frac{|\omega_n|}{c}r}, & D = 3. \end{cases} \qquad (4.15)$$

where $K_0(x)$ is the modified Bessel function of the second kind.

We would like to note that the large distance scaling of $G_r^{(0)}(\omega_n)$ is universal and can be expressed in the form

$$G_r^{(0)}(\omega_n) \underset{r\frac{|\omega_n|}{c}\gg 1}{\sim} |\omega_n|^{\frac{D+1}{2}} r^{-\frac{D-1}{2}} e^{-\frac{|\omega_n|}{c}r}. \qquad (4.16)$$

Due to the exponential dependence of $G_r^{(0)}(\omega_n)$ on the energy, the leading contribution to the Casimir effect comes from low energies $\omega_n \ll \omega_n^* = c/r$
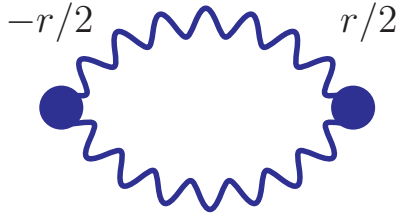
Figure 4.4. $U_{Cas}(r)$ in the second order of the perturbation theory.

at large distance.

4.4.1 Second order of perturbation theory

The lowest order term in g contributing to the Casimir force is of the second order, which is given by the diagram depicted in Fig. 4.4. Integrating this derivative of the thermodynamic potential, we obtain the Casimir energy

$$U_{Cas}(r) = \int_0^\infty \frac{d\omega_n}{2\pi} \left(g G_r^{(0)}(\omega_n) \right)^2 . \qquad (4.17)$$

Using the expression for $G_r^{(0)}(\omega_n)$ given by Eq. (4.15) and Eq. (4.16), we get that the Casimir potential in the second order of the perturbation theory obeys the law $U_{Cas}(r) \sim r^{-(2D+1)}$. In $D = 1..3$, we get the following expressions:

$$U_{Cas}(r) = \begin{cases} -\frac{g^2 c}{32\pi r^3}, & D = 1, \\ -\frac{27 g^2 c}{2048 r^5}, & D = 2, \\ -\frac{3 g^2 c}{64\pi^2 r^7}, & D = 3. \end{cases}$$

The expression for $D = 1$ agrees with early obtained in [51, 114].

4.4.2 T-matrix approximation

Continuum limit. Keeping only the leading terms in the low energy expansion, one can write down the single impurity $T_1(\omega_n)$-matrix of the phonon-impurity scattering in the following form (see for details Section 4.7.2):

$$T_1(\omega_n) \simeq \begin{cases} \frac{1}{a^{-1}+A_1\frac{|\omega_n|}{c}}, & D = 1, \\[3mm] \frac{1}{a^{-1}+A_2\frac{|\omega_n|^2}{c^2}\log|\frac{\omega_c}{\omega_n}|}, & D = 2, \\[3mm] \frac{1}{a^{-1}+A_3\frac{|\omega_n|^2}{c^2}}, & D \geq 3. \end{cases} \qquad (4.18)$$

The coefficients a, A_D and ω_c can be determined in various transport experiments and can be considered as phenomenological parameters. Then Eq. (11) directly relates the Casimir interaction to the physical properties of the phonon - single impurity scattering amplitude. This parameter cannot be found in the frame of the considered microscopic theory, since it emerges as a consequence of the linear spectrum possessed by an effective low-energy theory. For numerical estimations of the Casimir forces we use further a mapping of the continuum model with linear dispersion on the lattice model presented in the next paragraph.

For the finite value of a, the T_1-matrix can be approximately put $T_1 \to a$ at small values of $\omega_n \ll \omega_n^*$. As one can see from Eq.(4.18), the characteristic energy ω_n^* depends on the dimensionality and for $D = 1..3$ reads: $\omega_{n,1D}^* = c/(aA_1)$, $\omega_{n,2D}^* = c\sqrt{1/(aA_2|\log\omega_c(\sqrt{aA_2}/c)|)}$, $\omega_{n,3D}^* = c\sqrt{1/(aA_3)}$.

Since $G_r^{(0)}(\omega_n)$ exponentially depends on $\omega_n r$, the leading contribution to the Casimir energy, as seen from Eq.(4.13), comes from the ener-

gies $\omega_n \lesssim c/r$. It naturally defines the characteristic length $r_a \sim c/\omega_n^*$
of the change of the scaling behavior of the Casimir interaction. At
these energies, the $T_1(\omega_n)$ matrix can be approximated by the constant
a. As a result, at large distances between the impurities $r \gg r_a$, the
scaling of the Casimir interaction is the same as in the second order of
the perturbation theory with the renormalized phonon-impurity coupling
$U_{Cas}(r) \sim T_1^2(\omega_n = 0)/r^{(2D+1)}$.

For $g = g_{cr}$, $a \to \infty$ and $r_a \to \infty$. Hence, the energy dependence of $T_1(\omega_n)$
matrix becomes important. The evaluation of Eq. (4.13) with $T_1(\omega_n)$ from
Eq. (4.18) in the unitary limit shows that the Casimir interaction scaling
in the leading order triggers to

$$
U_{Cas}(r) \sim \begin{cases} \frac{1}{r}, & D = 1, \\ \frac{1}{r\log^2 r}, & D = 2, \\ \frac{1}{r^{2D-1}}, & D \geq 3. \end{cases} \tag{4.19}
$$

The analysis of the intermediate case of large but finite r_a shows that
at small distances $r \ll r_a$ the scaling in the leading approximation is
described by Eq. (4.19).

Lattice model. Now we map the model on a lattice in order to study
the general properties of the T-matrix. We analyze the ideal harmonic
cubic lattice described discussed earlier and described by $H_0 = \sum_i \frac{\hat{p}_i^2}{2m} +$
$\frac{m\omega_0^2}{2} \sum_{<i,j>} (\hat{u}_i - \hat{u}_j)^2$, with two embedded impurity atoms with their mass
different from the mass of the atoms of the lattice. Here $\hat{p}_i$ and $\hat{u}_i$ are the
momentum and coordinate operators, m is the mass of the atoms of the

cubic lattice and $m\omega_0^2$ is the potential term, $\omega_0 = c/\delta$, δ is the lattice constant. For simplicity, we put $\delta = 1$.

The harmonic Hamiltonian expressed via bosonic operators reads $H_0 = \sum_{\mathbf{k}} \omega_{\mathbf{k}} (b_{\mathbf{k}}^\dagger b_{\mathbf{k}} + \frac{1}{2})$. The dispersion of the phonons on a lattice is given as $\omega_{\mathbf{k}} = c\sqrt{2D - 2\sum_\delta \cos(\mathbf{k}\delta)}$, where the summation is done over the nearest neighbors. The effect of the introduced impurity atoms can be considered as a perturbation to the kinetic part of the Hamiltonian: $V = \frac{g}{2m}(\hat{p}_a^2 + \hat{p}_b^2)$, a and b are impurity positions. The coupling constant $g = (1 - m/M)$ with m being the mass of atom of the ideal lattice, M the mass of the impurity atoms, similar to Chapter 2. The momentum operator $\hat{p}_{\mathbf{k}}$ is quantized as $\hat{p}_{\mathbf{k}} = i\sqrt{\frac{m\omega_{\mathbf{k}}}{2}}(\hat{b}_{\mathbf{k}}^\dagger - \hat{b}_{\mathbf{k}})$. This term V is an equivalent of the phonon-impurity coupling given at Eq.(4.5). In terms of the bosonic operators $\hat{b}_{\mathbf{k}}, \hat{b}_{\mathbf{k}}^\dagger$, it reads

$$
\begin{aligned}
V(\mathbf{r}) \;=\;& g\sum_{\mathbf{k},\mathbf{k}'} \sqrt{\omega_{\mathbf{k}}}\sqrt{\omega_{\mathbf{k}'}} \left(-\hat{b}_{\mathbf{k}}^\dagger \hat{b}_{\mathbf{k}'} \cos\frac{(\mathbf{k}-\mathbf{k}')\mathbf{r}}{2} \right. \\
+\;& \left. \hat{b}_{\mathbf{k}}\hat{b}_{\mathbf{k}'} \cos\frac{(\mathbf{k}+\mathbf{k}')\mathbf{r}}{2} + h.c. \right),
\end{aligned}
$$

$\mathbf{r} = \mathbf{r}_b - \mathbf{r}_a$, according to the previous chapter. Rewriting this expression in terms of π and $\bar{\pi}$, one obtains Eq.(4.5). Then we define the Green's functions in accord with Eqs.(4.6), (4.8) and (4.9). Integrations in $G_r^{(0)}(\omega_n)$ and $G(\omega_n)$ are performed over the Brillouin zone, and the integrals in Eqs. (4.8),(4.9) become finite:

$$
\begin{aligned}
G_r^{(0)}(\omega_n) \;&=\; V_c^D \int_{BZ} \frac{d^D k}{(2\pi)^D} \cos\mathbf{k}\mathbf{r}\, \frac{\omega_{\mathbf{k}}^2}{\omega_n^2 + \omega_{\mathbf{k}}^2}, \\
G^{(0)}(\omega_n) \;&=\; V_c^D \int_{BZ} \frac{d^D k}{(2\pi)^D} \frac{\omega_{\mathbf{k}}^2}{\omega_n^2 + \omega_{\mathbf{k}}^2},
\end{aligned} \tag{4.20}
$$

V_c^D is the elementary cell volume in D dimensions.

Now we evaluate $G_r^{(0)}(\omega_n)$, $G^{(0)}(\omega_n)$, $T_1(\omega_n)$ and the Casimir interaction for the cubic lattice with the phonon spectrum $\omega_{\mathbf{k}}$:

$$\omega_{\mathbf{k}} = 2c\sqrt{\sum_{i=1}^{D} \sin^2 \frac{k_i}{2}}, \tag{4.21}$$

where D is the dimensionality. The Green's functions $G_r^{(0)}(\omega_n)$ and $G^{(0)}(\omega_n)$ are

$$G_r^{(0)}(\omega_n) = -f_D\left(\frac{|\omega_n|}{2c}\right),$$

$$G^{(0)}(\omega_n) = 1 - f_D\left(\frac{|\omega_n|}{2c}\right),$$

where the function $f_D(x, r)$ does not contain any divergences and falls off exponentially with energy and distance. It can be analytically calculated in $D = 1$ (see [114]) and estimated in the leading approximation for higher dimensions.

The $T_1(\omega_n)$-matrix can be found exactly by summation of the contributing diagrams:

$$T_1(\omega_n) = \frac{1}{\frac{1-g}{g} + f_D\left(\frac{|\omega_n|}{2c}, 0\right)}, \tag{4.22}$$

The value $g = 1$ corresponds to the unitary limit $a = g/(1 - g) \to \infty$. Namely, this limit corresponds to the scattering of bosons on a static impurity considered in [50]. Far away from this limit, the low energy part of the T-matrix can be considered as constant.

The function f_{1D} is diven by Eq.(3.14) and reads

$$f_{1D}(x) = \frac{x}{\sqrt{1+x^2}}(x+\sqrt{1+x^2})^{-2r}$$

This expression in the limit of small ω_n gives Eq.(4.18), with $a = \frac{g}{1-g}$ and $A = \frac{1}{2c}$.

For the dimensions $D = 2, 3$, a and A are evaluated numerically. For a cubic lattice in 2D and 3D, $G_r(\omega_n)$ in the leading approximation is identical to Eq.(4.15) in the limit of small Matsubara frequencies $\omega_n \ll c/\delta$. The coefficients a, A_D, ω_c in the analytical expressions given above are fitted to match these numerical results. It gives us: $G^{(0)}(\omega_n) = 1 - \frac{\omega_n^2}{2\pi c^2} \log \left| \frac{\omega_c}{\omega_n} \right|$ in 2D. While the coefficient in front of the log is universal in 2D, the value of ω_c depends on the parameters of the lattice. For the square lattice one can approximate $\omega_c^2 \simeq 28$ in units of energy. The same calculation for the hexagonal lattice leads to the phonon spectrum $\omega_{\mathbf{k}}^2 = \frac{8}{3}\left(\sin^2 \frac{k_x}{2} + \sin^2 \frac{k_x+\sqrt{3}k_y}{4} + \sin^2 \frac{k_x-\sqrt{3}k_y}{4}\right)$, with $\omega_c^2 \approx 32$. In 3D, $G^{(0)}(\omega_n) = 1 - \frac{1}{4c^2}\omega_n^2$ in the leading approximation for low energies.

This allows us to approximate the Casimir interaction for the linearized spectrum as:

$$U_{Cas}^{(1D)}(r) = \int_0^\infty \frac{d\omega_n}{2\pi} \log\left[1 - \left(\frac{\frac{|\omega_n|}{2c}e^{-\frac{|\omega_n|}{c}r}}{(1-g)/g + \frac{|\omega_n|}{2c}}\right)^2\right], \qquad (4.23)$$

$$U_{Cas}^{(2D)}(r) = \int_0^\infty \frac{d\omega_n}{2\pi} \log\left[1 - \left(\frac{\frac{|\omega_n|^2}{2\pi c^2}K_0(\frac{|\omega_n|}{c}r)}{(1-g)/g + \frac{|\omega_n|^2}{2\pi c^2}\log|\frac{\omega_c}{\omega_n}|}\right)^2\right], \qquad (4.24)$$

$$U_{Cas}^{(3D)}(r) \simeq \int_0^\infty \frac{d\omega_n}{2\pi} \log\left[1 - \left(\frac{\frac{|\omega_n|^2}{4\pi r c^2}e^{-\frac{|\omega_n|}{c}r}}{(1-g)/g + \frac{|\omega_n|^2}{4c^2}}\right)^2\right], \qquad (4.25)$$

The r dependence of the Casimir interaction is given by Eqs.(4.23)-
(4.25) for various g and $D = 1..3$ is illustrated in Figs.4.5, 4.6. There
are two regions, which are determined by the characteristic distance r_a.
For $r \gg r_a$, one finds the universal scaling $U_D \sim \frac{1}{r^{2D+1}}$. At distances
$r \lesssim r_a$ this interaction is not universal. But at very short distances,
$r \ll r_a = c/\omega_n^*$, the Casimir interaction can be approximated in the lead-
ing order as Eq. (4.19).

In the unitary limit $g \to 1$ (the static limit in terms of the lattice model),
due to the energy dependence of $T_1(\omega_n)$, $U_{1D}(r) \sim 1/r$, $U_{2D}(r) \sim 1/(r \log^2 r)$
and $U_D(r) \sim 1/r^{2D-3}$ for $D \geq 3$ at any r, since $r_a \to \infty$.

4.4.3   Casimir interaction at finite temperatures

Finite temperatures affect the scaling of the Casimir interaction at large
distances since the phonons get damping due to temperature.

The Casimir interaction at finite temperatures is given by Eq.(4.14).
Since $G_r^{(0)}(\omega_n) \sim e^{-\omega_n r/c}$, there are two limiting cases of $r \gg \lambda_T$ and
$r \ll \lambda_T$, where $\lambda_T = c/(2\pi T)$ is the thermal de Broglie wavelength. In
the former case, one restricts the summation by the first term. While
in the latter case, one has to perform the summation over all Matsubara
frequencies.

To illustrate this point, it is worth to consider a 1D system again. In
the explicit form, the thermodynamic potential reads:

$$U_{Cas}^{1D}(r) = T \sum_{n=1}^{\infty} \log \left[1 - \left(\frac{e^{-nr/\lambda_T}}{2\lambda_T(na)^{-1} + 1} \right)^2 \right],$$

where we use $a = g/(1 - g)$. Now there are two characteristic lengths:

(a)

(b)

(c)
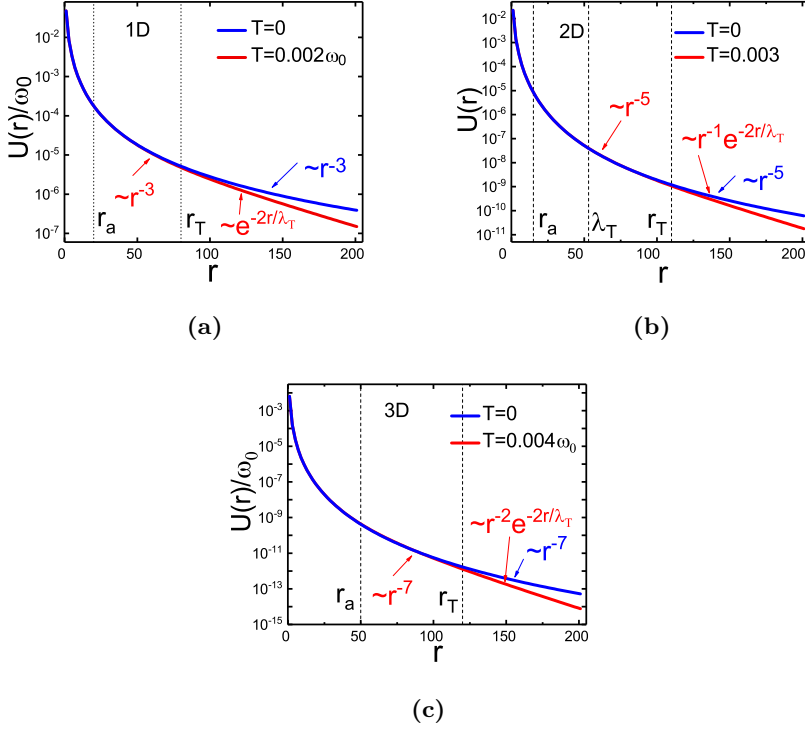
Figure 4.5. Casimir interaction of dynamic impurities at finite temperature and at $T = 0$. r_T is the effective length of the potential. In the units of energy: (a) 1D system with parameter $g = 0.95$. Red line: $T = 0.002\omega_0$. Blue line: $T = 0$. (b) 2D system with $g = 0.99$. Red line: $T = 0.003$. Blue line: $T = 0$. $\lambda_T \simeq 53$ is the de Broglie wavelength, $r_T \simeq 110$. (c) 3D system with $g = 0.999$. Red line: $T = 0.004$. Blue line: $T = 0$.

the characteristic length r_a and r_T of the order of the thermal de Broglie length $r_T \simeq \lambda_T$ (generally speaking, this parameter has a weak dependence on g in $D > 1$ and can differ from λ_T by a numerical factor of the order of 1, as illustrated in Fig.4.5b). For $r \gg r_T$, the sum is dominated by the first Matsubara term and we get a universal exponential decay of the

interaction:

$$U_{Cas}^{1D}(r) \approx -T \frac{e^{-2r/\lambda_T}}{(2\lambda_T/a + 1)^2}, \qquad (4.26)$$

For $r \ll r_a, r_T$ the Casimir interaction follows r^{-1} law. For the intermediate distances $r_a \ll r \ll r_T$, the Casimir interaction falls off as r^{-3}. A special consideration is required when we are exactly in the unitary limit $a \to \infty$. The decay of the Casimir interaction for $r \ll r_T$ in this case is precisely r^{-1}, and it further transfers to the exponential behavior Eq.(4.26) for $r \gg \lambda_T$. These dependencies can be seen at Fig.4.5 and Fig.4.6, in which the Casimir interaction at finite temperatures and at $T = 0$ are presented. As a guideline, we depict approximate borders of the change of the Casimir law r_a and r_T. The detailed derivation of various limits is provided in Section 4.7.3.

The effect of temperature in 2D and 3D systems can be calculated in the same way. The calculations lead to:

$$U_{Cas}^{2D} = T \sum_{n=1}^{\infty} \log \left[1 - \frac{2(K_0(\frac{nr}{\lambda_T}))^2}{\left(\frac{4\pi\lambda_T^2}{n^2 a} + \log \frac{\lambda_T^2 \omega_c^2 + (cn)^2}{(cn)^2} \right)^2} \right]$$

and

$$U_{Cas}^{3D} = T \sum_{n=1}^{\infty} \log \left[1 - \left(\frac{\frac{1}{\pi r} e^{-\frac{nr}{\lambda_T}}}{\frac{4\lambda_T^2}{an^2} + 1} \right)^2 \right].$$

For $r \gg r_T$, the leading contribution to the thermodynamic potential

(a)

(b)

(c)
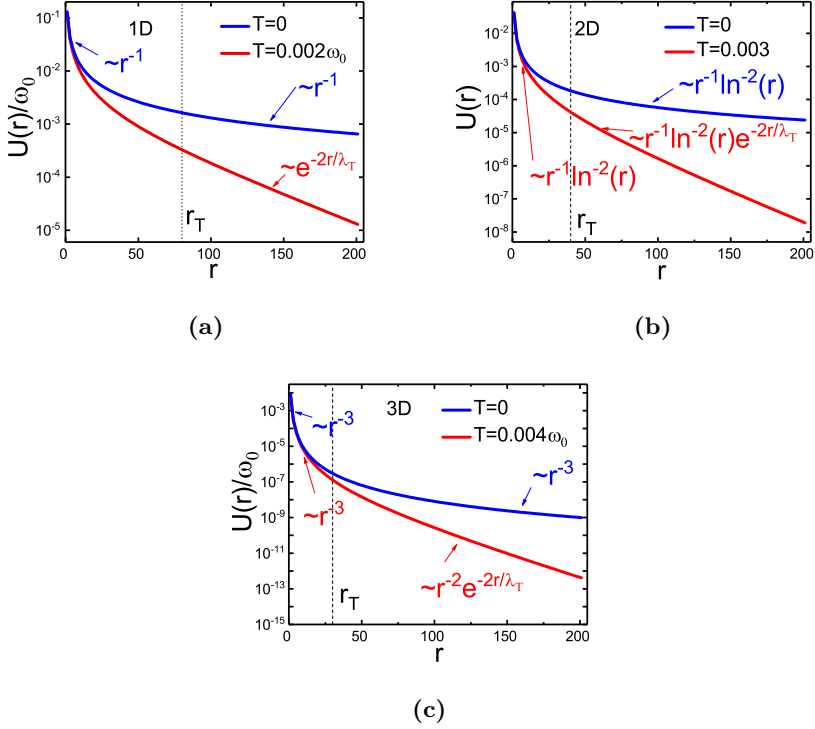
Figure 4.6. Casimir interaction of dynamic impurities in the unitary limit ($g = 1$). (a) 1D system. Red line: $T = 0.002$. Blue line: $T = 0$; (b) 2D system. Red line: $T = 0.003$. Blue line: $T = 0$; (c) 3D system. Red line: $T = 0.004$. Blue line: $T = 0$.

comes from the first Matsubara frequency:

$$U^{2D}_{Cas} \underset{r \gg r_T}{\simeq} - \frac{\frac{\pi T \lambda_T}{4r} e^{-\frac{2r}{\lambda_T}}}{\left(\frac{2\pi \lambda_T^2}{a} + \log\left|\frac{\lambda_T \omega_c}{c}\right| \right)^2} \tag{4.27}$$

and

$$U^{3D}_{Cas} \underset{r \gg r_T}{\simeq} \frac{g^2 T}{r^2 \pi^2} \frac{e^{-\frac{2r}{\lambda_T}}}{(\frac{4\lambda_T^2}{a} + 1)^2}, \tag{4.28}$$

correspondingly. The typical behavior is demonstrated in Figs. 4.5a and

4.5b. Note that, the value of r_T in 2D and 3D is different from de Broglie wave length by some factor. This difference can be clearly seen in Fig. 4.5b.

One can see that at large distances $r \gg r_T$ the decay of the Casimir interaction is exponential in all dimensions. For $r \ll r_T$ and $g < 1$, there is a crossover from the short distance law to the $T = 0$ long range law $r^{-(2D+1)}$.

The Casimir interaction in the unitary limit given in Fig.4.6 demonstrates the asymptotic behavior Eq.(4.19) with the temperature corrections similar to the ones given in Fig.4.5 for the non-unitary case.

4.5 Model for localized impurities in an external field

Now we consider the $\varphi\bar{\varphi}$ interaction. It corresponds to the external potential applied to two given atoms and trapping them at fixed positions. This situation was studied in [50, 114] for the one dimensional case. This case may be relevant for an experimental set-up with trapped quantum gases proposed in [76, 50]. It corresponds to the interaction for the field $\varphi(\mathbf{x})$ from Eq.(4.4):

$$\hat{H}_{int} = g\omega_0^2 \left(\varphi(\mathbf{x})\bar{\varphi}(\mathbf{x})\big|_{\mathbf{x}=-\frac{\mathbf{r}}{2}} + \varphi(\mathbf{x})\bar{\varphi}(\mathbf{x})\big|_{\mathbf{x}=\frac{\mathbf{r}}{2}} \right),$$

(4.29)

The strength of the external potential is given by value $g > 0$, ω_0 is a unit of energy.

The Green's functions for this case are defined as

$$\tilde{G}^{(0)}(\mathbf{x}, \mathbf{x}', \omega_n) = - \int_0^{\frac{1}{T}} d\tau e^{-i\omega_n \tau} \langle T_\tau(\varphi(\mathbf{x}, \tau)\bar{\varphi}(\mathbf{x}', 0)) \rangle.$$

For the calculations, we need two Green's functions at the points $-\frac{\mathbf{r}}{2}, \frac{\mathbf{r}}{2}$, which we denote as

$$\begin{aligned}
\tilde{G}_r^{(0)}(\omega_n) &\equiv& \tilde{G}^{(0)}\left(+\frac{\mathbf{r}}{2}, -\frac{\mathbf{r}}{2}, \omega_n\right) = \tilde{G}^{(0)}\left(-\frac{\mathbf{r}}{2}, +\frac{\mathbf{r}}{2}, \omega_n\right), \\
\tilde{G}^{(0)}(\omega_n) &\equiv& \tilde{G}^{(0)}\left(+\frac{\mathbf{r}}{2}, +\frac{\mathbf{r}}{2}, \omega_n\right) = \tilde{G}^{(0)}\left(-\frac{\mathbf{r}}{2}, -\frac{\mathbf{r}}{2}, \omega_n\right).
\end{aligned}$$

Their explicit expressions are

$$\begin{aligned}
\tilde{G}_{\mathbf{r}}^{(0)}(\omega_n) &=& \int \frac{d^D \mathbf{k}}{(2\pi)^D} \frac{\omega_0^2}{\omega_n^2 + \omega_{\mathbf{k}}^2} e^{-i\mathbf{k}\mathbf{r}}, \\
\tilde{G}^{(0)}(\omega_n) &=& \int \frac{d^D \mathbf{k}}{(2\pi)^D} \frac{\omega_0^2}{\omega_n^2 + \omega_{\mathbf{k}}^2}.
\end{aligned}$$

The explicit form of $\tilde{G}_r^{(0)}(\omega_n)$ is given by the integration above and reads

$$\tilde{G}_r^{(0)}(\omega_n) = \begin{cases} \frac{\omega_0^2}{2|\omega_n|c} e^{-\frac{|\omega_n|}{c}r}, & D = 1, \\ \frac{\omega_0^2}{2\pi c^2} K_0\left(\frac{|\omega_n|}{c}r\right), & D = 2, \\ \frac{\omega_0^2}{4\pi c^2 r} e^{-\frac{|\omega_n|}{c}r}, & D = 3. \end{cases} \tag{4.30}$$

The second order of the perturbation theory in $D = 1$ for $T = 0$ is given by

$$\tilde{U}_{Cas}^{(2)}(r) = \int_0^\infty \frac{d\omega_n}{2\pi} \frac{g^2 \omega_0^4 e^{-2\frac{|\omega_n|}{c}r}}{4\omega_n^2 c^2}.$$

The integral diverges at the lower limit. This divergence can not be elimi-

(a)

(b)

(c)
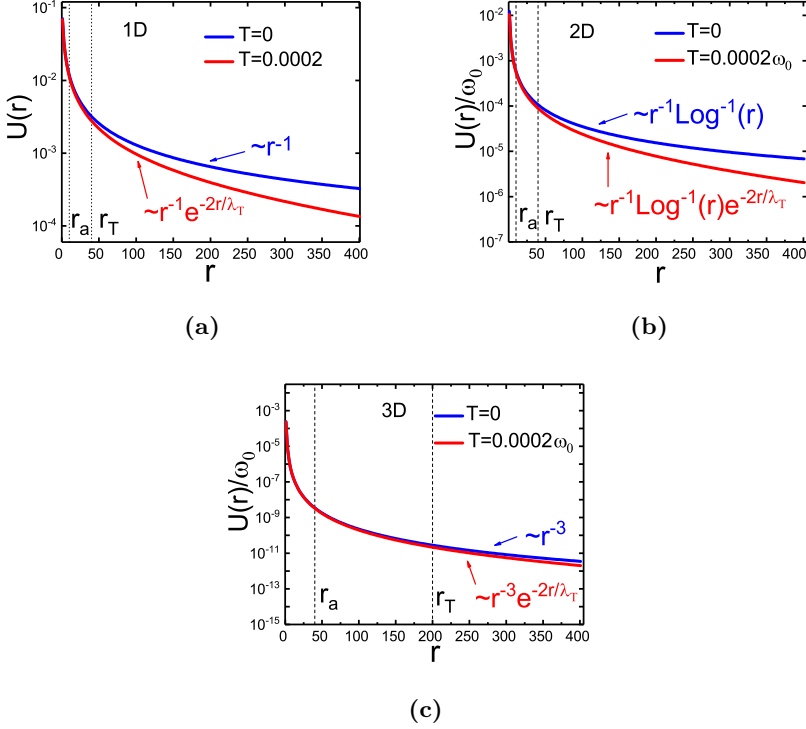
Figure 4.7. Casimir interaction for atoms trapped by external potential at a finite temperature and at $T = 0$. r_T is the effective length of the interaction, $g = 2$, $\omega_0 = 1$. Blue line: $T = 0$, red line: $T = 0.0002$. (a) 1D system. (b) 2D system.(c) 3D system.

nated by introduction of the lattice model. The same infra-red divergence emerges in any order of the perturbation theory. However, the single impurity matrix $\tilde{T}_1(\omega_n)$, which is the sum of the diagrams in Fig.4.2, allows us to renormalize this divergence.

$\tilde{T}_1(\omega_n)$ is defined as

$$\tilde{T}_1(\omega_n) = \frac{g}{1 - g\tilde{G}^{(0)}(\omega_n)}. \tag{4.31}$$

The explicit form of Eq.(4.31) is:

$$
\tilde{T}_1(\omega_n) \simeq
\begin{cases}
\dfrac{-g}{1+\dfrac{g\omega_0^2}{|\omega_n|c}}, & D = 1, \\[4ex]
\dfrac{-g}{1+\dfrac{g\omega_0^2}{2\pi c^2}\log|\frac{\omega_0}{\omega_n}|}, & D = 2, \\[4ex]
\dfrac{-g}{1+\dfrac{g\omega_0^2}{4c^2}}, & D = 3.
\end{cases}
\tag{4.32}
$$

Note that the T-matrix vanishes in the limit $\omega_n \to 0$ in $D = 1, 2$. It means that the impurities become essentially transparent for long-range phonons. The leading contribution comes from phonons of the energy c/r. Therefore, the Casimir interaction cannot be approximated via scatterings at zero energy in the contrast to the model of dynamic impurities.

Substituting Eq.(4.30) and Eq.(4.32) into Eq.(4.14), we calculate the Casimir interaction. It remains finite, since the $\tilde{T}_1(\omega_n)$ cancels the divergence of $\tilde{G}_r^{(0)}(\omega_n)$ at $\omega_n \to 0$.
The results are presented in Fig.4.7. In the long-range limit $r \gg r_a$, the Casimir potential scales as

$$
U_{Cas}(r) \sim
\begin{cases}
\dfrac{1}{r}, & D = 1, \\[3ex]
\dfrac{1}{r\log^2 r}, & D = 2, \\[3ex]
\dfrac{1}{r^3}, & D = 3.
\end{cases}
\tag{4.33}
$$

The characteristic length r_a of the crossover to the long-range limit is smaller than for the dynamic impurities. The difference stems from the low energy behavior of the T-matrix. In contrast to the dynamic impurities, the T-matrix goes quickly to the saturation point. The characteristic

length r_a is fully determined by the saturation energy $\omega^*_{n,D}$ of the T-matrix as $r_a \sim c/\omega^*_{n,D}$. The saturation energies are: $\omega^*_{n,1D} \sim g\omega_0^2/c$, $\omega^*_{n,2D} \sim \omega_0 e^{-\frac{g\omega_0^2}{2\pi c^2}}$. Since $\tilde{T}_1 \simeq const$ for $D = 3$, $r_{a,3} = 0$, and the $\frac{1}{r^3}$-law is fulfilled at all distances.

Comparing the long-range behavior with the unitary limit of the dynamic impurities, one finds that the scaling is exactly the same. It is originated from the fact that the both cases describe the same physical picture of two classical localized impurities of infinite mass. Mathematically, it follows from the identity (see Section 4.7.4):

$$T_1\,(\omega_n)|_{g=1}\,G_r^{(0)}(\omega_n) = \tilde{T}_1\,(\omega_n)|_{g=\infty}\,\tilde{G}_r^{(0)}(\omega_n). \qquad (4.34)$$

Similar to the model of dynamic impurities, the power law changes to exponential at finite temperatures at long distances. The characteristic length r_T is determined by the thermal de Broglie length with $r_T \sim c/2\pi T$. The crossover to the thermal regime is demonstrated in Fig. 4.7.

4.6   Discussion

Through the chapter, we considered the Casimir interaction mediated by acoustic phonons. The phonon-mediated Casimir interaction between the dynamic impurities scales as $r^{-(2D+1)}$ in D dimensions for large distance in a continuum model. The result remains the same for large distances in a lattice model. A small difference can be found only at short distances $r \ll r_a$. The Casimir interaction at long distances is universal. The comparison of the Casimir interaction for the lattice model and the continuum model is given in Section 4.7.5. The reason for the similarity of the results is the

dominating contribution of low-energy phonons, for which the spectrum can be linearized.

It is worth to outline the relation between the considered model and the phonon mediated Casimir interaction in the Luttinger liquid in 1D. The model, in contrast to the Luttinger liquid, does not contain vertex corrections to the phonon-impurity scattering [107, 105, 106, 51]. To map the Luttinger liquid model to our model, we assume the phonon-impurity amplitude as a phenomenological parameter. The bare phonon-impurity interaction element coincides with that derived in the leading order in the Supplementary material of [51]. For 1D systems, our results for dynamic impurities in the second order of perturbation theory are identical to the model of [51]. The results for static impurities are identical to the one considered in [50]. Further, we demonstrated that the results for the two models converge in the limit of infinite mass of the impurities.

An impurity in a Luttinger liquid may be dressed by a density depletion cloud [139]. These depletion clouds are relevant for interactions between static impurities in a Bose gas [50, 84], but neglectable for dynamic impurities [51] and for static impurities in a Fermi gas [50]. Our model corresponds two latter cases.

The model is restricted only on the phonon mediated interaction. In real gases of cold atoms in addition to the phonon mediated interaction, dipole-dipole interactions can arise [112], but the phonon-induced Casimir interaction falls off much slower and therefore dominates over the dipole-dipole interactions as estimed in the previous chapter.

The Casimir interaction for cold atoms in 1D the phonon-induced interaction may be observable. As estimated in [51], for the experimental

set-up [79] of ^{40}K atoms with ^{87}Rb atoms as impurities, the Casimir interaction is expected to be $\sim 1kHz$ at $0.14\mu m$ separation between the impurities. For the parameters of this set-up, we estimate $\omega_0 \simeq 400kHz$ and the red line given in Fig.4.5a corresponds to $T = 40nK$, with $r_T \simeq 6\mu m$ (the interaction parameter g used in our paper is the low-energy scattering amplitude given in [51]).

An observable phonon induced Casimir interaction may also arise in two and three dimensional lattices with high Debye frequency. Particularly interesting material for this is solid hydrogen with deuterium impurities, since in addition to high Debye frequency, this system has a relatively large coupling parameter $g = \frac{1}{2}$ (due to the mass ratio $\frac{m_D}{m_H} = 2$). With the phonon energies are the order of $10meV$ [94], the Casimir energy between nearest neighbors impurities is expected to be $U_{Cas} \simeq 2\mu eV$. Other promising systems from this point of view are hydrates like H_3S [140], and superhydrides, as LaH_{10} [141], etc. These materials, synthesized under high pressures, currently attract enormous attention due to unusually high critical temperatures of superconductivity, which is a consequence of high Debye frequencies. But consideration of multi-atomic lattices is out of the scope of the present thesis.

4.7 Appendices

4.7.1 Appendix A. The lattice model

In this section, we derive the effective phonon-impurity interaction for a cubic harmonic lattice in terms of the field $\pi(x)$ and $\phi(x)$ following

Chapter 2 closely. The lattice is determined by the following Hamiltonian:

$$H = \sum_i \frac{\hat{\mathbf{p}}_i^2}{2m} + \frac{m\omega_0^2}{2} \sum_{|i-j|=1} (\hat{\mathbf{u}}_i - \hat{\mathbf{u}}_j)^2,$$

where m is the mass of the atoms and ω_0 is the characteristic energy of the nearest-neighbors interaction. After quantization and the Bogolubov transformation the Hamiltonian takes the standard form for free phonons:

$$H = \sum_{\mathbf{k}} \omega_{\mathbf{k}} \left(b_{\mathbf{k}}^\dagger b_{\mathbf{k}} + \frac{1}{2} \right),$$

where $b_{\mathbf{k}}^\dagger$, $b_{\mathbf{k}}$ are creation and annihilation phonon operators and their dispersion in D dimensions is

$$\omega_{\mathbf{k}} = \omega_0 \sqrt{2D\nu_{\mathbf{k}}}; \; \nu_{\mathbf{k}} = 1 - \frac{1}{D} \sum_{i=1}^{D} \cos(q_i\delta),$$

with δ being a lattice constant. For $q\delta \ll 1$ one gets $\omega_k = ck$ with the sound velocity $c\omega_0\delta$.

Below, we consider two types of the perturbations at the site i: *a)* the mass of the atom at site i is changed to M without modification of the interaction with the nearest atoms (isotopic substitution). *b)* a local external harmonic potential is applied to the atom at position i.

a) The perturbation is determined by the difference of the kinetic energy of the impurity atom at the site i in comparison to the regular atom of

the lattice:

$$\hat{H}_{int} = \frac{\hat{\mathbf{p}}_i^2}{2} \left(\frac{1}{M} - \frac{1}{m} \right).$$

Introducing $g = \left(1 - \frac{m}{M} \right)$, one can rewrite the expression in terms of phonon operators:

$$H_{int} = -g \sum_{\mathbf{k},\mathbf{k}'} \sqrt{\omega_{\mathbf{k}} \omega_{\mathbf{k}'}} \left(b_{\mathbf{k}} b_{\mathbf{k}'}^\dagger e^{-i\mathbf{r}_i(\mathbf{k}-\mathbf{k}')} + b_{\mathbf{k}}^\dagger b_{\mathbf{k}'} e^{i\mathbf{r}_i(\mathbf{k}-\mathbf{k}')} \right.$$
$$\left. - b_{\mathbf{k}} b_{\mathbf{k}'} e^{-i\mathbf{r}_i(\mathbf{k}+\mathbf{k}')} - b_{\mathbf{k}}^\dagger b_{\mathbf{k}'}^\dagger e^{i\mathbf{r}_i(\mathbf{k}+\mathbf{k}')} \right),$$

which is in the short form:

$$H_{int} = -g\pi(\mathbf{r}_i)\bar{\pi}(\mathbf{r}_i).$$

b) The perturbation is

$$H_{int} = gm\omega_0^2 \left(\hat{\mathbf{u}}_i^2 \right),$$

The expression in terms of phonon operators:

$$H_{int} = g \sum_{\mathbf{k},\mathbf{k}'} \frac{1}{\sqrt{\omega_{\mathbf{k}} \omega_{\mathbf{k}'}}} \left(b_{\mathbf{k}} b_{\mathbf{k}'}^\dagger e^{-i\mathbf{r}_i(\mathbf{k}-\mathbf{k}')} + b_{\mathbf{k}}^\dagger b_{\mathbf{k}'} e^{i\mathbf{r}_i(\mathbf{k}-\mathbf{k}')} \right.$$
$$\left. + b_{\mathbf{k}} b_{\mathbf{k}'} e^{-i\mathbf{r}_i(\mathbf{k}+\mathbf{k}')} + b_{\mathbf{k}}^\dagger b_{\mathbf{k}'}^\dagger e^{i\mathbf{r}_i(\mathbf{k}+\mathbf{k}')} \right),$$

which is in the short form:

$$H_{int} = g\omega_0^2 \varphi(\mathbf{r}_i)\bar{\varphi}(\mathbf{r}_i).$$

4.7.2 Appendix B. Evaluation of $G_r^{(0)}(\omega_n)$, $G^{(0)}(\omega_n)$ and $T_1(\omega_n)$

Linear spectrum. Here we evaluate Eq.(4.8) for the linear spectrum $\omega_n = c|\mathbf{k}|$ at large distances. For $r \neq 0$, it reads

$$G_r^{(0)}(\omega_n) = -\int \frac{dk_\parallel d^{D-1}\mathbf{k}_\perp}{(2\pi)^D} \frac{\omega_n^2}{\omega_n^2 + c^2 k_\perp^2 + c^2 k_\parallel^2} e^{-ik_\parallel r},$$

where D is the number is dimensions. We represented the vector $\mathbf{k}$ as $\mathbf{k} = \mathbf{k}_\perp + \mathbf{k}_\parallel$ and chose $\mathbf{k}_\parallel$ along $\mathbf{r}$. After integration over $k_\parallel$, we have

$$-C_D \left(\frac{\omega_n}{c}\right)^2 \int_0^\infty dk_\perp \frac{k_\perp^{D-2}}{\sqrt{(\frac{\omega_n}{c})^2 + k_\perp^2}} e^{-\sqrt{(\frac{\omega_n}{c})^2 + k_\perp^2}\, r},$$

where $C_D = \frac{\pi}{(2\pi)^D} \int d\Omega_{D-1}$ is a constant containing all angular integrations.

We renomalize the momentum introducing a new dimensionless variable q defined as: $k_\perp \to q\frac{\omega_n}{c}$. The contribution of large values of the momentum to the integral is exponentially small, so only small momenta matter here. It turns the integral into

$$-\ C_D \left(\frac{|\omega_n|}{c}\right)^D \int_0^\infty dq \frac{q^{D-2}}{1+q^2} e^{-\sqrt{1+q^2}\frac{|\omega_n|}{c} r} \underset{r\frac{|\omega_n|}{c} \gg 1}{\simeq}$$

$$-\ C_D \left(\frac{|\omega_n|}{c}\right)^D e^{-\frac{|\omega_n|}{c} r} \int_0^\infty q^{D-2} e^{-\frac{q^2}{2}\frac{\omega_n}{c} r} dq.$$

The remaining integral can be evaluated exactly and gives $2^{\frac{D-3}{2}} (\frac{|\omega_n|}{c} r)^{-\frac{D-1}{2}} \Gamma(\frac{D-1}{2})$. It leads us to Eq.(4.16):

$$G_r^{(0)}(\omega_n) \simeq C_D 2^{\frac{D-3}{2}} \Gamma\left(\frac{D-1}{2}\right) \left(\frac{|\omega_n|}{c}\right)^{\frac{D+1}{2}} r^{-\frac{D-1}{2}} e^{-\frac{|\omega_n|}{c} r}.$$

$G^{(0)}(\omega_n)$ diverges on the upper limit. Therefore, a cut-off ω_c is introduced. This cut-off is used here formally, all the divergent terms are included into the T-matrix. Its value for impurity-phonon scatterings can be measured experimentally and, therefore, there are no real divergences in this approach. Then the integration yields:

$$G^{(0)}(\omega_n) \simeq \begin{cases} \frac{\omega_c}{\pi c} - \frac{|\omega_n|}{2c}, & D = 1, \\ \frac{\omega_c^2}{4\pi c^2} - \frac{|\omega_n|^2}{2\pi c^2} \log\left|\frac{\omega_c}{\omega_n}\right|, & D = 2, \\ \frac{\omega_c^3}{6\pi^2 c^3} - \frac{\omega_c |\omega_n|^2}{2\pi^2 c^3}, & D = 3. \end{cases}$$

Since the $T_1(\omega_n)$-matrix is given by the diagrams Fig.4.2, it has the form

$$T_1(\omega_n) = \frac{g}{1 - g G^{(0)}(\omega_n)}. \tag{4.35}$$

Substitution of $G^{(0)}(\omega_n)$ gives in the low energy limit the form of the T-matrix given in Eq. (4.18).

Lattice. The integrals (4.8) and (4.9) are convergent on the lattice:

$$G_x^{(0)}(\omega_n) = V_c \int_{BZ} \frac{d^D k}{(2\pi)^D} \frac{\omega_{\mathbf{k}}^2}{\omega_n^2 + \omega_{\mathbf{k}}^2} e^{i\mathbf{k}\cdot\mathbf{x}} = V_c \int_{BZ} \frac{d^D k}{(2\pi)^D} e^{i\mathbf{k}\cdot\mathbf{x}}$$

$$- V_c \int_{BZ} \frac{d^D k}{(2\pi)^D} \frac{\omega_n^2}{\omega_n^2 + \omega_{\mathbf{k}}^2} e^{i\mathbf{k}\cdot\mathbf{x}} = \delta_{x,0} - f_D\left(\frac{|\omega_n|}{2c}, x\right).$$

For $D = 1$, on a square lattice it results into $G^{(0)}(\omega_n) = 1 - f_1(\frac{|\omega_n|}{2c}, 0)$, with $f_1(x, r) = \frac{x}{\sqrt{1+x^2}}(x + \sqrt{1+x^2})^{-2r}$. In the small ω_n limit, this function turns into $G^{(0)}(\omega_n) = 1 - \frac{|\omega_n|}{2c}$. For higher dimensions, the structure $1 - f_D(\frac{|\omega_n|}{2c}, 0)$, with some finite function f_D, remains.

For $D \geq 3$, the Green function $G^{(0)}(\omega_n)$ can be approximated:

$$G^{(0)}(\omega_n) = 1 - \omega_n^2 V_c \int_{BZ} \frac{d^D k}{(2\pi)^D} \frac{1}{\omega_n^2 + \omega_{\mathbf{k}}^2} \simeq 1 - \omega_n^2 V_c \int_{BZ} \frac{d^D k}{(2\pi)^D} \frac{1}{\omega_{\mathbf{k}}^2}.$$

It means, that $G^{(0)}(\omega_n) \simeq 1 - A_D \omega_n^2$, with constant A_D.

For $D = 1$, one gets $G^{(0)}(\omega_n) - 1 \sim \omega_n$.

For $D = 2$ the integral is $G^{(0)}(\omega_n) - 1 \sim \omega_n^2 \log |\omega_n|$.
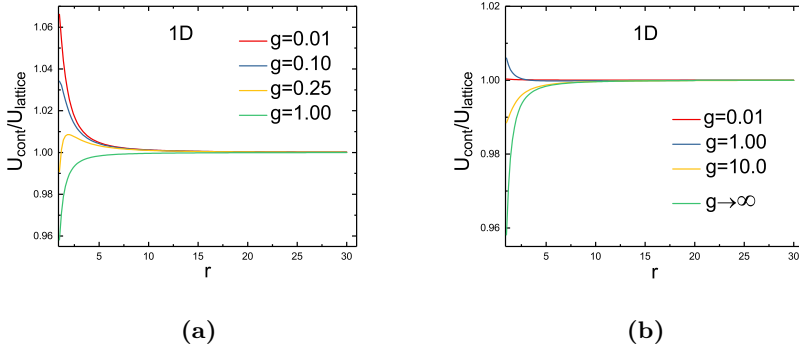
Figure 4.8. The ratio of the 1D Casimir interaction in the continuum limit U_{cont} and the lattice model $U_{lattice}$. Here T=0, **(a)** dynamic impurities, red line – $g = 0.01$, blue line – $g = 0.1$, yellow line – $g = 0.25$, green line – $g = 1$. **(b)** impurities localized in the external potential, red line – $g = 0.01$, blue line – $g = 1$, yellow line – $g = 10$, green line – $g \to \infty$.

4.7.3 Appendix C. Asymptotic behavior of the Casimir interaction at finite temperatures

Low temperature corrections in 1D. At low temperatures and short distances, when $r \ll \lambda_T$, we use the Euler-Maclaurin formula up to the

first term to approximate the sum:

$$U_{Cas}^{1D}(r) \underset{r \ll \lambda_T}{\simeq} c \int_0^\infty \frac{dx}{2\pi r} \log \left[1 - \left(\frac{\frac{gx}{2r} e^{-x}}{1 - g + \frac{gx}{2r}} \right)^2 \right]$$

$$- \frac{1}{12} \frac{d}{dn} T \log \left[1 - \left(\frac{\frac{g\pi nT}{c} e^{-2\pi^2 n \frac{r}{\lambda_T}}}{1 - g + \frac{g\pi nT}{c}} \right)^2 \right]^2 \Bigg|_{n=1}.$$

At $g = 1$ it gives

$$U_{Cas}^{1D}(r) \underset{r \ll \lambda_T}{\simeq} -\frac{\pi c}{24r} + \frac{2\pi^2 rT}{\lambda_T},$$

while for small g it gives

$$U_{Cas}^{1D}(r) \underset{r \ll \lambda_T}{\simeq} -\frac{g^2 c}{32\pi r^3} + \frac{g^2 \pi^6 rT}{\lambda_T^3}.$$

Low temperature corrections in 2D. In the same way as in the one dimensional case, there are two limiting cases for $r \ll \lambda_T$. For $g \ll 1$ we have:

$$U_{Cas}^{2D}(r, T) \underset{r \ll \lambda_T}{\simeq} -\frac{g^2 c}{128\pi r^5} + \frac{4g^2}{3}\pi^2 T^5 \log^2 \left(\frac{r}{\lambda_T} \right)$$

At $g = 1$, the leading terms are:

$$U_{Cas}^{2D}(r, T) \underset{r \ll \lambda_T}{\simeq} -\frac{1}{2} \left(\frac{1}{r \log \omega_c r} - \frac{1}{r \log^2 \omega_c r} \right)$$

$$- \frac{\pi}{6} T \frac{\log \left(\frac{r}{\lambda_T} \right)}{\log^2 \omega_c^2}.$$

Low temperature corrections in 3D. For $r \ll \lambda_T$, we again consider two cases. At $g = 1$, we have:

$$U_{Cas}^{3D} \underset{r \ll \lambda_T}{\simeq} -\frac{c}{8\pi r} Li_2 \left(\frac{1}{r^2 \pi^2} \right) + \frac{2T}{\pi r c},$$

where $Li_2(x)$ is the polylogarithmic function.

And $g \ll 1$ gives us:

$$U_{Cas}^{3D} \underset{r \ll \lambda_T}{\simeq} -\frac{g^2 c}{256 \pi^3 r^7} + \frac{2g^2 \pi^2 T^5}{r^2 c^4} - \frac{2g^2 \pi^3 T^6}{r c^5}.$$

Casimir energy at non-zero temperature in the second order of the perturbation theory. Here we evaluate the Casimir energy at non-zero temperature in the second order in relation to the parameter g. The energy is given by:

$$U_{Cas}^{(2)}(r) = T \sum_{n=1}^{\infty} \left(g G_r^{(0)}(\omega_n) \right)^2,$$

$G_r(\omega_n)$ is taken from Eq.(4.15).

In the one-dimensional case, the energy reads as:

$$U_{1D}^{(2)} = Tg^2 \sum_{n=1}^{\infty} \left(\frac{\pi n T}{c} \right)^2 e^{-\frac{4\pi n T r}{c}} = \frac{g^2 T^3 \pi^2}{4c^2} \frac{\cosh\left(\frac{r}{\lambda_T} \right)}{\sinh^3\left(\frac{r}{\lambda_T} \right)}.$$

This expression is in accordance with the result given in the Supplemental Material of [51].

In the three-dimensional case, the energy turns into:

$$
\begin{aligned}
U_{3D}^{(2)} &= Tg^2 \sum_{n=1}^{\infty} \left(\frac{\pi n^2 T^2}{rc^2} \right)^2 e^{-2\frac{r}{\lambda_T}} \\
&= \frac{g^2 \pi^2 T^5}{4r^2 c^4} \frac{\cosh^3(\frac{r}{\lambda_T}) + 2\cosh\left(\frac{r}{\lambda_T}\right)}{\sinh^5(\frac{r}{\lambda_T})}.
\end{aligned}
$$

4.7.4 Appendix D. Infinitely heavy dynamical impurities vs impurities in an external potential

In this subsection, we demonstrate the identity Eq.(4.34). For the system with dynamical impurities, it means that their masses $M \to \infty$. For the system of impurities in external potential, it means $g\omega_0 \to \infty$, so in both cases the impurities are completely static. We consider our systems on a lattice with a general spectrum and dimensionality.

For the $\pi\bar{\pi}$ interaction, the Green's functions are given by Eq.(4.20). For the $\varphi\bar{\varphi}$ interaction, the corresponding Green's functions are

$$
\begin{aligned}
\tilde{G}_{\mathbf{r}}^{(0)}(\omega_n) &= V_c^D \int_{BZ} \frac{d^D \mathbf{k}}{(2\pi)^D} \cos \mathbf{kr} \frac{\omega_0^2}{\omega_n^2 + \omega_{\mathbf{k}}^2}, \\
\tilde{G}^{(0)}(\omega_n) &= V_c^D \int_{BZ} \frac{d^D \mathbf{k}}{(2\pi)^D} \frac{\omega_0^2}{\omega_n^2 + \omega_{\mathbf{k}}^2}.
\end{aligned}
$$

The T_1- and $\tilde{T}_1$-matrices are defined by Eq.(4.35) and Eq.(4.31) correspondingly. In the limit of static impurities they take form

$$
\begin{aligned}
T_1\left(\omega_n\right)\big|_{g=1} &= \frac{1}{1 - V_c^D \int_{BZ} \frac{d^D\mathbf{k}}{(2\pi)^D}\left(1 - \frac{\omega_n^2}{\omega_n^2 + \omega_\mathbf{k}^2}\right)} \\
&= \frac{1}{V_c^D \int_{BZ} \frac{d^D\mathbf{k}}{(2\pi)^D} \frac{\omega_n^2}{\omega_n^2 + \omega_\mathbf{k}^2}}, \\
\tilde{T}_1\left(\omega_n\right)\big|_{g=\infty} &= -\frac{1}{V_c^D \int_{BZ} \frac{d^D\mathbf{k}}{(2\pi)^D} \frac{\omega_0^2}{\omega_n^2 + \omega_\mathbf{k}^2}}.
\end{aligned}
$$

Multiplying them by $G_r^{(0)}(\omega_n)$ and $\tilde{G}_r^{(0)}(\omega_n)$ correspondingly, we have

$$
\begin{aligned}
T_1\left(\omega_n\right)\big|_{g=1} G_r^{(0)}(\omega_n) &= -\frac{\int_{BZ} d^D\mathbf{k}\frac{\cos\mathbf{kr}}{\omega_n^2 + \omega_\mathbf{k}^2}}{\int_{BZ} d^D\mathbf{k}\frac{1}{\omega_n^2 + \omega_\mathbf{k}^2}}, \\
\tilde{T}_1\left(\omega_n\right)\big|_{g=\infty} \tilde{G}_r^{(0)}(\omega_n) &= -\frac{\int_{BZ} d^D\mathbf{k}\frac{\cos\mathbf{kr}}{\omega_n^2 + \omega_\mathbf{k}^2}}{\int_{BZ} d^D\mathbf{k}\frac{1}{\omega_n^2 + \omega_\mathbf{k}^2}}.
\end{aligned}
$$

Therefore, these two expressions are identical.

4.7.5 Appendix E. Proof of Eq.(4.34)

In this section, we consider effects of the weak non-linearities in the spectrum of phonons.

For this reason, we compare the $1D$ lattice model with continuum limit at $T = 0$. The spectrum in the lattice model is $\omega_k = 2c|\sin\frac{k}{2}|$. We put the lattice constant $\delta = 1$ further.

Considering dynamical impurities ($\pi\bar{\pi}$-interaction), we need the Green's

functions for this spectrum. These Green's functions were found in [114]:

$$
\begin{aligned}
G_r^{(0)}(\omega_n) &= -\frac{\frac{\omega_n}{2c}}{\sqrt{1 + \left(\frac{\omega_n}{2c}\right)^2}} \left(\frac{\omega_n}{2c} + \sqrt{1 + \left(\frac{\omega_n}{2c}\right)^2}\right)^{-2r}, \\
G^{(0)}(\omega_n) &= 1 - \frac{\frac{\omega_n}{2c}}{\sqrt{1 + \left(\frac{\omega_n}{2c}\right)^2}}.
\end{aligned}
$$

In the low energy limit, these expressions can be simplified as

$$
\begin{aligned}
G_r^{(0)}(\omega_n) &\simeq -\frac{\omega_n}{2c} e^{-\frac{\omega_n}{c} r}, \\
G^{(0)}(\omega_n) &\simeq 1 - \frac{\omega_n}{2c},
\end{aligned}
$$

giving us the Green's function for the linear spectrum.

For localized impurities ($\varphi\bar{\varphi}$-interaction), the corresponding Green's functions read

$$
\begin{aligned}
\tilde{G}_r^{(0)}(\omega_n) &= \frac{\frac{\omega_0^2}{2\omega_n c}}{\sqrt{1 + \left(\frac{\omega_n}{2c}\right)^2}} \left(\frac{\omega_n}{2c} + \sqrt{1 + \left(\frac{\omega_n}{2c}\right)^2}\right)^{-2r}, \\
\tilde{G}^{(0)}(\omega_n) &= \frac{\frac{\omega_0^2}{2\omega_n c}}{\sqrt{1 + \left(\frac{\omega_n}{2c}\right)^2}}.
\end{aligned}
$$

The low energy limit Green's functions (corresponding to the case of linear spectrum) are

$$
\begin{aligned}
\tilde{G}_r^{(0)}(\omega_n) &\simeq \frac{\omega_0^2}{2\omega_n c} e^{-\frac{\omega_n}{c} r}, \\
\tilde{G}^{(0)}(\omega_n) &\simeq \frac{\omega_0^2}{2\omega_n c}.
\end{aligned}
$$

The ratios between the potentials for continuous ($U_{cont}(r)$) and lattice ($U_{lattice}(r)$) spectra are given in Fig.4.8. It demonstrates that small corrections to the result ($\sim 1\%$ of potential for the linear spectrum), appear at $r \sim \delta$ and quickly vanish.

Chapter 5

Single hole propagation in a two dimensional ferromagnet

5.1   Ferromagnetism in two dimensional systems

Nowadays, two-dimensional (quasi-two-dimensional) magnets attract a lot of attention due to a variety of novel physical phenomena [142, 143]. It has been known for quite long that two-dimensional antiferromagnets possess rich families of transitions between classical, quantum and quantum critical phases [144, 145, 146, 147, 148].

Recent years, two-dimensional ferromagnetic atomic crystals were predicted [149, 150, 151, 152, 153, 154] and observed experimentally [155]. It has led to a surge of interest to these structures due to their potential in device applications [156].

The ferromagnetic order is reported in thin layers, up to a single layer, in such transition metal-based compounds as $CrBr_3$ [157], CrI_3 [158], K_2CuF_4 [150], $Cr_2Ge_2Te_6$ [159, 155]. They exists because the Mermin-Wagner theorem's restriction on the stability of ferromagnetism [160] is lifted in these compounds by their quasi-two-dimensionality and strong magnetocrystalline anisotropy [161]. A recent study [157] of heterostructures based on $CrBr_3$ shows magnon-assisted tunnelling in this system, which gives an opportunity for creation of new spintronics devices, such as spin-filtering tunneling of the tunnel current.

In this chapter, we consider how a charged quasiparticle propagates in ferromagnetic material if the propagation process is accompanied by the spin-flip processes. We discuss the physical relevance of such models with two systems. The first one is a quasiparticle in a system of two ferromagnetic layers coupled antiferromagnetically (this configuration is reported for $CrCl_3$ [149, 162]). The second is a model of a hole in a ferromagnetic monolayer with strong spin-orbit coupling. Then we develop a theory for the single-hole propagation within such a two-dimensional ferromagnet considering as well a finite magnetic field and analyze the spectral function of the hole. We show that for certain magnetic fields the hole quasiparticle spectral weight vanishes.

The problem of hole propagation was studied in detail in the context of the metal-insulator transitions in two-dimensional antiferromagnets close to half-filling [163]. Numerous studies show that the system can be described in the polaronic quasiparticle formalism [164, 165, 163, 166, 167, 168, 169]. A single hole propagating in the system changes

the local spin configuration and creates magnetic excitations. This cloud of magnons strongly renormalizes the hole, resulting into the so-called spin polaron. The same mechanism is applicable for the so-called orbital polarons appearing as a consequence of the orbital order distortion by the hole [170, 171, 172]. The existence of such polarons in the system means that the renormalized holes propagate through the material, giving it metallic properties. In contrast, if too many magnons are created by a hole, they can effectively prevent propagation, lead to localization of the charges and thus render the material insulating. In contrast to isotropic antiferromagnets where the Goldstone mode is linear $\omega \propto k$, the Goldstone mode in isotropic ferrmagnets is quadratic, $\omega \propto k^2$. One expects that the effects of the magnon excitations can be more pronounced in the ferromagnets. Such ferromagnetic systems were not investigated so far and is the main topic of the consideration below.

5.2   Hole propagation in two ferromagnetic layers

In this section we consider two ferromagnetic layers of localized spins which are ordered antiferromagnetically between the layers. For the quasi-two-dimensional van der Waals crystals, the interlayer magnetic coupling is much weaker than the intralayer coupling and the hopping matrix elements of the electron [155], therefore we neglect the interlayer interaction, even if this coupling will affect the spectrum of magnons as very low energies. A single electron introduced into this system can then propagate due to either intralayer or interlayer hopping. At the same time, the elec-

tron interacts with the localized spins. The full Hamiltonian includes the spin-spin intra- and interlayer interaction part

$$H_S = \sum_{<i,j>} \left[J\vec{\mathbf{S}}_{ai}\vec{\mathbf{S}}_{aj} + J\vec{\mathbf{S}}_{bi}\vec{\mathbf{S}}_{bj} + J_{ab}\vec{\mathbf{S}}_{ai}\vec{\mathbf{S}}_{bj} \right].$$

It defines the spectra of magnons in layers a and b. We assume that J is the same in both layers, $J_{ab} \ll J, t, t_0$.

The interaction is described by the ferromagnetic Kondo model. The Hamiltonian for this model reads

$$
\begin{aligned}
H_{sd} &= -\sum_{\mathbf{k},\alpha} \left[\varepsilon_{\mathbf{k}} \left(c^\dagger_{\mathbf{k}a\alpha}c_{\mathbf{k}a\alpha} + c^\dagger_{\mathbf{k}b\alpha}c_{\mathbf{k}b\alpha} \right) + t \left(c^\dagger_{\mathbf{k}a\alpha}c_{\mathbf{k}b\alpha} + c^\dagger_{\mathbf{k}b\alpha}c_{\mathbf{k}a\alpha} \right) \right] \\
&+ J_K \sum_{\mathbf{k},\mathbf{q},\alpha,\beta} \left(c^\dagger_{\mathbf{k}a\alpha}\vec{\sigma}_{\alpha\beta}c_{\mathbf{k}-\mathbf{q}a\beta}\vec{\mathbf{S}}_{\mathbf{q}a} + c^\dagger_{\mathbf{k}b\alpha}\vec{\sigma}_{\alpha\beta}c_{\mathbf{k}-\mathbf{q}b\beta}\vec{\mathbf{S}}_{\mathbf{q}b} \right), \quad (5.1)
\end{aligned}
$$

where $c^\dagger_{\mathbf{k}a\alpha}$ ($c_{\mathbf{k}a\alpha}$) are creation (annihilation) operators of electron, α, β are spin indexes, a, b are layer indexes, $\vec{\mathbf{S}}$ are operators of the localized spins.

Couplings J_K between the localized spin and spin of itinerant electron at each site of both layers are assumed to be identical. $\varepsilon_{\mathbf{k}} = 2t_0 \left(\cos k_x + \cos k_y \right)$ (at the square lattice), t and t_0 are interlayer and intralayer hopping parameters respectively.

Let us start with the case when there are no spin-spin interactions, so we have only hopping terms in Eq. (5.1):

$$H_{hopping} = -\sum_{\mathbf{k},\alpha} \begin{pmatrix} c^\dagger_{\mathbf{k}a\alpha} & c^\dagger_{\mathbf{k}b\alpha} \end{pmatrix} \begin{pmatrix} \varepsilon_{\mathbf{k}} & t \\ t & \varepsilon_{\mathbf{k}} \end{pmatrix} \begin{pmatrix} c_{\mathbf{k}a\alpha} \\ c_{\mathbf{k}b\alpha} \end{pmatrix}$$

Introducing symmetric and antisymmetric operators
$d_{\mathbf{k},\alpha} = \frac{1}{\sqrt{2}}\left(c_{\mathbf{k},b,\alpha} + c_{\mathbf{k},a,\alpha}\right)$, $\tilde{d}_{\mathbf{k},\alpha} = \frac{1}{\sqrt{2}}\left(c_{\mathbf{k},b,\alpha} - c_{\mathbf{k},a,\alpha}\right)$, we bring the hopping Hamiltonian to the form

$$H_{hopping} = -\sum_{\mathbf{k}}\left[(\varepsilon_{\mathbf{k}} + t)d^{\dagger}_{\mathbf{k}\alpha}d_{\mathbf{k}\alpha} + (\varepsilon_{\mathbf{k}} - t)\tilde{d}^{\dagger}_{\mathbf{k}\alpha}\tilde{d}_{\mathbf{k}\alpha}\right]. \qquad (5.2)$$

For simplicity, we assume $t \gg t_0$, so the anti-symmetric state $\tilde{d}$ has much higher energy than the symmetric one and can be neglected. In general, most of the results remain the same for the full model Eq. (5.2).

We choose a laboratory system of coordinates along the localized spins in the layer a. To describe the spins of the layer b in this system, we rotate the local coordinates of this layer along x-axis. Thus, the spins in the layer b are transformed as $\tilde{S}^{z}_{b} \rightarrow -S^{z}_{b}$, $\tilde{S}^{x}_{b} \rightarrow S^{x}_{b}$, $\tilde{S}^{y}_{b} \rightarrow -S^{y}_{b}$. Expressing the Kondo part of the full Hamiltonian via the operators d, $\tilde{d}$ and retaining only the leading (quadratic) terms in the symmetric operator d, we obtain

$$\begin{aligned}
H_{K} &= J_{K}\left(\mathbf{s}_{a}\mathbf{S}_{a} + \mathbf{s}_{b}\tilde{\mathbf{S}}_{b}\right) = J_{K}\left[\frac{S^{z}_{a} - S^{z}_{b}}{2}\left(d^{\dagger}_{\uparrow}d_{\uparrow} - d^{\dagger}_{\downarrow}d_{\downarrow}\right)\right. \\
&+ \left.\frac{S^{x}_{b} + S^{x}_{a}}{2}\left(d^{\dagger}_{\uparrow}d_{\downarrow} + d^{\dagger}_{\downarrow}d_{\uparrow}\right) + \frac{S^{y}_{b} - S^{y}_{a}}{2i}\left(d^{\dagger}_{\uparrow}d_{\downarrow} - d^{\dagger}_{\downarrow}d_{\uparrow}\right)\right].
\end{aligned}$$

Using the Holstein-Primakoff transformation and restricting our-self by the one-magnon processes, we get

$$H_{K} = \frac{J_{K}}{2}\sqrt{\frac{S}{2}}d^{\dagger}_{\mathbf{k}\uparrow}d_{\mathbf{k}-\mathbf{q}\downarrow}\left(a^{\dagger}_{-\mathbf{q}} + b_{\mathbf{q}}\right) + H.c. \qquad (5.3)$$

Here the sum over $\mathbf{k}$ and $\mathbf{q}$ is omitted for simplicity of notations. It is important to note that the vertex of the hole-magnon coupling is constant

in Eq. (5.3).

Combining the hopping Hamiltonian Eq. (5.2) and the Kondo Hamiltonian Eq. (5.3), we get the full Hamiltonian describing propagation of the hole in the two-layered quasi-two-dimensional system

$$H = -\sum_{\mathbf{k}}(\varepsilon_{\mathbf{k}} + t)(d^\dagger_{\mathbf{k},\uparrow}d_{\mathbf{k},\uparrow}) + \frac{J_K}{2}\sqrt{\frac{S}{2}}\sum_{\mathbf{k},\mathbf{q}}d^\dagger_{\mathbf{k},\uparrow}d_{\mathbf{k}-\mathbf{q},\downarrow}\left(a^\dagger_{-\mathbf{q}} + b_{\mathbf{q}}\right) + H.c. \tag{5.4}$$

Similar effective models can also emerge in different physical context, for instance, a single hole propagating in a two-dimensional ferromagnet when spin-flip processes are present in the system. We show below that both models can be reduced to Eq. (5.4) in a one-magnon approximation.

5.3 Hole propagation in a two-dimensional ferromagnet

In this section we develop a theory of a single hole propagating in a two dimensional ferromagnetic system $S = \frac{1}{2}$ accompanied by the spin-flip processes. The propagating hole can be accompanied by spin flip processes if the hopping in the system occur via ligands possesing the spin-orbit coupling in a ferromagnet due to different kinds of interactions [173, 174, 175, 176]. It is shown by Jackeli and Khaliullin [177, 178] that d^5-systems with strong spin orbital coupling can be effective described by pseudospin-$\frac{1}{2}$, since the system retains $SU(2)$ symmetry. The treatment of pseudospins as spins remains correct even in presence of an external magnetic field [179].

We consider a ferromagnetic $t - J$ model. The Hamiltonian of this

model reads

$$H_{tJ} = -\sum_{<i,j>} \left(\sum_{\sigma,\sigma'} t_{\sigma\sigma'} c_{i\sigma}^{\dagger} c_{j\sigma'} + H.c. + \sum_{\alpha} J^{\alpha} S_i^{\alpha} S_j^{\alpha} \right),$$

(5.5)

where the hopping part has the general form

$$t_{\sigma\sigma'} = t_1 \delta_{\sigma,\sigma'} + t_2 \delta_{\sigma,-\sigma'}.$$

$c_{\sigma}^{\dagger}$, $c_{\sigma'}$ are the hole creation and annihilation operators, J^{α} are coefficients of the (anisotropic) exchange interaction, t_1, t_2 are hopping parameters, σ, σ' are spin indexes. Two types of hopping are possible - the hole hopping can either conserve its spin or the spin is flipped in this process due to strong spin-orbit interaction in the strong spin-orbit limit.

5.4   Two-dimensional ferromagnet in external magnetic field at half-filling

Let us consider the spin-spin interaction $\sum_{<i,j>} J^{\alpha} S_i^{\alpha} S_j^{\alpha}$ in Eq. (5.5) in presence of magnetic hield. We assume XXZ ferromagnetic interaction, the Hamiltonian of the system reduces to

$$H = -\sum_{<i,j>} \left((J+K) S_i^z S_j^z + J(S_i^x S_j^x + S_i^y S_j^y) \right) - \mathbf{h} \cdot \mathbf{S}_i,$$

(5.6)

$J > 0, |K| \ll J, S = \frac{1}{2}$. The effective g-factor is absorbed in $|\mathbf{h}|$.

If $K > 0$, the system is an easy axis ferromagnet, while for $K < 0$ it is an easy plane ferromagnet. Variation of the external magnetic field allows us to manipulate the system and change its ground state and excitation spectrum of magnons.

5.4.1 Ground state and excitations of the ferromagnet in a magnetic field along z-axis

Let us suppose that the magnetic field is applied along z-axis, i.e. $\mathbf{h} = (0, 0, h)$, and find the classical ground state of the system. The energy of the classical spins of Eq. (5.6) is

$$H = -JS^2 - KS^2 \cos^2 \theta - hS \cos \theta, \qquad (5.7)$$

where θ is the angle between the z-axis and the orientation of spins in the classical ground state, $0 \le \cos \theta \le 1$. Minimization of the energy by the angle θ gives us the classical ground state. There are two extrema solutions for Eq.(5.7):

$$\cos \theta = -\frac{h}{2KS} \qquad (5.8)$$

or

$$\cos \theta = 1. \qquad (5.9)$$

For $K < 0$ and the magnetic field along the z-axis $h < h_{sat}$, the minimum of the energy is given by Eq. (5.8). The system in this case is tilted in a weak magnetic field of strength $h < h_{sat}$ on the angle θ. If $h > h_{sat}$ or $K > 0$ (easy axis ferromagnet) the mininum of the energy corresponds to

Eq. (5.9) with spins aligned along the magnetic field.

We use the Holstein-Primakoff transformation, where we keep the leading terms in the $1/S$ expansion:

$$S_i^x \simeq \sqrt{2S}\frac{b_i + b_i^\dagger}{2}, \; S_i^- \simeq \sqrt{2S}\frac{b_i - b_i^\dagger}{2i}, \; S_i^z = S - b_i^\dagger b_i. \tag{5.10}$$

When $K > 0$ or the magnetic field is stronger than the saturation field ($h \geq h_{sat}$), spins are aligned along z-axis, so the Hamiltonian (5.6) reads in momentum space

$$H = \sum_{\mathbf{q}} \left[JzS(1 - \gamma_{\mathbf{q}}) + zKS + \frac{h}{2} \right] \left(b_{\mathbf{q}} b_{\mathbf{q}}^\dagger + b_{\mathbf{q}}^\dagger b_{\mathbf{q}} \right). \tag{5.11}$$

The spectrum of the spin-wave excitations in this case is

$$E_{\mathbf{q}} = 2zJS(1 - \gamma_{\mathbf{q}}) + 2zKS + h, \tag{5.12}$$

where $\gamma_{\mathbf{q}} = \frac{1}{z}\sum_\delta e^{i\mathbf{q}\delta}$, the sum is taken over the nearest neighbors, the coordination number $z = 4$ for a square lattice, we absorb it into J and K further from now on and put the lattice constant $\delta = 1$. This spectrum is gapped. At small $|\mathbf{q}|$ it takes the form $E_{\mathbf{q}} = (h + 2KS) + JS\mathbf{q}^2$, with $h \geq 0$ if $K > 0$, and $E_{\mathbf{q}} = (h - 2KS) + JS\mathbf{q}^2$ if $h \geq h_{sat}$ and $K < 0$.

Let us now consider a situation when $K < 0$ and the value of the magnetic field does not exceed h_{sat}. We rotate the coordinate system, choosing a new $\tilde{z}$-axis along the classical spin alignment given by Eq.(5.8).

It requires the following transformation:

$$S^y \longrightarrow \tilde{S}^y,$$
$$S^z \longrightarrow \tilde{S}^z \cos\theta - \tilde{S}^x \sin\theta, \tag{5.13}$$
$$S^x \longrightarrow \tilde{S}^x \cos\theta + \tilde{S}^z \sin\theta.$$

Thus, the Hamiltonian takes form:

$$H = \sum_{\mathbf{q}} \left[\left(JS(1 - \gamma_{\mathbf{q}}) + \frac{1}{2}|K|S\gamma_{\mathbf{q}} - \frac{h^2}{8|K|S}\gamma_{\mathbf{q}} \right) \left(b_{\mathbf{q}} b_{\mathbf{q}}^\dagger + b_{\mathbf{q}}^\dagger b_{\mathbf{q}} \right) + \right.$$
$$\left. \left(\frac{1}{2}|K|S\gamma_{\mathbf{q}} - \frac{h^2}{8|K|S}\gamma_{\mathbf{q}} \right) \left(b_{\mathbf{q}} b_{-\mathbf{q}} + b_{\mathbf{q}}^\dagger b_{-\mathbf{q}}^\dagger \right) \right]. \tag{5.14}$$

This Hamiltonian is diagonalized by appying the Bogolibov transformation which introduces operators of magnons $\beta_{\mathbf{q}} = u_{\mathbf{q}} b_{\mathbf{q}} - v_{\mathbf{q}} b_{-\mathbf{q}}^\dagger$, $\beta_{\mathbf{q}}^\dagger = u_{\mathbf{q}} b_{\mathbf{q}}^\dagger - v_{\mathbf{q}} b_{-\mathbf{q}}$, where $u_{\mathbf{q}}$ and $v_{\mathbf{q}}$ satisfy the equation $u_{\mathbf{q}}^2 - v_{\mathbf{q}}^2 = 1$. For a non-diagonal Hamiltonian of the form $H = \sum_{\mathbf{q}}[A_{\mathbf{q}}(b_{\mathbf{q}}^\dagger b_{\mathbf{q}} + b_{\mathbf{q}} b_{\mathbf{q}}^\dagger) + B_{\mathbf{q}}(b_{\mathbf{q}}^\dagger b_{-\mathbf{q}}^\dagger + b_{\mathbf{q}} b_{-\mathbf{q}})]$, where $A_{\mathbf{q}}$ and $B_{\mathbf{q}}$ are some coefficients, $E_{\mathbf{q}} = \sqrt{A_{\mathbf{q}}^2 - B_{\mathbf{q}}^2}$ is the energy of the system, the Bogolubov coefficients are expressed as $u_{\mathbf{q}} = \sqrt{\frac{A_{\mathbf{q}}}{2E_{\mathbf{q}}} + \frac{1}{2}}$, $v_{\mathbf{q}} = -\frac{B_{\mathbf{q}}}{\sqrt{2E_{\mathbf{q}}(A_{\mathbf{q}} + E_{\mathbf{q}})}}$.

After the Bogolubov transformation, the Hamiltonian (5.14) acquires the diagonal form

$$H = \sum_{\mathbf{q}} E_{\mathbf{q}}(\beta_{\mathbf{q}} \beta_{\mathbf{q}}^\dagger + \beta_{\mathbf{q}}^\dagger \beta_{\mathbf{q}}),$$

so the spectrum of magnons in this case is

$$E_{\mathbf{q}} = 2\sqrt{JS\left[(1 - \gamma_{\mathbf{q}})\right]\left[JS(1 - \gamma_{\mathbf{q}}) + |K|S\gamma_{\mathbf{q}} - \frac{h^2}{4|K|S}\gamma_{\mathbf{q}}\right]}. \tag{5.15}$$

It's gapless. At small q dispersion of the excitations is linear $E_{\mathbf{q}} \sim c|\mathbf{q}|$.

At h_{sat} the spins in the ground state become aligned along the z axis ($\cos\theta = 1$). As a consequence, the dispersion is the one of the isotropic ferromagnetic Heisenberg model with the quadratic spectrum $E_{\mathbf{q}} \simeq JS\mathbf{q}^2$. For $h > h_{sat}$, the energy is given by Eq. (5.12)

Note that the Hamiltonian in Eq. (5.11) is already diagonal and does not require a Bogolubov transform, so there magnon operators $\beta_{\mathbf{k}} \equiv b_{\mathbf{k}}$.

5.4.2 Ground state and excitations of the system with magnetic field along x-axis

The similar approach is used to find the ground state of the Hamiltonian (5.6) if the magnetic field is applied along the x-axis, $\mathbf{h} = (h, 0, 0)$. The classical Hamiltonian becomes

$$H = -JS^2 - KS^2 \cos^2\theta - hS\sin\theta. \tag{5.16}$$

Minimizing it with regard to the angle θ, we obtain two solutions:

$$\cos\theta = 0. \tag{5.17}$$

if $K < 0$ or $h > h_{sat}$, or

$$\sin\theta = \frac{h}{2KS} \tag{5.18}$$

if $K > 0$ and $h < h_{sat}$.

Eq.(5.17) means that spins are aligned along x-axis and corresponds to a system with the excitation spectrum

$$E_{\mathbf{q}} = 2\sqrt{\left[JS(1 - \gamma_{\mathbf{q}}) + \frac{h}{2}\right]\left[JS(1 - \gamma_{\mathbf{q}}) + |K|S\gamma_{\mathbf{q}} + \frac{h}{2}\right]}. \tag{5.19}$$

At $h = 0$ and small $|\mathbf{q}|$, the spectrum becomes linear, $E_{\mathbf{q}} \simeq \sqrt{2J|K|}S|\mathbf{q}|$. Eq.(5.18) corresponds to the ground state with spins tilted on angle θ with respect to z-axis. The energy of magnons

$$E_{\mathbf{q}} = 2\sqrt{\left[JS(1 - \gamma_{\mathbf{q}}) + KS\right]\left[JS(1 - \gamma_{\mathbf{q}}) + KS - \frac{h^2}{4KS}\gamma_{\mathbf{q}}\right]} \qquad (5.20)$$

is again gapped with the gap $\Delta = 2\sqrt{KS\left(KS - \frac{h^2}{4KS}\right)}$ but the gap vanishes at $h = h_{sat}$, the energy of magnons read in this case $E_{\mathbf{q}} \simeq \sqrt{2K(J + K)}S|\mathbf{q}|$.

5.5   Self-energy of the hole

Now, when we have established the properties of the system at exact half-filling, we can consider the limit of a single hole in the system.

The full Hamiltonian of the system takes hopping processes into account. Since the hopping processes with and without flips of the spin are possible in the system, the configuration space of the $\frac{1}{2}$-spin system consists of three elements: $|\uparrow\rangle$, $|\downarrow\rangle$, $|0\rangle$. We use the axis along the direction of the spins in the $t - J$ model. There are four types of hopping possible in the system and depicted by Eqs. (5.21-5.24).

$$|0\rangle_i\,|\uparrow\rangle_j \longrightarrow |\uparrow\rangle_i\,|0\rangle_j\,, \qquad (5.21)$$

$$|0\rangle_i\,|\downarrow\rangle_j \longrightarrow |\downarrow\rangle_i\,|0\rangle_j\,, \qquad (5.22)$$

$$|0\rangle_i\,|\uparrow\rangle_j \longrightarrow |\downarrow\rangle_i\,|0\rangle_j\,, \qquad (5.23)$$

$$|0\rangle_i\,|\downarrow\rangle_j \longrightarrow |\uparrow\rangle_i\,|0\rangle_j\,. \qquad (5.24)$$

We introduce an operator $f_i^\dagger$ that creates a hole at site i from the spin-up state: $f_i \left| \uparrow \right\rangle = \left| 0 \right\rangle$. The process given by Eq.(5.21) does not change the spin configuration of the system, so the spin-up state is annihilated at the site j and created at the site i, $f_i f_j^\dagger \left| 0 \right\rangle_i \left| \uparrow \right\rangle_j = \left| \uparrow \right\rangle_i \left| 0 \right\rangle_j$. We restrict our consideration to the one-magnon processes. The hopping shown in Eq. (5.22) corresponds to the hopping of the hole in a perturbed state $\left| \downarrow \right\rangle$. It involves two-magnon processes and can be neglected [163]. Eqs. (5.23, 5.24) describe the spin-slip process involving the one-magnon processes. The change of the spin is described by the ladder operators $S^\pm$: $S_i^- f_i f_j^\dagger \left| 0 \right\rangle_i \left| \uparrow \right\rangle_j = \left| \downarrow \right\rangle_i \left| 0 \right\rangle_j$, $f_i f_j^\dagger S_j^+ \left| 0 \right\rangle_i \left| \downarrow \right\rangle_j = \left| \uparrow \right\rangle_i \left| 0 \right\rangle_j$.

Summing all hopping terms and using the Holstein-Primakoff transformation, we obtain the hopping Hamiltonian

$$H_t = - \sum_{<i,j>} f_i f_j^\dagger \left[2St_1 + \sqrt{2S}t_2 \left(b_i^\dagger + b_j \right) \right] + H.c. \qquad (5.25)$$

The part corresponding to the hopping without the spin flips does not perturb the magnetic structure of the system, so we consider it as a shift of the hole spectrum. With the effective Hamiltonian (5.25), we can calculate the self-energy of a single hole hopping with spin flips. We do it in the framework of the non-crossing diagrams approximation. The corresponding self-energy is depicted diagrammatically in Fig. 5.1. Only the spin-flip hopping involves interaction with magnons. It corresponds to the second part of Eq. (5.25) proportional to t_2, where Bose operators $b^\dagger$, b has to be expressed via operators of magnons that diagonalize the Hamiltonian in Eq. (5.6). This is done via the Bogolubov transform described in the previous section. The magnon-involving hopping Hamiltonian is written
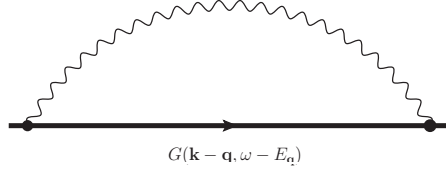
$$G(\mathbf{k} - \mathbf{q}, \omega - E_q)$$

Figure 5.1. The self energy of the hole in the self-consistent non-crossing diagrams approximation. $G(\mathbf{k} - \mathbf{q}, \omega - E_\mathbf{q})$ is the renormalized Green's of the hole, $E_\mathbf{q}$ - energy of a magnon.

then as

$$\tilde{H}_t = - \sum_{<i,j>} \sqrt{2S} t_2 f_i f_j^\dagger \left(b_i^\dagger + b_j \right) + H.c. \tag{5.26}$$

The Green's function of the hole can be reduced to the Green's function of the "slave"-fermions, as we replace Bose operators by $\sqrt{2S}$ values.

$$G(i, j, \omega) = \int_{-\infty}^{\infty} dt e^{i\omega t} \langle T[f_i(t) f_j(0)^+] \rangle \tag{5.27}$$

With this Green's function, the self-consistent perturbation theory can be constructed. The self-energy can be written in the frame of this approach as

$$\Sigma(\mathbf{k}, \omega) = \sum_\mathbf{q} f(\mathbf{k}, \mathbf{q}) G(\mathbf{k} - \mathbf{q}, \omega - E_\mathbf{q}) \tag{5.28}$$

$f(\mathbf{k}, \mathbf{q})$ contains information about the coupling of the hole to magnons. It is obtained from Eq. (5.26) as $f(\mathbf{k}, \mathbf{q}) = 2S t_2^2 |\gamma_{\mathbf{k}-\mathbf{q}} u_\mathbf{q} + \gamma_\mathbf{k} v_\mathbf{q}|^2$. If the spins in the ground state are aligned along z-axis (it corresponds to the energy of magnons defined by Eq. (5.12) for an arbitrary magnetic field along z-axis or by Eq. (5.15) for $h = h_{sat}$), $f(\mathbf{k}, \mathbf{q}) = 2S t_2^2 \gamma_{\mathbf{k}-\mathbf{q}}^2$ (the Bogolubov coefficient are trivial in this case: $u_\mathbf{q} = 1$, $v_\mathbf{q} = 0$). For the low energy of magnons which give the main contribution to Eq. (5.28),

this function is in leading order constant: $f(\mathbf{k}, \mathbf{q}) \simeq 2St_2^2$. While for the tilted ground state of spins $f(\mathbf{k}, \mathbf{q}) \sim |\mathbf{q}|$ at the bottom of the band if the excitation spectrum is linear and $f(\mathbf{k}, \mathbf{q})$ is constant if the excitation spectrum is gapped, which is defined by Eqs. (5.15), (5.20), (5.19). The explicit form of the Green's function for our problem reads

$$G(\mathbf{k}, \omega) = \frac{1}{\omega + 2St_1\gamma_{\mathbf{k}} - \sum_{\mathbf{q}} f(\mathbf{k}, \mathbf{q})G(\mathbf{k} - \mathbf{q}, \omega - E_{\mathbf{q}})}, \qquad (5.29)$$

$E_{\mathbf{q}}$ is the spectrum of magnons provided in the previous section for various cases by Eqs. (5.12), (5.15), (5.19), (5.20).

For the multi-layered system discussed above, Eq. (5.29) retains its form. But the hole-magnon interaction in this model is unrelated to hopping and occurs at the same site, therefore the only difference for this case is that the coupling function $f(\mathbf{k}, \mathbf{q})$ does not contain the $\gamma_{\mathbf{k}-\mathbf{q}}$-factor, and it is exactly constant if spins are aligned along z-axis.

As it follows from the analysis of $f(\mathbf{k}, \mathbf{q})$, if the spectrum of magnons is gapless and linear, the problem of a propagating single hole in an easy plane ferromagnet is identical to the problem of a propagating single hole in an isotropic two-dimensional antiferromagnet studied in details by Kane et al. in [163]. They showed that the spectral function of the hole in this system contains a quasiparticle peak at the bottom of the spectrum. If the system is gapped, the quasiparticle peak is separated from the incoherent part of the spectrum since for the hole there are no states with lower energy to scatter during creating of the spin excitation.

5.6 Spectral function of the hole coupled to magnons with quadratic dispersion

Let us estimate the analytical behavior of the self-energy of the hole when the low-energy magnons in the system have quadratic dispersion $E_{\mathbf{q}} = \Delta + JSq^2$. This situation can be realized by a manipulation of the external magnetic field applied along z axis. The gap $\Delta = 2KS + h$ is given by Eq.(5.12) for $h \geq 0$, $\Delta = 0$ when we consider an easy plane ferromagnet in the saturation field $h = h_{sat}$ described by Eq.(5.15). The self-energy of the hole is given by Eq. (5.28). For analysis of the lowest energy excitations, we stay at the bottom of the band, so we consider $\mathbf{k} = 0$. For the considered ferromagnetic alignment of the spins along z axis, the leading term of the hole-magnon vertex is constant: $f(0, \mathbf{q}) \simeq 2t_2^2 S^2$, the next term is proportional to $\sim q^2$ and can be neglected in the low-energy limit. Let us for a moment assume that the hole-magnon coupling is small, so we may treat the self-energy of the hole near the quasiparticle pole perturbatively. In the lowest order of the perturbation theory, the self-energy is defined by the single loop contribution depicted in Fig. 5.2a and reads

$$
\begin{aligned}
\Sigma^{(1)}(\omega) &= \frac{t^2 S}{2\pi} \int \frac{q\,dq}{\omega - \Delta - JSq^2 + t_1(1 - \frac{q^2}{2}) - i\delta} \\
&\simeq -\kappa \ln \left| \frac{\Delta - \tilde{\omega}}{\Lambda} \right|,
\end{aligned}
$$

where $\kappa = \frac{t_2^2 S}{\pi(JS + \frac{t_1}{2})}$ is the effective coupling constant, $\tilde{\omega} = \omega + t_1$ ($\tilde{\omega} = 0$ at the position of the quasiparticle hole), Λ is the ultraviolet cut-off, $\delta \to 0_+$. The second order of the perturbation theory in the non-crossing

approximation is shown in Fig. 5.2b and the sum of the single loop and the two loop contributions reads

$$
\begin{aligned}
\Sigma^{(2)}(\omega) &= \Sigma^{(1)}\left(\omega - \kappa \ln\left|\frac{\Delta - \tilde{\omega}}{\Lambda}\right|\right) \\
&\simeq \Sigma^{(1)}(\omega) + \frac{\kappa^2}{\Delta - \tilde{\omega}} \ln\left|\frac{\Delta - \tilde{\omega}}{\Lambda}\right|.
\end{aligned}
\tag{5.30}
$$

The perturbative approach is justified as long as $\frac{\kappa}{\Delta - \tilde{\omega}} \ll 1$, but this analysis is no longer valid when $\frac{\kappa}{\Delta - \tilde{\omega}} \gtrsim 1$. Since the gap Δ vanishes in the easy-plane ferromagnet inside the saturation field, the perturbation theory breaks down even for an arbitrary small hole-magnon coupling. It is necessary to use a nonperturbative approach in this case.

(a)   (b)
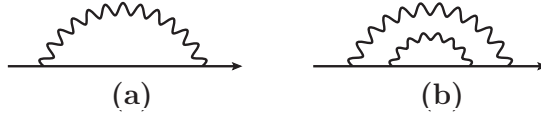
Figure 5.2. **(a)** Single loop contribution to the hole self-energy. **(b)** Two loop contribution to the impurity sef-energy. The solid line corresponds to the hole, the curved line corresponds to the magnon.

When the gap $\Delta = 0$, the self-energy is given by

$$
\Sigma(\omega) = \frac{2S^2 t^2}{\pi} \int \frac{q\,dq}{\omega - J_z S q^2 - \Sigma(\omega - J_z S q^2)}.
\tag{5.31}
$$

For simplicity, we can assume that $t_1 = 0$. We use an ansatz for the spectral function in the form $\Sigma(\omega) = \omega_c + A(\omega - \omega_c)^\alpha$. ω_c is the characteristic frequency where the spectral weight appears, A is some constant. Putting this form of Σ in Eq.(5.31), we have

$$
\omega_c + A(\omega - \omega_c)^\alpha = \frac{t^2}{\pi J} \int_0^\Lambda \frac{dx}{\omega - \omega_c - x - A(\omega - \omega_c - x)^\alpha},
\tag{5.32}
$$

Λ is some cut-off value for the energy. Eq.(5.32) is satisfied for $|\omega - \omega_c| \ll \omega_c$ if $\alpha = \frac{1}{2}$, and the spectral function reads

$$\Sigma(\omega) \underset{\omega \to \omega_c}{\simeq} \omega_c + A(\omega - \omega_c)^{\frac{1}{2}},$$

with constant $A = \sqrt{\frac{2t^2}{J\pi}}$.

This self-energy gives us the Green's function

$$G(\omega) = \frac{1}{\omega - \omega_c - A(\omega - \omega_c)^{\frac{1}{2}}}. \qquad (5.33)$$

It diverges at the threshold ω_c of the band as $G(\omega - \omega_c) \sim \omega^{-\frac{1}{2}}$. Due to this scaling, there is no quasiparticle pole in this case.

5.7 Numerical evaluation of the spectral function

Now we solve the equation (5.29) numerically and compare it with the qualitative results from the previous section.

The case of $t_2 = 0$ is trivial. The hole hops through the ferromagnetic background without flips, so there are no magnons in the system. The spectral function in this case is simply a δ-function peak at the bottom of the band.

The case of $t_1 = t_2$ for an isotropic ferromagnet is shown in Fig. 5.3. There is no quasiparticle hole in this case, the self-energy at the bottom of the band is rather obey $\Sigma(\omega) = \sqrt{\omega - \omega_c}$ (depicted by the dotted line for $\mathbf{k} = (0,0)$). The hopping processes without flip of the spin causes shift of the relative spectral weight from the bottom of the band to the position the δ-peak for $t_2 = 0$ used to be.
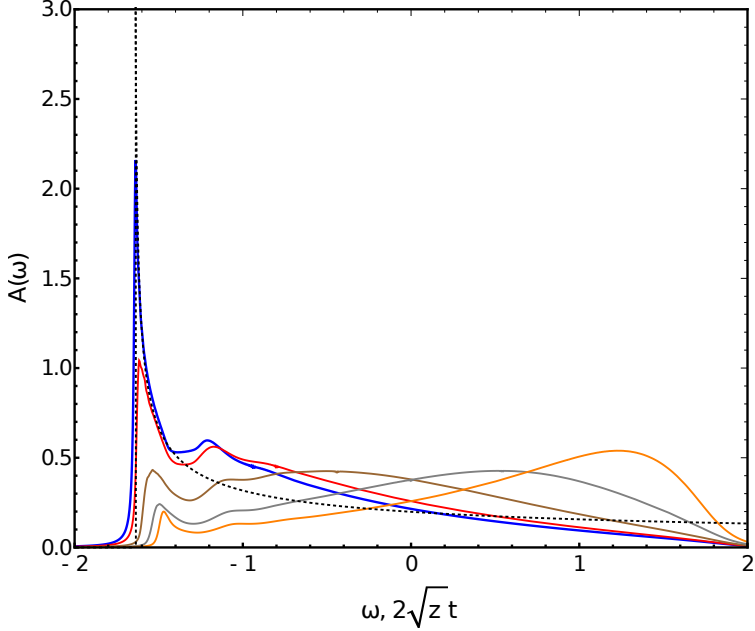
Figure 5.3. Spectral function of the hole at the bottom of the band with the spin-flip processes. Only processes involving spin flips are allowed: $t_1 = t_2$. $h = h_{sat}$, $J = 0.5t_2$. Thick blue line: spectral function for gapless magnons, $\mathbf{k} = (0,0)$, $\Delta = 0$. Dashed black line $\sim \frac{1}{\pi} Im[(\omega - \omega_c)^{-\frac{1}{2}}]$. Red line: $\mathbf{k} = (\frac{\pi}{5}, \frac{\pi}{5})$, brown line: $\mathbf{k} = (\frac{2\pi}{5}, \frac{2\pi}{5})$, gray line: $\mathbf{k} = (\frac{3\pi}{5}, \frac{3\pi}{5})$, orange line: $\mathbf{k} = (4\frac{\pi}{5}, \frac{4\pi}{5})$.

In Fig.5.4a we show the spectral function $A(\omega) = -\frac{1}{\pi} ImG(\omega)$ for the itinerant electron in the two-layered system with a gapless spectrum of ferromagnetic magnons. The coupling of the itinerant electron to magnons is given for this case by Eq. (5.3), t_0 is put to zero for the simplicity, e.g. only the interlayer hopping is present in the system. This spectral function does not depend on the wave-vector $\mathbf{k}$. At the bottom of the band, this spectral function behaves as $A\omega \propto (\omega - \omega_c)^{-\frac{1}{2}}$ in accordance with our ansatz solution Eq. (5.33). If the spectrum of magnons is gapped, there is a distinctive quasiparticle pole in the system separated from the incoherent part of the band, as shown in Fig. 5.4b.

(a)   **(b)**
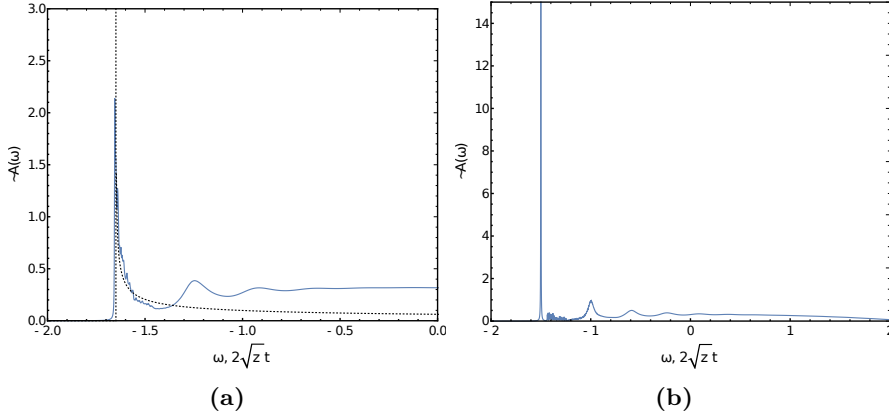
Figure 5.4. Spectral function of the itinerant electron in the two layered van der Waals crystal. (a) Isotropic case $\Delta = 0$. Only processes involving spin flip are allowed - $t_1 = 0$, $J = 0.1t_2$. Dashed black line $\sim \frac{1}{\pi} Im[(\omega - \omega_c)^{-\frac{1}{2}}]$. (b) Anisotropic (easy axis) case $\Delta = 0.6J$.

5.8 Comparison to the two-dimensional antiferromagnet

Our results of two previous sections clearly demonstrate that a hole in a two-dimensional ferromagnet has a special regime, shown in Table 5.1 ($K < 0$, $h = h_{sat}$ and $K = 0$, $h - 0$) where the quasiparticle weight $Z = \left(1 - \frac{\partial \Sigma(\omega)}{\partial \omega}|_{\omega=\omega_c}\right)^{-1}$ vanishes and the Green's function scales as $G(\omega) \propto \sqrt{\omega - \omega_c}^{-1}$. It is caused by the magnon spectrum $E_{\mathbf{q}} \sim \mathbf{q}^2$. If the spectrum of magnons is gapped or linear, one obtains again coherent polarons. This situation is contrasted to a two-dimensional antiferromagnet, which always can be described by coherent quasiparticles [163]. We have shown that this non-quasiparticle regime can be achieved in anisotropic ferromagnets by manipulation of an external magnetic field applied to the system. If this behavior survives at finite charge densities, manipulation of the

magnetic field allows experimental control of the Fermi liquid-non-Fermi liquid properties.

	Δ	$E_{\mathbf{q}}$	$Z(\omega)$
$K > 0,\ h^z \geq 0$	$h + 2KS$	$\Delta + c\mathbf{q}^2$	finite
$K > 0,\ h^x < h_{sat}$	$2\sqrt{KS(KS - \frac{h^2}{4KS})}$	$\Delta + c\mathbf{q}^2$	finite
$K > 0,\ h^x \geq h_{sat}$	$\sqrt{h(h + 2KS)}$	$\Delta + c\mathbf{q}^2$	finite
$K < 0,\ h^z > h_{sat}$	$h - 2KS$	$\Delta + c\mathbf{q}^2$	finite
$K < 0,\ h^x > 0$	$\sqrt{h(h + 2KS)}$	$\Delta + c\mathbf{q}^2$	finite
$K < 0,\ h^z < h_{sat}$	0	$c\|\mathbf{q}\|$	finite
$K < 0,\ h^z = h_{sat}$	0	$c\mathbf{q}^2$	$0,\ G(\omega) \propto (\omega - \omega_c)^{-\frac{1}{2}}$
$K = 0,\ h^z = h^x = 0$	0	$c\mathbf{q}^2$	$0,\ G(\omega) \propto (\omega - \omega_c)^{-\frac{1}{2}}$

Table 5.1. Gap Δ, spectrum of magnons $E_{\mathbf{q}}$ and quasiparticle spectral weight $Z(\omega)$ for different values of anisotropy K and magnetic field h. c is a function of S, J, K, h

Chapter 6

Conclusions of the thesis

In this thesis we studied several aspects of the manifestation of the fluctuating Goldstone modes in condensed matter physics. For the large part of the thesis, we focused on the phonon-mediated Casimir interaction between impurities in lattice and continuum systems both numerically and analytically. The obtained exact solution of the considered model for the phonon-induced Casimir interaction brings together the results of earlier studies in the field and explains discrepancy between them. In particular, we demonstrated that the model of Schecter and Kamenev [51] in the limit of the infinite impurity masses is equivalent to the model of Recati et al. [50].

As we found in our research, heavy or light impurities in atomic chains with periodic boundary conditions create weak perturbing potential interaction between the impurity atoms. The low-energy phonons are weakly affected by this change, while higher-energy phonons become gapped, i.e. optical branches appear in the spectrum. The Casimir interaction stems

from the low-energy part of the spectrum, so the resulting attractive interaction can be treated perturbatively. That kind of interaction immediately makes phonon spectrum gapped and eliminates an acoustic branch from the spectrum, but does not substantially affect higher energy modes.

In Chapter 2, we analyzed numerically the evolution of the phonon-induced Casimir interaction between two impurity atoms embedded in an ideal atomic lattice. We showed the mapping of the Luttinger liquid with impurities to the continuum limit of the introduced lattice model. As we found, this interaction in one dimension at small distances differs from the power law $1/r^{(3)}$ predicted by Schecter and Kamenev for large separations between the impurities. For static impurities without kinetic energy the interaction asymptotically tends to the $1/r$ law, restoring the results of Recati et al. We found that the latter spacial law is the short-distance limit of the interaction between the dynamic impurities. At intermediate distance the Casimir interaction is nonuniversal and has a crossover between these two limits of $\frac{1}{r}$ and $\frac{1}{r^3}$.

The reasons for such behavior and the characteristic scale of the crossover are found in the Chapter 3. In this Chapter we developed the model for the phonon-mediated Casimir interaction. We showed that this model can be solved exactly by the full summation of the infinite series given by the perturbation theory. The characteristic distance of the system is defined by the coupling constant of the phonon-impurity interaction. For the lattice case, this constant depends only on the ratio between masses of the impurities and atoms of the ideal lattice.

The obtained long-ranged interaction can be observed experimentally in ultra cold atomic gases in the experimental setup of Catani et al. [79]

described in Chapter 1. As it follows from this chapter, we show that the real Casimir interaction for dynamic impurities is stronger than it is given by the second order of the perturbation theory, which was available in the literature so far. In particular, our results based on the exact solution for the setup considered in [51] give the value of the Casimir interaction three times larger than the second order of the perturbation theory and increases even further in systems with large phonon-impurity scattering amplitudes close to the unitary limit. It gives hope that the Casimir interaction can can be found experimentally in atomic gases in optical traps.

In Chapter 4, we formulated the theory of the phonon-mediated Casimir interaction via the T-matrix formalism for the phonon-impurity scattering. This allowed us to express all microscopical parameters of the model via the phenomenological experimentally observable constants and generalize the model for two- and three-dimensional systems. Our results demonstrate that the multiple phonon scattering processes occurring at each impurity are crucial for the correct evaluation of the Casimir interaction. We show that the energy dependence of the T-matrix determines the power law decrease of the Casimir interaction at short distances and at large distances in the unitary limit at $T = 0$. For the weak impurity scatterings, the Casimir interaction is universal at large distances. This T-matrix method is especially important for the consideration of the Casimir forces between two atoms in external potential and allows to obtain the non-perturbative results. At finite temperatures, a new characteristic scale of the order of the thermal de Broglie wavelength appears. For distances much larger the de Broglie wave length, the Casimir interaction decays exponentially with the distance between the impurities.

The obtained temperature corrections may be relevant to the proposed experimental set-ups of [76, 79].

In Chapter 5 we developed the theoretical description of a singe hole propagating in the two-dimensional ferromagnet in external magnetic field with spin-flips. We found that interaction of the itinerant quasiparticle with magnons leads to the strong renormalization of the spectral weight of quasiparticles. We showed that an external magnetic field can be used to manipulate the properties of this system. At the saturation value of the magnetic field applied to an easy plane ferromagnet, the Green's function demonstrates $G(\omega) \propto \omega^{-\frac{1}{2}}$ behavior. It is contrasted to the systems of an itinerant quasiparticle in the antiferromagnetic background where the the quasiparticle retains the finite quasiparticle weight. We showed that the anisotropic system with a gapped spectrum of magnons demonstrates clear quasiparticle poles separated from the incoherent part of the band. The obtained results for the effective renormalization of a single hole by magnons in ferromagnets open possibility to develop a theory for the magnon-mediated Casimir interaction between two impurities in a two-dimensional ferromagnet in addition to the existent descriptions of the magnon-mediated Casimir forces in to dimensional antiferromagnets [180].

As the conclusion of this thesis, we developed the description of the phonon-mediated Casimir interaction taking into account multiple phonon-impurity scatterings, that strongly renormalize the resulting interaction between the impurities. Our results generalize previous studies of the Casimir interaction between different kind of impurities. We developed the theory for magnon scattering processes on a single itinerant impurity in a two-dimensional ferromagnet that can be used further for study of

the magnon-mediated Casimir interaction in quasi-two-dimensional ferro-magnets.

Bibliography

[1]   H. B. G. Casimir. In: *Proc. Kon. Ned. Akad. Wetenschap. Ser. B* 51 (1948), p. 793.

[2]   H. B. G. Casimir and D. Polder. In: *Phys. Rev.* 73 (1948), p. 360.

[3]   W. E. Lamb and R. C. Retherford. "Fine Structure of the Hydrogen Atom by a Microwave Method". In: *Phys. Rev.* 72 (3 1947), pp. 241–243. DOI: 10.1103/PhysRev.72.241.

[4]   H. A. Bethe. "The Electromagnetic Shift of Energy Levels". In: *Phys. Rev.* 72 (4 1947), pp. 339–341. DOI: 10.1103/PhysRev.72.339.

[5]   T. A. Welton. "Some Observable Effects of the Quantum-Mechanical Fluctuations of the Electromagnetic Field". In: *Phys. Rev.* 74 (9 1948), pp. 1157–1167. DOI: 10.1103/PhysRev.74.1157.

[6]   J. Schwinger. "On Quantum-Electrodynamics and the Magnetic Moment of the Electron". In: *Phys. Rev.* 73 (4 1948), pp. 416–417. DOI: 10.1103/PhysRev.73.416.

[7]   V. Weisskopf. "Probleme der neueren Quantentheorie des Elektrons". In: *Naturwissenschaften* 23.37 (1935), pp. 631–637. ISSN: 1432-1904. DOI: `10.1007/BF01492012`.

[8]   V. M. Mostepanenko and N. N. Trunov. *The Casimir Effect and its applications*. Oxford University Press, New York, 1997.

[9]   K.A.Milton. *The Casimir Effect: Physical Manifestations of Zero-Point Energy*. World Scientific, Singapore, 2001.

[10] J. Mehra. "Temperature correction to the casimir effect". In: *Physica* 37.1 (1967), pp. 145 –152. ISSN: 0031-8914. DOI: `https://doi.org/10.1016/0031-8914(67)90115-2`.

[11] B. V. Deriagin and I. I. Abrikosova. "Direct measurement of the molecular attraction of solid bodies. I. Statement of the problem and method of measuring forces by using negative feedback". In: *Sov. Phys. JETP* 3 (1957). [Zh. Eksp. Teor. Fiz.30, 993 (1956)], pp. 819–829.

[12] B. V. Deriagin and I. I. Abrikosova. "Direct measurement of the molecular attraction of solid bodies. II. Method for Measuring the Gap. Results of Experiments". In: *Sov. Phys. JETP* 4 (1957). [Zh. Eksp. Teor. Fiz.31, 3 (1956)], pp. 2–10.

[13] E.M. Lifshitz. "The Theory Of Molecular Attractive Forces Between Solids". In: *J. Exp. Theor. Phys.* 2.1 (1956), p. 73.

[14] I.E. Dzyaloshinskii, E.M. Lifshitz, and L.P. Pitaevskii. "The General Theory Of Van Der Waals Forces". In: *Adv. Phys.* 10.38 (1961), p. 165.

[15]   Julian Schwinger. "Casimir effect in source theory". In: *Letters in Mathematical Physics* 1.1 (1975), pp. 43–47. ISSN: 1573-530. DOI: `10.1007/BF00405585`.

[16]   M.J. Sparnaay. "Measurements Of Attractive Forces Between Flat Plates". In: *Physica* 24.9 (1958), p. 751.

[17]   A. Kitchener and A. P. Prosser. "Direct measurement of the long-range van der Waals forces". In: *Proceedings of the Royal Society of London. Series A. Mathematical and Physical Sciences* 242.1230 (1957), pp. 403–409. DOI: `10.1098/rspa.1957.0184`.

[18]   W. Black et al. "Measurements of retarded Van Der Waals forces". In: *Trans. Faraday Soc.* 56 (0 1960), pp. 1597–1608. DOI: `10.1039/TF9605601597`.

[19]   D. Tabor and R. H. S. R. H. S. Winterton. "Surface Forces: Direct Measurement of Normal and Retarded van der Waals Forces". In: *Nature* 219.5159 (1968), pp. 1120–1121. DOI: `10.1038/2191120a0`.

[20]   E. S. Sabisky and C. H. Anderson. "Verification of the Lifshitz Theory of the van der Waals Potential Using Liquid-Helium Films". In: *Phys. Rev. A* 7 (2 1973), pp. 790–806. DOI: `10.1103/PhysRevA.7.790`.

[21]   S. K. Lamoreaux. "Demonstration of the Casimir Force in the 0.6 to $6\mu m$ Range". In: *Phys. Rev. Lett.* 78 (1 1997), pp. 5–8. DOI: `10.1103/PhysRevLett.78.5`.

[22]   U. Mohideen and Anushree Roy. "Precision Measurement of the Casimir Force from 0.1 to $0.9\mu m$". In: *Phys. Rev. Lett.* 81 (21 1998), pp. 4549–4552. DOI: `10.1103/PhysRevLett.81.4549`.

[23] R. H. French et al. "Long range interactions in nanoscale science". In: *Rev. Mod. Phys.* 82 (2 2010), pp. 1887–1944. DOI: `10.1103/RevModPhys.82.1887`.

[24] HB Chan et al. "Quantum mechanical actuation of microelectromechanical systems by the Casimir force". In: *Science* 291.5510 (2001), p. 1941.

[25] R. S. Decca et al. "Measurement of the Casimir Force between Dissimilar Metals". In: *Phys. Rev. Lett.* 91 (5 2003), p. 050402. DOI: `10.1103/PhysRevLett.91.050402`.

[26] S. J. Rahi et al. "Nonmonotonic effects of parallel sidewalls on Casimir forces between cylinders". In: *Phys. Rev. A* 77 (3 2008), p. 030101. DOI: `10.1103/PhysRevA.77.030101`.

[27] J. L. Garrett, D. A. T. Somers, and J. N. Munday. "Measurement of the Casimir Force between Two Spheres". In: *Phys. Rev. Lett.* 120 (4 2018), p. 040401. DOI: `10.1103/PhysRevLett.120.040401`.

[28] A. Le Cunuder et al. "Measurement of the Casimir force in a gas and in a liquid". In: *Phys. Rev. B* 98 (20 2018), p. 201408. DOI: `10.1103/PhysRevB.98.201408`.

[29] C. J. Cao, M. van Caspel, and A. R. Zhitnitsky. "Topological Casimir effect in Maxwell electrodynamics on a compact manifold". In: *Phys. Rev. D* 87 (10 2013), p. 105012. DOI: `10.1103/PhysRevD.87.105012`.

[30] A. G. Grushin and A. Cortijo. "Tunable Casimir Repulsion with Three-Dimensional Topological Insulators". In: *Phys. Rev. Lett.* 106 (2 2011), p. 020403. DOI: `10.1103/PhysRevLett.106.020403`.

[31]   A. Martín-Ruiz, M. Cambiaso, and L. F. Urrutia. "A Green's function approach to the Casimir effect on topological insulators with planar symmetry". In: *Europhysics Letters (EPL)* 113.6 (2016), p. 60005. DOI: `10.1209/0295-5075/113/60005`.

[32]   C.-J. Feng and X.-Z. Li. "Quantum spring from the Casimir effect". In: *Physics Letters B* 691.3 (2010), pp. 167 –172. ISSN: 0370-2693. DOI: `https://doi.org/10.1016/j.physletb.2010.06.030`.

[33]   D. Karabali and V. P. Nair. "Casimir effect in $(2+1)$-dimensional Yang-Mills theory as a probe of the magnetic mass". In: *Phys. Rev. D* 98 (10 2018), p. 105009. DOI: `10.1103/PhysRevD.98.105009`.

[34]   P. Hays. "Vacuum fluctuations of a confined massive field in two dimensions". In: *Annals of Physics* 121.1 (1979), pp. 32 –46. ISSN: 0003-4916. DOI: `https://doi.org/10.1016/0003-4916(79)90090-3`.

[35]   J. Ambjørn and S. Wolfram. "Properties of the vacuum. I. Mechanical and thermodynamic". In: *Annals of Physics* 147.1 (1983), pp. 1–32. ISSN: 0003-4916. DOI: `https://doi.org/10.1016/0003-4916(83)90065-9`.

[36]   R. L. Jaffe. "Casimir effect and the quantum vacuum". In: *Phys. Rev. D* 72 (2 2005), p. 021301. DOI: `10.1103/PhysRevD.72.021301`.

[37]   A. Scardicchio. "Casimir dynamics: Interactions of surfaces with codimension > 1 due to quantum fluctuations". In: *Phys. Rev. D* 72 (6 2005), p. 065004. DOI: `10.1103/PhysRevD.72.065004`.

[38] D. Zhabinskaya, J. M. Kinder, and E. J. Mele. "Casimir effect for massless fermions in one dimension: A force-operator approach". In: *Phys. Rev. A* 78 (6 2008), p. 060103. DOI: 10.1103/PhysRevA.78.060103.

[39] F. S. Khoo and L. P. Teo. "Finite temperature Casimir effect of massive fermionic fields in the presence of compact dimensions". In: *Physics Letters B* 703.2 (2011), pp. 199 –207. ISSN: 0370-2693. DOI: https://doi.org/10.1016/j.physletb.2011.07.072.

[40] T. H. Boyer. "Van der Waals forces and zero-point energy for dielectric and permeable materials". In: *Phys. Rev. A* 9 (5 1974), pp. 2078–2084. DOI: 10.1103/PhysRevA.9.2078.

[41] O. Kenneth et al. "Repulsive Casimir Forces". In: *Phys. Rev. Lett.* 89 (3 2002), p. 033001. DOI: 10.1103/PhysRevLett.89.033001.

[42] M. Levin et al. "Casimir Repulsion between Metallic Objects in Vacuum". In: *Phys. Rev. Lett.* 105 (9 2010), p. 090403. DOI: 10.1103/PhysRevLett.105.090403.

[43] D. T. Alves et al. "Repulsive Maxwell–Chern–Simons Casimir effect". In: *Physics Letters A* 374.21 (2010), pp. 2113 –2116. ISSN: 0375-9601. DOI: https://doi.org/10.1016/j.physleta.2010.03.012.

[44] U. Leonhardt and T. G. Philbin. "Quantum levitation by left-handed metamaterials". In: *New Journal of Physics* 9.8 (2007), pp. 254–254. DOI: 10.1088/1367-2630/9/8/254.

[45] J. N. Munday, F. Capasso, and V. A. Parsegian. "Measured long-range repulsive Casimir–Lifshitz forces". In: *Nature* 457.7226 (2009), pp. 170–173. DOI: `10.1038/nature07610`.

[46] Q.-D. Jiang and F. Wilczek. "Chiral Casimir forces: Repulsive, enhanced, tunable". In: *Phys. Rev. B* 99 (12 2019), p. 125403. DOI: `10.1103/PhysRevB.99.125403`.

[47] R. Garcia and M. H. W. Chan. "Critical Casimir Effect near the $^{3}He - ^{4}He$ Tricritical Point". In: *Phys. Rev. Lett.* 88 (8 2002), p. 086101. DOI: `10.1103/PhysRevLett.88.086101`.

[48] T. Ueno et al. "Critical Casimir Effect and Wetting by Helium Mixtures". In: *Phys. Rev. Lett.* 90 (11 2003), p. 116102. DOI: `10.1103/PhysRevLett.90.116102`.

[49] A. Mukhopadhyay and B. M. Law. "Critical Casimir Effect in Binary Liquid Wetting Films". In: *Phys. Rev. Lett.* 83 (4 1999), pp. 772–775. DOI: `10.1103/PhysRevLett.83.772`.

[50] A. Recati et al. "Casimir forces between defects in one-dimensional quantum liquids". In: *Phys. Rev. A* 72 (2 2005), p. 023616. DOI: `10.1103/PhysRevA.72.023616`.

[51] Michael Schecter and Alex Kamenev. "Phonon-Mediated Casimir Interaction between Mobile Impurities in One-Dimensional Quantum Liquids". In: *Phys. Rev. Lett.* 112 (15 2014), p. 155301. DOI: `10.1103/PhysRevLett.112.155301`.

[52] E. Eisenriegler and U. Ritschel. "Casimir forces between spherical particles in a critical fluid and conformal invariance". In: *Phys.*

Rev. B 51 (19 1995), pp. 13717–13734. DOI: `10.1103/PhysRevB.51.13717`.

[53] J. N. Fuchs, A. Recati, and W. Zwerger. "Oscillating Casimir force between impurities in one-dimensional Fermi liquids". In: *Phys. Rev. A* 75 (4 2007), p. 043615. DOI: `10.1103/PhysRevA.75.043615`.

[54] P. Wächter, V. Meden, and K. Schönhammer. "Indirect forces between impurities in one-dimensional quantum liquids". In: *Phys. Rev. B* 76 (4 2007), p. 045123. DOI: `10.1103/PhysRevB.76.045123`.

[55] Eugene B. Kolomeisky, Joseph P. Straley, and Michael Timmins. "Casimir effect in a one-dimensional gas of free fermions". In: *Phys. Rev. A* 78 (2 2008), p. 022104. DOI: `10.1103/PhysRevA.78.022104`.

[56] A. V. Shytov, D. A. Abanin, and L. S. Levitov. "Long-Range Interaction between Adatoms in Graphene". In: *Phys. Rev. Lett.* 103 (1 2009), p. 016806. DOI: `10.1103/PhysRevLett.103.016806`.

[57] M. Bordag et al. "Casimir interaction between a perfect conductor and graphene described by the Dirac model". In: *Phys. Rev. B* 80 (24 2009), p. 245406. DOI: `10.1103/PhysRevB.80.245406`.

[58] C. K. Law. "Interaction between a moving mirror and radiation pressure: A Hamiltonian formulation". In: *Phys. Rev. A* 51 (3 1995), pp. 2537–2541. DOI: `10.1103/PhysRevA.51.2537`.

[59] Alejandro W. Rodriguez, Federico Capasso, and Steven G. Johnson. "The Casimir effect in microstructured geometries". In: *Nat. Photon.* 5.4 (2011), p. 211. ISSN: 1749-4885. DOI: `10.1038/NPHOTON.2011.39`.

[60]   M. Antezza, L. P. Pitaevskii, and .S Stringari. "Effect of the Casimir-Polder force on the collective oscillations of a trapped Bose-Einstein condensate". In: *Phys. Rev. A* 70 (5 2004), p. 053619. DOI: `10.1103/PhysRevA.70.053619`.

[61]   F. Meier and H. Walliser. "Quantum corrections to baryon properties in chiral soliton models". In: *Physics Reports* 289.6 (1997), pp. 383 –448. ISSN: 0370-1573. DOI: `https://doi.org/10.1016/S0370-1573(97)00012-4`.

[62]   R. S. Decca et al. "Novel constraints on light elementary particles and extra-dimensional physics from the Casimir effect". In: *Eur. Phys. J. C* 51.4 (2007), p. 963.

[63]   M Fabinger and P Horava. "Casimir effect between world-branes in heterotic M-theory". In: *Nucl. Phys. B* 580.1 (2000), p. 243.

[64]   E Elizalde. "Matching the observational value of the cosmological constant". In: *Phys. Lett. B* 516.1 (2001), p. 143.

[65]   Emilio Elizalde et al. "Casimir effect in de Sitter and anti–de Sitter braneworlds". In: *Phys. Rev. D* 67 (6 2003), p. 063515. DOI: `10.1103/PhysRevD.67.063515`.

[66]   L. H. Ford. "Quantum vacuum energy in general relativity". In: *Phys. Rev. D* 11 (12 1975), pp. 3370–3377. DOI: `10.1103/PhysRevD.11.3370`.

[67]   Y. Srivastava, A. Widom, and M. H. Friedman. "Microchips as Precision Quantum-Electrodynamic Probes". In: *Phys. Rev. Lett.* 55 (21 1985), pp. 2246–2248. DOI: `10.1103/PhysRevLett.55.2246`.

[68]   E. Buks and M. L. Roukes. "Stiction, adhesion energy, and the Casimir effect in micromechanical systems". In: *Phys. Rev. B* 63 (3 2001), p. 033402. DOI: 10.1103/PhysRevB.63.033402.

[69]   M. Bordag, U. Mohideen, and V. M. Mostepanenko. "New developments in the Casimir effect". In: *Phys. Rep.* 353.1 (2001), p. 1.

[70]   H. B. Chan et al. "Quantum Mechanical Actuation of Microelectromechanical Systems by the Casimir Force". In: *Science* 291.5510 (2001), pp. 1941–1944. ISSN: 0036-8075. DOI: 10.1126/science.1057984.

[71]   M. Kardar and R. Golestanian. "The "friction" of vacuum, and other fluctuation-induced forces". In: *Rev. Mod. Phys.* 71 (4 1999), pp. 1233–1245. DOI: 10.1103/RevModPhys.71.1233.

[72]   N.K. Mahale and M. W. Cole. "Ordering and phase separation of adsorbed binary mixtures". In: *Surface Science* 176.1 (1986), pp. 319 –326. ISSN: 0039-6028. DOI: https://doi.org/10.1016/0039-6028(86)90178-0.

[73]   P. Kapitza. "Viscosity of Liquid Helium below the λ-Point". In: *Nature* 141.3558 (1938), pp. 74–74. DOI: 10.1038/141074a0.

[74]   I. Bloch, J. Dalibard, and W. Zwerger. "Many-body physics with ultracold gases". In: *Rev. Mod. Phys.* 80 (3 2008), pp. 885–964. DOI: 10.1103/RevModPhys.80.885.

[75]   H. Moritz et al. "Exciting Collective Oscillations in a Trapped 1D Gas". In: *Phys. Rev. Lett.* 91 (25 2003), p. 250402. DOI: 10.1103/PhysRevLett.91.250402.

[76] Henning Moritz et al. "Confinement Induced Molecules in a 1D Fermi Gas". In: *Phys. Rev. Lett.* 94 (21 2005), p. 210401. DOI: 10.1103/PhysRevLett.94.210401.

[77] B. L. Tolra et al. "Observation of Reduced Three-Body Recombination in a Correlated 1D Degenerate Bose Gas". In: *Phys. Rev. Lett.* 92 (19 2004), p. 190401. DOI: 10.1103/PhysRevLett.92.190401.

[78] T. Kinoshita, T. Wenger, and D. S. Weiss. "Observation of a One-Dimensional Tonks-Girardeau Gas". In: *Science* 305.5687 (2004), pp. 1125–1128. ISSN: 0036-8075. DOI: 10.1126/science.1100700.

[79] J. Catani et al. "Quantum dynamics of impurities in a one-dimensional Bose gas". In: *Phys. Rev. A* 85 (2 2012), p. 023623. DOI: 10.1103/PhysRevA.85.023623.

[80] K. M. O'Hara et al. "Stable, Strongly Attractive, Two-State Mixture of Lithium Fermions in an Optical Trap". In: *Phys. Rev. Lett.* 85 (10 2000), pp. 2092–2095. DOI: 10.1103/PhysRevLett.85.2092.

[81] M. Köhl et al. "Fermionic Atoms in a Three Dimensional Optical Lattice: Observing Fermi Surfaces, Dynamics, and Interactions". In: *Phys. Rev. Lett.* 94 (8 2005), p. 080403. DOI: 10.1103/PhysRevLett.94.080403.

[82] A. G. Volosniev, H.-W. Hammer, and N. T. Zinner. "Real-time dynamics of an impurity in an ideal Bose gas in a trap". In: *Phys. Rev. A* 92 (2 2015), p. 023623. DOI: 10.1103/PhysRevA.92.023623.

[83] P. Wächter, V. Meden, and K. Schönhammer. "Indirect forces between impurities in one-dimensional quantum liquids". In: *Phys.*

Rev. B 76 (4 2007), p. 045123. DOI: 10 . 1103 / PhysRevB . 76 . 045123.

[84] B. Reichert, Z. Ristivojevic, and A. Petković. "The Casimir-like effect in a one-dimensional Bose gas". In: *New Journal of Physics* 21.5 (2019), p. 053024. DOI: 10.1088/1367-2630/ab1b8e.

[85] G. Xianlong and W. Wonneberger. "Two-component Fermi gas in a one-dimensional harmonic trap". In: *Phys. Rev. A* 65 (3 2002), p. 033610. DOI: 10.1103/PhysRevA.65.033610.

[86] A. Recati et al. "Spin-Charge Separation in Ultracold Quantum Gases". In: *Phys. Rev. Lett.* 90 (2 2003), p. 020401. DOI: 10.1103/ PhysRevLett.90.020401.

[87] F. Gleisberg and W. Wonneberger. "Coupling constants for a degenerate Fermi gas confined to a quasi-one-dimensional harmonic trap". In: *Journal of Physics B: Atomic, Molecular and Optical Physics* 37.7 (2004), S59–S72. DOI: 10.1088/0953-4075/37/7/ 053.

[88] I. V. Tokatly. "Dilute Fermi Gas in Quasi-One-Dimensional Traps: From Weakly Interacting Fermions via Hard Core Bosons to a Weakly Interacting Bose Gas". In: *Phys. Rev. Lett.* 93 (9 2004), p. 090405. DOI: 10.1103/PhysRevLett.93.090405.

[89] G. E. Astrakharchik and L. P. Pitaevskii. "Motion of a heavy impurity through a Bose-Einstein condensate". In: *Phys. Rev. A* 70 (1 2004), p. 013608. DOI: 10.1103/PhysRevA.70.013608.

[90] Alexander Klein and Michael Fleischhauer. "Interaction of impurity atoms in Bose-Einstein condensates". In: *Phys. Rev. A* 71 (3 2005), p. 033605. DOI: 10.1103/PhysRevA.71.033605.

[91] Bernd Mohring et al. "Extracting atoms on demand with lasers". In: *Phys. Rev. A* 71 (5 2005), p. 053601. DOI: 10.1103/PhysRevA.71.053601.

[92] A. Recati et al. "Atomic Quantum Dots Coupled to a Reservoir of a Superfluid Bose-Einstein Condensate". In: *Phys. Rev. Lett.* 94 (4 2005), p. 040404. DOI: 10.1103/PhysRevLett.94.040404.

[93] J. Catani et al. "Entropy Exchange in a Mixture of Ultracold Atoms". In: *Phys. Rev. Lett.* 103 (14 2009), p. 140401. DOI: 10.1103/PhysRevLett.103.140401.

[94] M. Nielsen. "Phonons in Solid Hydrogen and Deuterium Studied by Inelastic Coherent Neutron Scattering". In: *Phys. Rev. B* 7 (4 1973), pp. 1626–1635. DOI: 10.1103/PhysRevB.7.1626.

[95] F. Capitani et al. "Spectroscopic evidence of a new energy scale for superconductivity in H3S". In: *Nature Physics* 13 (2017). Article, 859 EP.

[96] S.-I. Tomonaga. "Remarks on Bloch's Method of Sound Waves applied to Many-Fermion Problems". In: *Progress of Theoretical Physics* 5.4 (1950), pp. 544–569. DOI: 10.1143/ptp/5.4.544.

[97] J. M. Luttinger. "An Exactly Soluble Model of a Many-Fermion System". In: *Journal of Mathematical Physics* 4.9 (1963), pp. 1154–1162. DOI: 10.1063/1.1704046.

[98]   D. C. Mattis and E. H. Lieb. "Exact Solution of a Many-Fermion System and Its Associated Boson Field". In: *Journal of Mathematical Physics* 6.2 (1965), pp. 304–312. DOI: 10.1063/1.1704281.

[99]   F. D. M. Haldane. "'Luttinger liquid theory' of one-dimensional quantum fluids. I. Properties of the Luttinger model and their extension to the general 1D interacting spinless Fermi gas". In: *Journal of Physics C: Solid State Physics* 14.19 (1981), pp. 2585–2609. DOI: 10.1088/0022-3719/14/19/010.

[100]   F. D. M. Haldane. "Effective Harmonic-Fluid Approach to Low-Energy Properties of One-Dimensional Quantum Fluids". In: *Phys. Rev. Lett.* 47 (25 1981), pp. 1840–1843. DOI: 10.1103/PhysRevLett.47.1840.

[101]   J. Voit. "One-dimensional Fermi liquids". In: *Reports on Progress in Physics* 58.9 (1995), pp. 977–1116. DOI: 10.1088/0034-4885/58/9/002.

[102]   T. Giamarchi. *Quantum Physics in One Dimension*. Oxford University Press, 2003. DOI: 10.1093/acprof:oso/9780198525004.001.0001.

[103]   Elliott H. Lieb and Werner Liniger. "Exact Analysis of an Interacting Bose Gas. I. The General Solution and the Ground State". In: *Phys. Rev.* 130 (4 1963), pp. 1605–1616. DOI: 10.1103/PhysRev.130.1605.

[104]   Zoran Ristivojevic. "Excitation Spectrum of the Lieb-Liniger Model". In: *Phys. Rev. Lett.* 113 (1 2014), p. 015301. DOI: 10.1103/PhysRevLett.113.015301.

[105]   C. L. Kane and Matthew P. A. Fisher. "Transport in a one-channel Luttinger liquid". In: *Phys. Rev. Lett.* 68 (8 1992), pp. 1220–1223. DOI: 10.1103/PhysRevLett.68.1220.

[106]   C. L. Kane and Matthew P. A. Fisher. "Transmission through barriers and resonant tunneling in an interacting one-dimensional electron gas". In: *Phys. Rev. B* 46 (23 1992), pp. 15233–15262. DOI: 10.1103/PhysRevB.46.15233.

[107]   A. H. Castro Neto and Matthew P. A. Fisher. "Dynamics of a heavy particle in a Luttinger liquid". In: *Phys. Rev. B* 53 (15 1996), pp. 9713–9718. DOI: 10.1103/PhysRevB.53.9713.

[108]   G.E. Volovik. "Mesoscopic Casimir forces from effects of discrete particle number in the quantum vacuum." In: *JETP Lett.* 73 (2001), pp. 375–379.

[109]   A. Zee. *Quantum Field Theory in a Nutshell.* Princeton University Press, Princeton, 2007.

[110]   J. Friedel. "Metallic alloys". In: *Il Nuovo Cimento (1955-1965)* 7.2 (1958), pp. 287–311. ISSN: 1827-6121. DOI: 10.1007/BF02751483.

[111]   I. Y. Dzyaloshinskii A. A. Abrikosov L. P. Gorkov. *Methods of Quantum Field Theory in Statistical Physics.* Dover Publications, New York, 1975.

[112]   A. Derevianko et al. "High-Precision Calculations of Dispersion Coefficients, Static Dipole Polarizabilities, and Atom-Wall Interaction Constants for Alkali-Metal Atoms". In: *Phys. Rev. Lett.* 82 (18 1999), p. 3589. DOI: 10.1103/PhysRevLett.82.3589.

[113]   N. N. Bogoljubov. "On a new method in the theory of supercon-
        ductivity". In: *Il Nuovo Cimento (1955-1965)* 7.6 (1958), pp. 794–
        805. ISSN: 1827-6121. DOI: `10.1007/BF02745585`.

[114]   A. I. Pavlov, J. van den Brink, and D. V. Efremov. "Phonon-
        mediated Casimir interaction between finite-mass impurities". In:
        Phys. Rev. B 98 (16 2018), p. 161410. DOI: `10.1103/PhysRevB.`
        `98.161410`.

[115]   R. Englman. *The Jahn-Teller effect in molecules and crystals.* Wiley-
        Interscience, London, 1972.

[116]   M. V. Klein. "Some Properties of Phonon Thermal-Conductivity
        Resonances". In: *Phys. Rev.* 186 (3 1969), pp. 839–851. DOI: `10.`
        `1103/PhysRev.186.839`.

[117]   B. Halperin and R. Englman. "Scattering of lattice waves due to
        Jahn-Teller interaction". In: *Phys. Rev. B* 12 (1 1975), pp. 388–399.
        DOI: `10.1103/PhysRevB.12.388`.

[118]   Y. Kayanuma, H. Yamada, and S. Tanaka. "Resonant Scattering of
        Acoustic Phonons by Randomly Distributed Two-Level Systems".
        In: *Journal of the Physical Society of Japan* 54.7 (1985), pp. 2576–
        2587. DOI: `10.1143/JPSJ.54.2576`.

[119]   M. Rueff, E. Sigmund, and M. Wagner. "Resonance Scattering of
        Phonons at Trigonal Jahn-Teller Centres". In: *physica status solidi
        (b)* 81.2 (1977), pp. 511–520. DOI: `10.1002/pssb.2220810211`.

[120]   I. Ya. Polishchuk, L. A. Maksimov, and A. L. Burin. "Localization
        and propagation of phonons in crystals with heavy impurities". In:
        Physics Reports 288.1 (1997). I.M. Lifshitz and Condensed Matter

Theory, pp. 205 –222. ISSN: 0370-1573. DOI: `https://doi.org/`
`10.1016/S0370-1573(97)00025-2`.

[121] T. Emig et al. "Casimir Forces between Arbitrary Compact Ob-
jects". In: *Phys. Rev. Lett.* 99 (17 2007), p. 170403. DOI: `10.1103/`
`PhysRevLett.99.170403`.

[122] O. Kenneth and I. Klich. "Casimir forces in a T-operator approach".
In: *Phys. Rev. B* 78 (1 2008), p. 014103. DOI: `10.1103/PhysRevB.`
`78.014103`.

[123] L.D. Landau and E.M. Lifshitz. *Course of Theoretical Physics.*
Quantum Mechanics. Non-relativistic Theory. 3rd ed. Pergamon,
Oxford, 1977.

[124] B. A. Lippmann and J. Schwinger. "Variational Principles for Scat-
tering Processes. I". In: *Phys. Rev.* 79 (3 1950), pp. 469–480. DOI:
`10.1103/PhysRev.79.469`.

[125] J.J. Sakurai. *Modern Quantum Mechanics.* Revised. Prentice Hall,
New Jersey, 1993.

[126] C. Bena et al. "Quasiparticle scattering and local density of states
in the d-density-wave phase". In: *Phys. Rev. B* 69 (13 2004), p. 134517.
DOI: `10.1103/PhysRevB.69.134517`.

[127] Luuk J. P. Ament et al. "Resonant inelastic x-ray scattering stud-
ies of elementary excitations". In: *Rev. Mod. Phys.* 83 (2 2011),
pp. 705–767. DOI: `10.1103/RevModPhys.83.705`.

[128] Jörg Schmiedmayer et al. "Index of Refraction of Various Gases for Sodium Matter Waves". In: *Phys. Rev. Lett.* 74 (7 1995), pp. 1043–1047. DOI: `10.1103/PhysRevLett.74.1043`.

[129] Robert C. Forrey, A. Dalgarno, and Jörg Schmiedmayer. "Determining the electron forward-scattering amplitude using electron interferometry". In: *Phys. Rev. A* 59 (2 1999), R942–R945. DOI: `10.1103/PhysRevA.59.R942`.

[130] M. R. Matthews et al. "Dynamical Response of a Bose-Einstein Condensate to a Discontinuous Change in Internal State". In: *Phys. Rev. Lett.* 81 (2 1998), pp. 243–247. DOI: `10.1103/PhysRevLett.81.243`.

[131] D. S. Hall et al. "Dynamics of Component Separation in a Binary Mixture of Bose-Einstein Condensates". In: *Phys. Rev. Lett.* 81 (8 1998), pp. 1539–1542. DOI: `10.1103/PhysRevLett.81.1539`.

[132] C. A. Regal and D. S. Jin. "Measurement of Positive and Negative Scattering Lengths in a Fermi Gas of Atoms". In: *Phys. Rev. Lett.* 90 (23 2003), p. 230404. DOI: `10.1103/PhysRevLett.90.230404`.

[133] K. M. Mertes et al. "Nonequilibrium Dynamics and Superfluid Ring Excitations in Binary Bose-Einstein Condensates". In: *Phys. Rev. Lett.* 99 (19 2007), p. 190402. DOI: `10.1103/PhysRevLett.99.190402`.

[134] L. J. Challis, V. W. Rampton, and A. F. G Wyatt, eds. *Phonon Scattering in Solids.* Springer US, 1976. DOI: `10.1007/978-1-4613-4271-7`.

[135] J. A. Carruthers et al. "The thermal conductivity of germanium and silicon between 2 an d 300° K". In: *Proceedings of the Royal Society of London. Series A. Mathematical and Physical Sciences* 238.1215 (1957), pp. 502–514. DOI: 10.1098/rspa.1957.0014.

[136] A. M. Poujade and H. J. Albany. "Carrier-Concentration Dependence of Electron-Phonon Scattering in Te-Doped GaSb at Low Temperature". In: *Phys. Rev.* 182 (3 1969), pp. 802–807. DOI: 10.1103/PhysRev.182.802.

[137] A. Atland and B.D. Simons. *Condensed Matter Field Theory*. Cambridge University Press ; 2 edition, 2010.

[138] L. D. Landau and E.M. Lifshitz. *Course of Theoretical Physics*. 3rd ed. Vol. 5. Butterworth-Heinemann, 1996.

[139] M. Schecter, D.M. Gangardt, and A." Kamenev. "Dynamics and Bloch oscillations of mobile impurities in one-dimensional quantum liquids". In: *Annals of Physics* 327.3 (2012), pp. 639 –670. ISSN: 0003-4916. DOI: https://doi.org/10.1016/j.aop.2011.10.001.

[140] A. P. Drozdov et al. "Conventional superconductivity at 203 kelvin at high pressures in the sulfur hydride system". In: *Nature* 525.7567 (2015), pp. 73–76. DOI: 10.1038/nature14964.

[141] M. Somayazulu et al. "Evidence for Superconductivity above 260 K in Lanthanum Superhydride at Megabar Pressures". In: *Phys. Rev. Lett.* 122 (2 2019), p. 027001. DOI: 10.1103/PhysRevLett.122.027001.

[142] Ah H. Castro Neto and K. S. Novoselov. "New directions in science and technology: two−dimensional crystals". In: *Reports on Progress in Physics* 74.8 (2011), p. 082501. DOI: `10.1088/0034-4885/74/8/082501`.

[143] K. S. Novoselov et al. "Two dimensional atomic crystals". In: *Proceedings of the National Academy of Sciences* 102.30 (2005), pp. 10451–10453. DOI: `10.1073/pnas.0502848102`.

[144] Andrey V. Chubukov, Subir Sachdev, and Jinwu Ye. "Theory of two-dimensional quantum Heisenberg antiferromagnets with a nearly critical ground state". In: *Phys. Rev. B* 49 (17 1994), pp. 11919–11961. DOI: `10.1103/PhysRevB.49.11919`.

[145] Matthias Vojta, Chiranjeeb Buragohain, and Subir Sachdev. "Quantum impurity dynamics in two-dimensional antiferromagnets and superconductors". In: *Phys. Rev. B* 61 (22 2000), pp. 15152–15184. DOI: `10.1103/PhysRevB.61.15152`.

[146] O. P. Sushkov. "Spin-$\frac{1}{2}$ magnetic impurity in a two-dimensional magnetic system close to a quantum critical point". In: *Phys. Rev. B* 62 (18 2000), pp. 12135–12140. DOI: `10.1103/PhysRevB.62.12135`.

[147] Michael Holt et al. "Fermi Surface Reconstruction by Dynamic Magnetic Fluctuations". In: *Phys. Rev. Lett.* 109 (3 2012), p. 037001. DOI: `10.1103/PhysRevLett.109.037001`.

[148] Michael Holt et al. "Fermi surface reconstruction by dynamic magnetic fluctuations and spin-charge separation near an $O(3)$ quan-

tum critical point". In: *Phys. Rev. B* 87 (7 2013), p. 075109. DOI: 10.1103/PhysRevB.87.075109.

[149]   H. Wang, V. Eyert, and U. Schwingenschlögl. "Electronic structure and magnetic ordering of the semiconducting chromium trihalides CrCl3, CrBr3, and CrI3". In: *Journal of Physics: Condensed Matter* 23.11 (2011), p. 116003. DOI: 10.1088/0953-8984/23/11/116003.

[150]   B. Sachs et al. "Ferromagnetic two-dimensional crystals: Single layers of K_2CuF_4". In: *Phys. Rev. B* 88 (20 2013), p. 201402. DOI: 10.1103/PhysRevB.88.201402.

[151]   Xingxing Li, Xiaojun Wu, and Jinlong Yang. "Half-Metallicity in MnPSe3 Exfoliated Nanosheet with Carrier Doping". In: *Journal of the American Chemical Society* 136.31 (2014), pp. 11065–11069. DOI: 10.1021/ja505097m.

[152]   Xingxing Li and Jinlong Yang. "CrXTe3(X = Si, Ge) nanosheets: two dimensional intrinsic ferromagnetic semiconductors". In: *Journal of Materials Chemistry C* 2.34 (2014), p. 7071. DOI: 10.1039/c4tc01193g.

[153]   Wei-Bing Zhang et al. "Robust intrinsic ferromagnetism and half semiconductivity in stable two-dimensional single-layer chromium trihalides". In: *Journal of Materials Chemistry C* 3.48 (2015), pp. 12457–12468. DOI: 10.1039/c5tc02840j.

[154]   Nikhil Sivadas et al. "Magnetic ground state of semiconducting transition-metal trichalcogenide monolayers". In: *Phys. Rev. B* 91 (23 2015), p. 235425. DOI: 10.1103/PhysRevB.91.235425.

[155] Cheng Gong et al. "Discovery of intrinsic ferromagnetism in two-dimensional van der Waals crystals". In: *Nature* 546.7657 (2017), pp. 265–269. DOI: `10.1038/nature22060`.

[156] A. K. Geim and I. V. Grigorieva. "Van der Waals heterostructures". In: *Nature* 499.7459 (July 2013), pp. 419–425. DOI: `10.1038/nature12385`.

[157] D. Ghazaryan et al. "Magnon-assisted tunnelling in van der Waals heterostructures based on CrBr3". In: *Nature Electronics* 1.6 (2018), pp. 344–349. DOI: `10.1038/s41928-018-0087-z`.

[158] Michael A. McGuire et al. "Coupling of Crystal Structure and Magnetism in the Layered, withinetic Insulator CrI3". In: *Chemistry of Materials* 27.2 (2015), pp. 612–620. DOI: `10.1021/cm504242t`.

[159] Yao Tian et al. "Magneto-elastic coupling in a potential ferromagnetic 2D atomic crystal". In: *2D Materials* 3.2 (2016), p. 025035. DOI: `10.1088/2053-1583/3/2/025035`.

[160] N. D. Mermin and H. Wagner. "Absence of Ferromagnetism or Antiferromagnetism in One- or Two-Dimensional Isotropic Heisenberg Models". In: *Phys. Rev. Lett.* 17 (22 1966), pp. 1133–1136. DOI: `10.1103/PhysRevLett.17.1133`.

[161] B. Huang et al. "Layer-dependent ferromagnetism in a van der Waals crystal down to the monolayer limit". In: *Nature* 546.7657 (2017), pp. 270–273. DOI: `10.1038/nature22391`.

[162] Xinghan Cai et al. "Atomically Thin $CrCl_3$: An In−Plane Layered Antiferromagnetic Insulator". In: *Nano Letters* 19.6 (2019), pp. 3993–3998. DOI: `10.1021/acs.nanolett.9b01317`.

[163] C. L. Kane, P. A. Lee, and N. Read. "Motion of a single hole in a quantum antiferromagnet". In: *Phys. Rev. B* 39 (10 1989), pp. 6880–6897. DOI: `10.1103/PhysRevB.39.6880`.

[164] L. N. Bulaevskii, E. L. Nagaev, and D. I. Khomskii. "A new Type of auto−localized state of a conduction elecnron in an antiferromagnetic semiconductor". In: *Soviet Physics JETP* 27 (5 1968), pp. 836–838.

[165] W. F. Brinkman and T. M. Rice. "Single-Particle Excitations in Magnetic Insulators". In: *Phys. Rev. B* 2 (5 1970), pp. 1324–1338. DOI: `10.1103/PhysRevB.2.1324`.

[166] Gerardo Martinez and Peter Horsch. "Spin polarons in the t-J model". In: *Phys. Rev. B* 44 (1 1991), pp. 317–331. DOI: `10.1103/PhysRevB.44.317`.

[167] J. Bała, A. M. Oleś, and J. Zaanen. "Spin polarons in the t-t'-J model". In: *Journal of Magnetism and Magnetic Materials* 140-144 (1995). International Conference on Magnetism, pp. 1939 – 1940. ISSN: 0304-8853. DOI: `https://doi.org/10.1016/0304-8853(94)01438-8`.

[168] C. Brünger and F. F. Assaad. "Single-hole dynamics in the Kondo necklace and bilayer Heisenberg models on a square lattice". In: *Phys. Rev. B* 74 (20 2006), p. 205107. DOI: `10.1103/PhysRevB.74.205107`.

[169] C. Donnerer et al. "High-pressure insulator-to-metal transition in $Sr_3Ir_2O_7$ studied by x-ray absorption spectroscopy". In: *Phys. Rev. B* 97 (3 2018), p. 035106. DOI: `10.1103/PhysRevB.97.035106`.

[170] R. Kilian and G. Khaliullin. "Orbital polarons in the metal−insulator transition of manganites". In: *Phys. Rev. B* 60 (19 1999), pp. 13458–13469. DOI: `10.1103/PhysRevB.60.13458`.

[171] Krzysztof Wohlfeld, and Peter Horsch. "Orbitally induced string formation in the spin-orbital polarons". In: *Phys. Rev. B* 79 (22 2009), p. 224433. DOI: `10.1103/PhysRevB.79.224433`.

[172] Ekaterina M. Pärschke et al. "Correlation induced electron-hole asymmetry in quasi- two-dimensional iridates". In: *Nature Communications* 8.1 (22 Sept. 2017), p. 224433. DOI: `10.1038/s41467-017-00818-8`.

[173] A. Fert and Campbell I. A. "Electrical resistivity of ferromagnetic nickel and iron based alloys". In: *Journal of Physics F: Metal Physics* 6.5 (22 1976), pp. 849–871. DOI: `10.1088/0305-4608/6/5/025`.

[174] F. Beuneu and P. Monod. "Conduction-electron spin resonance in cold-worked Al, Cu, and Ag: The spin-flip cross section of dislocations". In: *Phys. Rev. B* 13 (8 1976), pp. 3424–3430. DOI: `10.1103/PhysRevB.13.3424`.

[175] A Fert. "Two-current conduction in ferromagnetic metals and spin wave-electron collisions". In: *Journal of Physics C: Solid State Physics* 2.10 (22 1969), pp. 1784–1788. DOI: `10.1088/0022-3719/2/10/311`.

[176] F. C. Schwerer and J. Silcox. "Electrical Resistivity of Nickel at Low Temperatures". In: *Phys. Rev. Lett.* 20 (3 1968), pp. 101–103. DOI: `10.1103/PhysRevLett.20.101`.

[177] G. Jackeli and G. Khaliullin. "Mott Insulators in the Strong Spin-Orbit Coupling Limit: From Heisenberg to a Quantum Compass and Kitaev Models". In: *Phys. Rev. Lett.* 102 (1 2009), p. 017205. DOI: `10.1103/PhysRevLett.102.017205`.

[178] George Jackeli and Giniyat Khaliullin. "Magnetically Hidden Order of Kramers Doublets in d^1 Systems: Sr_2VO_4". In: *Phys. Rev. Lett.* 103 (6 2009), p. 067205. DOI: `10.1103/PhysRevLett.103.067205`.

[179] B. J. Kim et al. "Novel $J_{eff} = 1/2$ Mott State Induced by Relativistic Spin-Orbit Coupling in Sr_2IrO_4". In: *Phys. Rev. Lett.* 101 (7 2008), p. 076402. DOI: `10.1103/PhysRevLett.101.076402`.

[180] Yaroslav A. Kharkov and Oleg P. Sushkov. "Casimir effect mechanism of pairing between fermions in the vicinity of a magnetic quantum critical point". In: *Phys. Rev. B* 91 (23 2015), p. 235105. DOI: `10.1103/PhysRevB.91.235105`.

Versicherung

Hiermit versichere ich, dass ich die vorliegende Arbeit ohne unzulässige Hilfe Dritter und ohne Benutzung anderer als der angegebenen Hilfsmittel angefertigt habe, die aus fremden Quellen direkt oder indirekt übernommenen Gedanken sind als solche kenntlich gemacht. Die Arbeit wurde bisher weder im Inland noch im Ausland in gleicher oder ännlicher Form einer anderen Prüfungsbehörde vorgelegt. Die vorliegende Dissertation wurde unter der Betreuung von Prof. Dr. Jeroen van den Brink und Dr. Dmitri V. Efremov im Institut für Theoretische Festkörperforschung des Leibniz-Institut für Festkörper- und Werkstoffforschung Dresden angefertigt.

Andrei Pavlov

Dresden, den 23.08.2019